

**Exploring the role of mechanosensors, with a focus on TMEM63B, in somatosensory coding**  
by

Daniel Jay Orlin

A dissertation submitted in partial fulfillment  
of the requirements for the degree of  
Doctorate in Philosophy  
Neuroscience Graduate program  
in the Oregon Health and Science University  
2024

Doctoral Committee:

Swetha Murthy, PhD, Mentor  
Kevin Wright, PhD, Chair  
Kelly Monk, PhD  
Eric Schnell, MD/PhD  
Elizabeth Moss, PhD

Daniel J. Orlin

Orlin@ohsu.edu

ORCID ID: 0000-0002-7100-4784

School of Medicine  
Oregon Health & Science University

---

Certificate of Approval

This is to certify that the PhD dissertation of  
Daniel J. Orlin  
Has been approved

---

Mentor/Advisor

---

Committee chair

---

Committee member

---

Committee member

---

Committee member

## Table of Contents

Acknowledgements.....	viii
Abstract .....	xiii
List of Tables .....	xiv
List of Figures .....	xv
List of Appendices .....	xix
Chapter 1 Introduction .....	1
1.1 MA ion channels and their role in biology .....	1
1.1.1 MA ion channels are used for cellular function.....	3
1.2 Somatosensory neurons of the dorsal root ganglion .....	6
1.2.1 High-threshold and low-threshold mechanoreceptors (HTMRs and LTMRs).....	7
1.3 Mechanically activated ion channels in DRG neurons: the search.....	11
1.3.1 PIEZO ion channel family: PIEZO2, the low-threshold mechanosensor. ....	12
1.3.2 PIEZO2's role in touch, interoception, and proprioception.....	14
1.3.3 What is beyond PIEZO2? .....	17
1.4 TMEM63B in C-LTMRs .....	21
Chapter 2 Exploring the Landscape of Mechanosensors in C-LTMRs .....	25
2.1 Introduction: Untangling PIEZO2 and TMEM63B's contributions to MA currents in C-LTMRs .....	25
2.2 Results:.....	27
2.2.1 Validation of Cre-mediated recombination in a Vglut3-IRES-Cre mouse line.....	27
2.2.2 Expression of MA ion channels Tmem63b and Piezo2 in C-LTMRs .....	31
2.2.3 Characterization of indentation- and stretch-activated currents in C-LTMRs.....	32

2.2.4 In situ hybridization reveals that the Vglut3 <sup>Cre</sup> line does not delete Tmem63b within C-LTMRs.....	35
2.3 Discussion.....	37
2.4 Methods.....	40
2.4.1 Animals .....	40
2.4.2 Whole DRG dissections.....	41
2.4.3 Dissociated DRG cultures.....	41
2.4.4 In situ hybridization .....	42
2.4.5 IHC.....	43
2.4.6 Primary antibodies .....	43
2.4.7 Imaging and analysis.....	44
2.4.8 Electrophysiology .....	47
Chapter 3 Investigating MA currents of cells over expressing of <i>Piezo2</i> and <i>Tmem63b</i> .....	50
3.1 Introduction:.....	50
3.2 Results: Indentation currents of cells co-expressing of <i>Piezo2</i> and <i>Tmem63b</i> .....	51
3.3 Discussion: .....	56
3.4 Methods: .....	58
3.4.1 Cell culture.....	58
3.4.2 Electrophysiology .....	59
Chapter 4 Discussion .....	61
4.1 MA currents in cultured DRG neurons. ....	62
4.1.1 Further studies on SA currents in C-LTMRs. ....	63
4.1.2 Reexamining PIEZO2's role in MA currents in cultured DRG neurons. ....	64
4.2 Tools to study PIEZO2 in DRG neurons. ....	67
4.3 TMEM63B, what does it do?.....	68
4.3.1 TMEM63B in humans. ....	68

4.3.2 TMEM63B in mice .....	69
4.3.3 TMEM63B and the scramblase hypothesis. ....	70
4.3.4 TMEM63B in DRG neurons and its role in touch .....	71
Bibliography .....	86

## **Acknowledgements**

Professors at Muhlenberg built my path to a career in science. I enjoyed the broad conversations in class with Dr. Gretchan Godhard and Dr. Amy Hark. I got experience conducting a ‘neuro-philosophy’ research project with a group of students lead by Dr. Jeff Rudski and presented that work at my first scientific conference. What made me realize science could be a career came from Dr. Jeremy Teissere. He grounded science in the community of people who conduct research, describing academic families and the environment within an R01 institution. His classes on ion channels and his advice led me to apply to the Vollum at OHSU.

After college I worked at Boston University in Dr. Howard Eichenbaum’s lab. Working for Howard alongside Denise Parisi was a pleasure. Denise supported me day to day helping me navigate Boston University. Howard was eager to get me started on a project and help me learn the field sending me to conferences and discussing projects I wanted to work on.

The Eichenbaum lab was special because of all the wonderful people. Our late nights at Cornwall’s after journal clubs, fantasy football drafts waiting to see which Patriots player Dr. Catherine Mikkelsen took first, and arguing with Dr. Daniel Sheehan about something around 2 pm made for a great place to work. Importantly, I learned to study learning and memory, Drs. Will Mau, Sam Levy, Dave Sullivan, and Nat Kinsky (in order of distance from my desk) all took time to teach me about calcium imaging and even more time to help me learn MATLAB. A special shout out to Nat for letting me help with his amnesia project. There are plenty more people from Boston University that I could thank, and I appreciated everyone there. Our group

could not have moved forward without the assistance of Drs. Michael Hasselmo, Steve Ramirez, and Marc Howard; all of you stepped up when our lab needed help and supported us.

Being accepted into graduate school by the Neuroscience Graduate Program was an honor, and the environment the program fosters helped prepare me to overcome obstacles and avoid many more. Beyond helping me navigate the administration, Jessica Parks has been a great sounding board when I want to chat about my career. My conversations with Drs. Antoinette Foster and Sarah Kissiwaa from the Racial Equity and Inclusion center at the Vollum Institute guided me through tough times during my professional relationships, emphasizing the importance of using non-violent communication to deal with conflict.

I did not stay locked in the lab my entire time in Portland. Thank you to my friends in Portland if you participated in any of these activities with me, I am grateful: hiking, camping, skiing, climbing, hanging out in various parks, playing basketball and volleyball, game nights, pickle ball tournaments, open mic nights, attending cheap Blazers and Thorns games, discovering new breweries and food carts, and Friendsgiving. All these activities have helped me de-stress and made these past 5 years fun.

The Murthy lab was integral to getting me across the finish line. You all helped in your own individual ways and as a group during lab meetings and practice talks. Socially it was a pleasure to go on hikes and share homemade dishes and drinks with all of you. Each one of you made this a special place to do science and you all taught me many fun facts, some of which helped shape my thesis project, many that will probably never come up again. I am thankful that I got to work with all of you and I do hope that our paths cross again.

Dr. Swetha Murthy, my P.I. and mentor, goes above and beyond for the lab. I know she wants the best for every member of the lab because she values us as people and not just as



students and technicians. She takes a complete view of all members of the lab considering things beyond our career goals and scientific accomplishments. I have trust in Swetha to put the long-term health and happiness of the people in her lab above short-term scientific success of the lab. I know these qualities will bring success to her and the lab. She is also a brilliant electrophysiologist, scientist, and teacher. She tirelessly assisted me when I began in the lab letting me pound on her office wall to summon her for immediate patching aid. Her feedback could be exacting, but that gave me confidence when I presented a figure or submitted written work.

My family and friends, there are too many to name here, but I have had the pleasure of being surrounded by supportive people throughout my life. My parents Jeff Orlin and Dr. Frances Keech, I know my education was a high priority for both of you, and maybe leaving me at school until 6-7 every night made me like school so much, I stayed until I am 30. As I grow up, I understand that your stressful days, long hours of work, and love for me gave me an amazing childhood. I am most grateful for the freedom you provided me throughout the years, big decisions were always a conversation where I felt heard and empowered, and I like to think I listened to your advice most of the time. Casey, my sister, is so caring. She would probably tell you she had nothing to do with this and is humble enough to be a tad surprised there was space for her in this ‘official’ document. We have shared so much together, and I wouldn’t be here in Portland if it wasn’t for her; Casey and I drove all the way out to Portland from our home in Newton. It was a grand adventure for the two of us, and I might have gotten a tad cranky camping with our dad’s sleeping pad from the 1980’s, but it was a life changing trip.

To switch gears... graduate school is about learning how to do science, and many people have taken time to train me. Both of my rotation mentors, Drs. Skyler Jackman and Eric Schnell,

are amazing teachers and many of the skills I learned during my rotations came in handy during my time in the Murthy lab. I wanted to list a few people that took the time to train me on experiments and microscopes even though not everything I learned was included in my thesis, Drs. Leire Abalde-Atristain, Julia Halford, Greg Duncan, Jennifer Jahncke, Matt Pomaville, and Tobias Stork.

People within the Vollum that did not directly assist me with scientific tasks but worked to support me with administrative and logistical matters. Chris Ghormley, Elizabeth Clarke, Kennedy Wambalama, Jason Cole, Teresa Newton, Ana Dagostin, Sara Strobaugh, Tim Donovan, and Travis Rogers should be recognized for the work they did.

The scientific work in this thesis was directly helped by the following people. The microscopy core for working with me to design staining experiments, training me on equipment, and seeing my project all the way through the image analysis phase: Drs. Stefanie Kaech-Petrie, Felice Kelly, Hannah Bronstein, and Brian Jenkins. Pamala Canady in the Flow cytometry core sorted DRG neurons for genotyping. Dr. Kevin Wright for offering resources in the form of microscopes, mice, and reagents for staining, and valuable opinions on fresh data. Drs. Skyler Jackman, Zhaozhu Qiu, and Kevin Wright helped by editing and making suggestions for a draft of my first author publication/chapter two of this thesis. Antonio Munoz collected data for the current clamp recordings in this thesis, and he helped with DRG dissections. Antonio Munoz, Desitny Semidey, Aidan Berryman, and Max Schreyer all contributed by genotyping, weaning, or tagging mice. My dissertation advisory committee, Drs. Kelly Monk, Eric Schnell, and Kevin Wright, all of you brought a different perspective to my project making committee meetings effective. In addition to your scientific advice each of you gave insights on my career and for that I am grateful. I always tell people I have an awesome committee, and it is because each of you

are thoughtful and kind individuals. Thank you to Dr. Elizabeth Moss who helped edit this thesis as my outside reader she provided great insights and helped clarify my ideas. Dr. Swetha Murthy trained me on a variety of methods used in this thesis, cell culture, electrophysiology, plasmid cloning, and more; she helped design and plan all experiments, interpret and visualize data, and gave feedback on this thesis and other written works I completed in the lab.

The funding from the T32:5T32NS007466-22, awarded to the Neuroscience graduate program supported me in my first two years. Funding from the Silver Family Foundation supported me and the resources I needed for this project.

I used a template created in consultation with the Horace H. Rackham School of Graduate Studies by the staff at **ScholarSpace**, a service of the University Library. This template made formatting and writing the thesis much easier, they are cited in the bibliography.

Absolutely none of this would not have been possible without my partner **Dr.** Katherine Lehmann. We met in graduate school, and she has contributed to all aspects of this thesis work, apart from directly funding me. In lab she taught me imaging analysis, lent me reagents, and helped edit parts of this document. Outside of lab she keeps me busy with countless activities with our (her) dog Roo; experiencing all the beauty of the Pacific Northwest is best done with someone else is what I've learned. I share absolutely all my thoughts and feelings with her and somehow it is never too much, or at least that's what she says. Unlike Katy, the person reading this probably does not care about **all** my thoughts and feelings, so I will leave it at this, I am too lucky to have met such a wonderful person who I get to share my life with, and this thesis is just a small yet significant part of that life.

## Abstract

The thesis aimed to investigate whether a newly identified mechanically activated (MA) ion channel, TMEM63B, transduces external force into neuronal signals within peripheral dorsal root ganglion (DRG) neurons. DRG neurons are part of the peripheral nervous system responsible for somatosensation. *Piezo2*, which encodes an MA ion channel, is expressed within many DRG neurons, and one of its roles is to transduce light forces into neuronal signals; this process gives rise to the sensation of light or gentle touch. Mice and humans lacking proper PIEZO2 function lose the ability to sense gentle forces but retain the ability to feel painful, noxious forces. There is a different mechanism by which DRG neurons initiate a response to noxious force, and I hypothesized that TMEM63B could allow DRG neurons to encode noxious stimuli. *Tmem63b* and *Piezo2* are co-expressed in many subtypes of DRG neurons, and one of these subtypes is C-fiber low threshold mechanoreceptors (C-LTMRs), which retain their response to noxious stimuli in *Piezo2* conditional knockout (cKO) mice. For this reason, I focused on C-LTMRs by characterizing *Tmem63b* expression and protein levels with staining experiments. I recorded MA currents from C-LTMRs and attempted to characterize TMEM63B's contribution to these currents, but after seeing no differences in the currents I ran a control experiment that showed the mouse lines I used did not generate a *Tmem63b* cKO. Recording MA currents in C-LTMRs demonstrated that the inactivation kinetics of the MA currents were slower compared to previous reports of PIEZO2-dependent currents. Follow-up studies could examine the MA currents of C-LTMR to understand what makes them different compared to other DRG subtypes that express *Piezo2*.

Another aim was to investigate if TMEM63B and PIEZO2 modulate each other's MA currents. Expression data from my experiments and other labs' RNA-sequencing experiments show that *Piezo2* and *Tmem63b* are co-expressed in many DRG neurons and other cell types within the body. I investigated how the co-expression of these two MA ion channels affects their MA currents. To do this, I overexpressed both channels in HEK293 *Piezo1* knockout cells (HEK P1KO) and recorded indentation currents. I found no differences in the indentation currents of *Piezo2* only expressing cells compared to *Piezo2* and *Tmem63b* co-expressing cells. These results indicate that these channels do not alter each other's function in these cells, so further tests in cell types with endogenous co-expression are required to make conclusions about how these two channels could alter each other's response to mechanical force.

## List of Tables

<b>Table 1.1: Comparison of PIEZO2 and TMEM63B relevant for this thesis.....</b>	<b>24</b>
<b>Table 2.1: DRG staining percentages for <i>Vglut3<sup>cre</sup></i>; <i>Ai9</i> characterization.....</b>	<b>31</b>
<b>Table 2.2: Electrical properties of C-LTMRs. ....</b>	<b>33</b>
<b>Table 3.1: Multiple t-test for each micron after threshold for maximum current. ....</b>	<b>53</b>
<b>Table 3.2: Multiple t-test for each micron after threshold for tau of inactivation. ....</b>	<b>53</b>
<b>Table 3.3: Multiple t-test for each micron after threshold for steady state percentage. ....</b>	<b>53</b>
<b>Table 3.4: Multiple t-test for each volage step for maximum current. ....</b>	<b>56</b>
<b>Table 3.5: Multiple t-test for each volage step for tau of inactivation. ....</b>	<b>56</b>
<b>Table 3.6: Multiple t-test for each volage step for tau of inactivation. ....</b>	<b>56</b>

## List of Figures

**Figure 1.1: Methods to stimulate and structures of known MA ion channels.** **A:** Outside out patch-clamp mode can induce stretch forces on the membrane by applying positive pressure to the pipette **B:** Cell attached patch-clamp mode can induce stretch forces on the membrane by applying negative pressure to the pipette **C:** In whole cell patch-clamp mode, indenting the cell with a blunt glass probe using a piezo-electric motor, can induce indentation forces. **D-G:** Structures of MA ion channels with amphipathic helices highlighted in red and pore lining helices in dark blue. **D:** Bacterial mechanosensitive channel large conductance (MscL) and small conductance (MscS). **E:** TREK-1 ion channel. **F:** OSCA1.2 ion channel. **G:** PIEZO1 ion channel. Cartoon patches were created by Dr. Swetha Murthy, Structure figures adapted from Kefauver *et al.*, 2020. .... 2

**Figure 1.2: Dorsal root ganglion anatomy and function.** **A:** The dorsal root ganglion (DRG) is composed of many neurons that send axons, which synapse on interneurons in the spinal cord. **B:** Neurons within the DRG have a T-shaped axon that sprouts from the cell body, one end projects to the spinal cord and the other to the periphery. **C:** The targets of DRG neurons include, but not limited to, bladder, colon, adipose tissue, skin, and muscle. **D:** The role of DRG neurons in the skin is to sense chemicals from plants and animals, temperature, and force. **E:** DRG neurons in the muscle sense stretch giving rise to proprioception. Cartoons made by: DBCLS spinal-cord, DBCLS sensory neuron, Servier bladder, Servier, adipocyte, Servier colon, Attendance Cute Mosquito, Kehan Thermometer, Namu Lobster. .... 6

**Figure 1.3: Dissociated DRG neurons produce indentation-induced MA currents with distinct inactivation times.** **A:** DRG neurons are dissected out of mice and the cell bodies are dissociated and cultured for the purpose of whole cell patch-clamp indentation recordings. **B:** Whole cell indentation recordings produce four different types of currents based on the inactivation kinetics. Figure adapted from Delmas *et al.*, 2011. Cartoons made by Dr. Swetha Murthy, DBCLS spinal-cord, DBCLS sensory neuron, Marcel Tisch Stem cell. .... 12

**Figure 1.4: The OSCA/TMEM63 are a family of MA ion channels.** **A:** Phylogenetic tree demonstrating sequence relationships of OSCA and TMEM63 family members. Sequences were aligned using MegAlign Pro and DrawTree created the plot. **B:** OSCA1.2 structure displayed with both subunits highlighted, PDB: 6MGV (Jojoa-Cruz *et al.*, 2018). **C:** Human TMEM63A transmembrane pore helices highlighted in blue, PDB 8GRS(Zhang *et al.*, 2023). . 21

**Figure 2.1: *Vglut3<sup>Cre</sup>* is specific and efficient in genetically labeling C-LTMRs.** **A-C:** Immunostaining of neuronal cell bodies from *Vglut3<sup>Cre</sup>;Ai9* mice for tdTomato and DRG subtype markers. **A:** Neurofilament-200 (Nf-200), **B:** Tyrosine Hydroxylase (TH), and **C:** Parvalbumin (PV) (scale bar: 200µm). **D:** Measure of *Cre* specificity by percent of tdTomato+ neurons overlapping with each DRG subtype marker (N=3 animals) **E:** Measure of *Cre*

efficiency by percent of neurons with a DRG subtype marker overlapping with tdTomato (N=3 animals). Bars represent mean  $\pm$  S.D. .... 28

**Figure 2.2: Staining of subtype markers and tdTomato is consistent across animals and experiments** **A:** Immunostaining of neuronal cell bodies from *Vglut3<sup>Cre</sup>;Ai9* mice stained for UCH-L1, tdTomato, and Nf-200 (top), TH (middle), or PV (bottom); overlap of all channels are also indicated (scale bar: 200  $\mu$ m). **B:** Percent of tdTomato+ neurons represented as UCH-L1 positive neurons that overlap with tdTomato separated by DRG subtype marker staining. **C:** Quantification of subtype abundance as a percent of UCH-L1 positive neurons that overlap with a DRG subtype marker. Bars represent mean  $\pm$  S.D. .... 30

**Figure 2.3: *Tmem63b* and *Piezo2* expression in C-LTMRs.** **A:** Thoracic DRG somas from *Vglut3<sup>Cre</sup>;Ai9* mice with Cre-dependent tdTomato fluorescence, co-labeled with *in situ* probes against *Tmem63b* and *Piezo2*. **B:** Percent of tdTomato+ neurons that co-express both *Tmem63b* and *Piezo2* calculated by mean fluorescence above negative probes (N = 3 animals). **C:** Thoracic DRG somas from *Tmem63b<sup>HA/HA</sup>* mice stained for TH, HA-tag, and overlay of both channels. **D:** Percent of TH positive DRG neurons with HA staining (N=3 animals). Bars represent mean  $\pm$  S.D. scale bars 100  $\mu$ m. .... 31

**Figure 2.4: Cultured C-LTMRs have MA currents in response to both indentation and stretch stimuli.** **A:** Representative trace of action potential of a tdTomato+ positive DRG neuron from *Tmem63b<sup>wt</sup>* (blue) vs *Tmem63b<sup>fl</sup>* (red) mice. **B:** Representative trace of indentation-induced whole-cell MA currents from *Tmem63b<sup>wt</sup>* and *Tmem63b<sup>fl</sup>* C-LTMRs. **C:** Half-width of action potentials within 0-4 pA of rheobase. Green indicates the example trace's corresponding measurement (*Tmem63b<sup>wt</sup>*; 3.07  $\pm$  0.63 ms, cells = 17 and animals = 4, *Tmem63b<sup>fl</sup>*; 2.84  $\pm$  0.80 ms, cells= 18 and animals= 4; unpaired t-test  $p$  = 0.34). **D:** Maximum peak current. Green indicates the example trace's corresponding measurement (*Tmem63b<sup>wt</sup>*; -244.1  $\pm$  200.4 pA, cells= 33 and animals= 6, *Tmem63b<sup>fl</sup>*; 218.7  $\pm$  193.7 pA, cells = 32 and animals = 6, unpaired t-test  $p$  = 0.61). **E:** Inactivation kinetics plotted on log<sub>10</sub> axis (*Tmem63b<sup>wt</sup>*; 154.7  $\pm$  149.4 ms, cells = 32 and animals = 6, *Tmem63b<sup>fl</sup>*; 183.9  $\pm$  132.3 ms, cells = 31 and animals = 6, unpaired t-test  $p$  = 0.42). **F:** Steady state current taken as a percentage of the peak current (*Tmem63b<sup>wt</sup>*; 34.42  $\pm$  25.82, cells = 33 and animals = 6, *Tmem63b<sup>fl</sup>*; 34.96  $\pm$  26.75, cells = 33 and animals = 6, unpaired t-test  $p$  = 0.93). **G:** Representative traces of outside-out stretch currents from *Tmem63b<sup>wt</sup>* and *Tmem63b<sup>fl</sup>*. **H:** P<sub>50</sub> of stretch response fit to a Boltzmann curve (*Tmem63b<sup>wt</sup>*; 38.28  $\pm$  6.24 mmHg, cells = 11 and animals = 3, *Tmem63b<sup>fl</sup>*; 51.32  $\pm$  32.39 mmHg, cells = 9 and animals = 3, unpaired t test  $p$  = 0.21). **I:** Current vs pressure relationship, current normalized to maximum response. Shown is a Boltzmann fit of the average values for each group, green indicates the representative trace's corresponding measurement (*Tmem63b<sup>wt</sup>*; cells = 11 and animals = 5, *Tmem63b<sup>fl</sup>*; cells = 10 and animals = 4, Boltzmann fit is not different  $p$  = 0.80). Bars represent mean  $\pm$  S.D. For all quantifications, green data points indicate the example trace's corresponding measurement. .... 35

**Figure 2.5: *Tmem63b* expression persists in tdTomato+ neurons from *Tmem63b<sup>fl</sup>* mice.** **A:** *In situ* hybridization and immunostaining of dissociated DRG neurons from *Tmem63b<sup>wt</sup>* for probe against *Tmem63b*-exon 5 (white) and tdTomato (red), respectively. Closed arrows denote tdTomato positive neurons with *Tmem63b* puncta. **B:** Same as **A**, but neurons are from *Tmem63b<sup>fl</sup>* mouse. Open arrows denote tdTomato+ neurons without *Tmem63b* puncta. scale

bars 50  $\mu\text{m}$ . **C:** *Tmem63b* expression measured by the percentage of tdTomato+ cells with a defined number of *in situ* hybridization puncta. Groups binned by the following levels, 0-1 puncta no expression (mean  $\pm$  SD %), 2-20 puncta medium expression (mean  $\pm$  SD %), 21-104 puncta high expression (mean  $\pm$  SD %). N = 3 animals per group. Chi-Square ( $p < 0.0001$   $\chi^2 = 22.76$ ,  $df = 2$ )..... 36

**Figure 2.6: Negative controls used to create threshold for ISH and IHC experiments. A:** Each tdTomato positive neuron's mean fluorescence from the *in situ* probes against *Tmem63b* and negative control probes across each section of DRG imaged for all three animals in the cohort. **B:** Same as above but *in situ* probe is for *Piezo2*. **C:** Mean fluorescence of HA antibody staining of TH positive DRG neurons in *Tmem63b*<sup>HA/HA</sup> vs *Tmem63b*<sup>WT/WT</sup>. Threshold made from the 99<sup>th</sup> percentile of mean fluorescence of HA staining from *Tmem63b*<sup>WT/WT</sup> DRG used as a cut off for *Tmem63b*<sup>HA/HA</sup> HA staining. Bars represent mean  $\pm$  S.D. .... 45

**Figure 3.1: Indentation responses of HEK P1KO cells expressing *Piezo2* alone or alongside *Tmem63b*. A:** Representative trace of indentation-induced currents at increasing forces in HEK P1KO cells overexpressing *Piezo2* (green) alone or co-expressing *Piezo2* and *Tmem63b* (purple). Black dots indicate the example trace's corresponding measurement. **B:** Maximum current response of increasing stimulation steps starting at the 1<sup>st</sup> responses until the cell popped, line mean response for each group (*Piezo2*; N=8, Co-express; N=10). **C:** Inactivation kinetics plotted on log<sub>10</sub> axis, line mean response for each group (*Piezo2*; N=8, Co-express; N=10). **D:** Steady state current taken as a percentage of the peak current, line mean response for each group (*Piezo2*; N=7, Co-express; N=9). Multiple unpaired t-test with Welch's correction. .... 52

**Figure 3.2: Repeated stimulation of HEK P1KO cells expressing *Piezo2* alone or alongside *Tmem63b*. A:** Representative trace of repeated indentation-induced currents in HEK P1KO cells overexpressing *Piezo2* (green) alone or co-expressing *Piezo2* and *Tmem63b* (Purple). Black outlines indicate the example trace's corresponding measurement. **B:** Maximum current response of the mean response after repeating the same indentation force (*Piezo2*;  $-1555 \pm 387.4$  pA, N=6, *Piezo2* & *Tmem63b*;  $-670.1 \pm 276.4$  pA, N=4, Unpaired t-test  $p = 0.004$ ). **C:** Inactivation kinetics plotted (*Piezo2*;  $13.3 \pm 8.2$  ms, N=6, *Piezo2* & *Tmem63b*;  $7.2 \pm 2.7$  ms, N=4, Unpaired t-test  $p = 0.2$ ). **D:** Steady state current taken as a percentage of the peak current (*Piezo2*;  $0.93 \pm 0.58$  %, N=6, *Piezo2* & *Tmem63b*;  $1.6 \pm 1.4$  %, N=4, Unpaired t-test  $p = 0.3$ ). Mean  $\pm$  S.D. .... 54

**Figure 3.3: Indentation responses of HEK P1KO cells expressing *Piezo2* alone or with *Tmem63b* at different voltages. A:** Representative trace of indentation-induced currents in HEK P1KO cells overexpressing *Piezo2* alone or co-expressing *Piezo2* and *Tmem63b* with voltage steps of 20 mV starting at -80 mV. **B:** Reversal potential calculated by a linear regression using the maximum current of the two sweeps where the polarity of the current flips (*Piezo2*;  $13.8 \pm 5.5$  pA N=6, *Piezo2* & *Tmem63b*;  $17.4 \pm 12.8$  pA, N=6, Unpaired t-test  $p = 0.5$ ). **C:** Maximum current response at each voltage step, line mean response for each group (*Piezo2*; N=6, *Piezo2* & *Tmem63b*; N=7). **C:** Inactivation kinetics plotted on log<sub>10</sub> axis, line mean response for each group (*Piezo2*; N=6, *Piezo2* & *Tmem63b*; N=7). **D:** Steady state current taken as a percentage of the peak current, line mean response for each group (*Piezo2*; N=6, *Piezo2* & *Tmem63b*; N=7). Mean  $\pm$  S.D. .... 55



**Figure 4.1: Stained sections of mouse hairy skin for neurons and TMEM63B.** **A:** HA and DAPI staining in skin sections from *Tmem63b<sup>wt</sup>* and *Tmem63b<sup>HA</sup>*. **B:** UCH-L1 marks something around hair follicles that overlaps with HA staining in *Tmem63b<sup>wt</sup>* and *Tmem63b<sup>HA</sup>*. **C:** Beta-Tubulin III stains neurons in the skin whereas UCH-L1 aligns with a subset of hair follicles. All scale bars are 50  $\mu$ m. .... 77

**Figure 4.2: Staining compared between skin sections and whole mount.** **A:** Skin sections with Beta-Tubulin III noted different in panel staining and auto-fluorescent hairs reveal neurons in the skin, Inset shows a lanceolate ending, specialized neuronal morphology that surround a hair. **B:** Same staining as **A** in whole mount skin shows each hair surrounded by multiple types of ending morphology in addition to free nerve endings. All scale bars 50 $\mu$ m. ... 78

**Figure 4.3: Whole mount skin staining for TMEM63B-HA channels has mixed results A-C:** Whole mount skin staining of mouse hairy skin. Left column: HA, TH, merged image of HA and TH channels, and overlap of HA and TH staining. Right column: TH-flip is a mirrored image of the TH channel, merged image of TH and TH-flip, merged image of HA and TH-Flip, and merge image of the overlap from the left column and the overlap-flip is the overlap of HA staining with the TH-flip channel. **A-B:** Representative images of whole mount skin from the same TMEM63B<sup>HA/HA</sup> mouse. **C:** Skin from a TMEM63B<sup>WT/WT</sup> mouse. **D:** Whole mount skin staining showing Top: Beta-Tubulin III staining and TH staining alone. Bottom: Merged image of Beta-Tubulin III and TH images, and the colocalization of the two antibody stains. ... 81

**Figure 4.4: Whole-cell indentation currents of C-LTMRs in *Piezo2<sup>fl</sup>* and *Tmem63b<sup>fl</sup>* & *Piezo2<sup>fl</sup>* and *in situ* hybridization showing *Piezo2<sup>fl</sup>*** **A:** Representative trace of indentation-induced whole-cell MA currents from *Piezo2<sup>wt</sup>* and *Piezo2<sup>fl</sup>* C-LTMRs. **D:** Maximum peak current. Green indicates the example trace's corresponding measurement (*Tmem63b<sup>wt</sup>*;  $-244.1 \pm 200.4$  pA, cells= 33 and animals= 6, *Piezo2<sup>fl</sup>*;  $-155.3 \pm 100.6$  pA, cells = 8 and animals = 1, *Tmem63b<sup>fl</sup>* & *Piezo2<sup>fl</sup>*;  $-355.7 \pm 241.7$  pA, cells = 10 and animals = 1). **E:** Inactivation kinetics plotted on log<sub>10</sub> axis (*Tmem63b<sup>wt</sup>*;  $154.7 \pm 149.4$  ms, cells= 32 and animals= 6, *Piezo2<sup>fl</sup>*;  $162.1 \pm 149.4$  ms, cells = 8 and animals = 1, *Tmem63b<sup>fl</sup>* & *Piezo2<sup>fl</sup>*;  $203.1 \pm 111.1$  ms, cells = 10 and animals = 1). **F:** Steady state current taken as a percentage of the peak current (*Tmem63b<sup>wt</sup>*;  $34.42 \pm 25.82$ , cells = 33 and animals = 6, *Piezo2<sup>fl</sup>*;  $58.45 \pm 17.69$ , cells = 8 and animals = 1, *Tmem63b<sup>fl</sup>* & *Piezo2<sup>fl</sup>*;  $61.6 \pm 10.2$  ms, cells = 10 and animals = 1). **E.** *In situ* hybridization staining of cultured DRG neurons from *Piezo2<sup>fl</sup>* mice with a probe against *Piezo2-Exon43-45* (blue) and natural tdTomato fluorescence (red). **F.** Mean fluorescence plotted on a log<sub>10</sub> axis of the ISH probe of every tdTomato+ cell in a *Piezo2<sup>wt</sup>* and *Peizo2<sup>fl</sup>* mouse. Threshold for a cell expressing *Piezo2* was based on the 99<sup>th</sup> percentile of mean fluorescence of a negative probe within tdTomato+ cells. .... 85

## **List of Appendices**

Appendix A: Skin Staining .....	75
Appendix B: <i>Piezo2</i> and <i>Tmem63b</i> double flox indentation induced currents in C-LTMRs.....	83

# Abbreviations:

calcium	Ca <sup>2+</sup>
c-fiber low threshold mechanoreceptors	C-LTMRs
conditional knock out	cKO
dithiothreitol	DTT
dorsal root ganglia	DRG
Dulbecco's Modified Eagle Medium	DMEM
haemagglutinin	HA
HEK293 <i>Piezol</i> KO	HEK P1KO
High-threshold mechanoreceptors	HTMRs
immunohistochemistry	IHC
<i>in situ</i> hybridization	ISH
intermediately adapting	IA
knocked down	KD
loss of function	LOF
low-threshold mechanoreceptors	LTMRs
mechanically activated	MA
neurofilament-200	Nf-200
Parvalbumin	PV
rapidly adapting	RA
slowly adapting	SA
trigeminal ganglion	TG
Tyrosine Hydroxylase	TH
ubiquitin carboxy-terminal hydrolase L1	UCH-L1
ultra slowly adapting	UA
<i>Vglut3<sup>Cre</sup>;Ai9;Tmem63b<sup>fl/fl</sup></i>	<i>Tmem63b<sup>fl</sup></i>
<i>Vglut3<sup>Cre</sup>;Ai9;Tmem63b<sup>wt/wt</sup></i>	<i>Tmem63b<sup>wt</sup></i>
<i>VGLUT3-IRES-Cre</i>	<i>Vglut3<sup>Cre</sup></i>
wildtype	WT

## Chapter 1 Introduction

**Mechanically activated** (MA) ion channels are membrane proteins that rapidly signal via current flow when force is applied to the cellular membrane. Responding to external force is one way animals use MA ion channels. By transducing force into neural signals MA ion channels give rise to sensations like hearing and touch. For a protein to be considered a bona fide MA ion channel, it must meet the criteria laid out for the mechanoelectrical transduction complex (MET) (Cunningham & Muller, 2019). First, the protein must be expressed in the cell type responsible for a given sensation. Second, the protein must be required for MA responses in the cell type of interest. Third, mutations/modifications to the protein should result in changes to the MA current response. And fourth, expressing the MA ion channel in a previously mechanically insensitive cell or lipid bilayer should imbue that membrane with MA responses. This thesis uses these criteria to assess TMEM63B as a mechanosensor for noxious stimuli in dorsal root ganglion (DRG) neurons.

### 1.1 MA ion channels and their role in biology

The gating of MA ion channels is a unique biological property that is currently not fully understood. There are two prevailing hypotheses for ways by which forces exerted on the membrane activates MA ion channels; force-from-lipid and force-from-filament (Cox *et al.*, 2019). The two major methods used in this thesis to activate MA channels with force are thought to disentangle the two proposed activation mechanism to some extent. First is stretching the cellular membrane in cell-attached or outside out patch-clamp mode, which is thought to

distend/thin the lipid membrane (**Figure 1.1A-B**). Second is indenting the cellular membrane with blunt glass probe, which applies tension between cytoskeletal elements and the membrane, but likely also causes stretching of the plasma membrane (**Figure 1.1C**). These two methods are the primary way to elicit currents from MA ion channels.

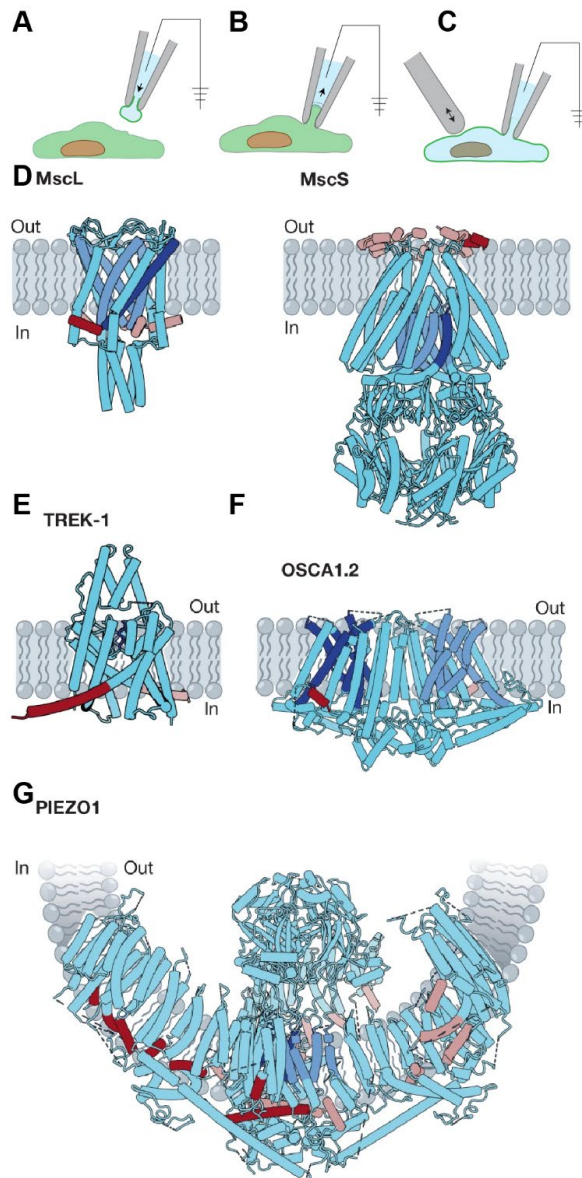


**Figure 1.1: Methods to stimulate and structures of known MA ion channels.** **A:** Outside out patch-clamp mode can induce stretch forces on the membrane by applying positive pressure to the pipette **B:** Cell attached patch-clamp mode can induce stretch forces on the membrane by applying negative pressure to the pipette **C:** In whole cell patch-clamp mode, indenting the cell with a blunt glass probe using a piezo-electric motor, can induce indentation forces. **D-G:** Structures of MA ion channels with amphipathic helices highlighted in red and pore lining helices in dark blue. **D:** Bacterial mechanosensitive channel large conductance (MscL) and small conductance (MscS). **E:** TREK-1 ion channel. **F:** OSCA1.2 ion channel. **G:** PIEZO1 ion channel. Cartoon patches were created by Dr. Swetha Murthy, Structure figures adapted from Kefauver *et al.*, 2020.

Activation by force-from-lipid is what makes a MA channel bona fide because no auxiliary cellular components are needed to gate the channel. There are structural models that suggest amphipathic helices, highlighted in red (**Figure 1.1D-G**), gate the channels using the

force-from-lipid, by allowing MA ion channels to interact with the surrounding lipids to sense membrane stretch/thinning (Kefauver *et al.*, 2020). All the channels depicted in **Figure 1.1** exhibit MA currents in proteoliposomes, a system where channels are reconstituted in pure lipid vesicles or bilayers. Thus, fulfilling the criteria laid out in Cunningham & Muller 2019 that for the channel to be inherently mechanosensitive, it must imbue a previously inert membrane with mechanosensitive properties.

Activation by force-from-filament is more nuanced among the different MA channels, but a good example is the Mechanoelectrical transduction (MET) complex in hair cells of the inner ear. The two pore-forming proteins, TMC1 and TMC2, are the essential ion channel components of the MET complex. To confirm that TMC1 is indeed the pore-forming subunit of the MET complex, researchers used homology modeling to the TMEM16A structure to identify pore lining residues, which when mutation and expressed in hair cells, altered the MET complex's MA currents (Ballesteros *et al.*, 2018; Pan *et al.*, 2018). However, the TMCs alone do not fit all the criteria laid out by Cunningham & Muller, 2019 because reconstitution of TMC1/2 proteins in lipid bilayer does not induce MA currents. Rather, TMC1/2 require several other proteins that form the MET complex at the tip of hair cells to generate a MA current (Pan *et al.*, 2018; Cunningham & Muller, 2019). Together the complex tether TMC1/2 to the tip links of stereocilia in hair cells. When sound waves deflect the stereocilia, the complex is stretched pulling open TMC1/2, thus causing activation by force-from-filament.

### **1.1.1 MA ion channels are used for cellular function.**

MA ion channels are fundamental to sensing external stimuli that give rise to sensations like touch and hearing in animals, but these proteins are also used to regulate basic cellular health and neuronal excitability. Using the criteria and methods outlined above only a handful of

channel families meet all the criteria of an MA channel. Shown in **Figure 1.1D-G** are representative structures of major channel families. MA ion channels within these families serve a variety of roles, including but not limited to, sensory perception in eukaryotic and prokaryotic organisms.

The mechanosensitive channels (Msc) found in prokaryotes were the first MA ion channel families identified (Sukharev *et al.*, 1993; Berrier *et al.*, 1996). These channels are named after their conductance; MscL channels have a large conductance and MscS channels have a small conductance (Kloda & Martinac, 2002). Early electrophysiological studies found evidence of multiple conductance states with non-inactivating responses to stretch stimulation in *Escherichia coli* (Sukharev *et al.*, 1993). These channels are responsible for maintaining cell health by relieving dangerously high pressure induced by cell swelling during osmotic shock. MscL and MscS do not inactivate so the channels stay open in the presence of osmotic shock, allowing osmolytes to escape the cell and close once the cellular pressure returns to safe levels. (Kloda & Martinac, 2002). Further studies discovered MscS-like proteins in plants, which were homologous to MscS channels in prokaryotes (Haswell & Meyerowitz, 2006). MSL2 and MSL3 are localized to the plastid organelle within plant cells and regulate its size and shape. Loss of these channels leads disfunction in these organelles and variegated leaves. These experiments show that MscS and MscL play role in maintaining the cell health of bacteria and plant cells. In addition to maintaining cellular health, plants repurposed some members of the Msc-like channels for sensing external mechanical stimuli. For example, the carnivorous Venus fly trap plants use FlyCatcher, an MA ion channel homologous to MSLs, at the base of their sensory organ to initiate the mechanically-induced prey-capture response (Procko *et al.*, 2021; Jojoa-

Cruz *et al.*, 2022). This is a good demonstration how different organisms can utilize MA ion channels for both external and internal forces.

Certain members of the two-pore potassium family (K2P) are MA and here I will focus on the role of MA K2P channels in neurons of the central and peripheral nervous system (Kefauver *et al.*, 2020). These channels were the first MA ion channel identified in mammals (Honore *et al.*, 2006). TREK-1(**Figure 1.1**), TREK-2, and TRAAK belong to the K2P family and are selective for potassium and can produce MA currents when reconstructed in a liposomes, suggesting that they are gated by force (Honore *et al.*, 2006; Enyedi & Czirjak, 2010; Brohawn *et al.*, 2014). Force is only one of many stimuli that activate this sub-family, and other activators include pH, temperature, voltage and many intracellular signaling molecules. Their roles are diverse and not always centered around their ability to respond to force. For example, at rest, these channels provide leak current to central and peripheral neurons that contribute to the resting membrane potential and therefore control neuronal excitability (Enyedi & Czirjak, 2010). The role of a leak channel may appear passive, but TRAAK channels localized to the nodes of Ranvier in mammals and are required for proper action potential propagation (Brohawn *et al.*, 2019). Additionally, TREK-1 and TRAAK exhibit both temperature and mechano-sensitivity as behavioral experiments show that global knockout of *Kcnk1* and *Kcnk4* (the genes that encode TREK-1/TRAAK/TREK-2) lowers the force and temperature response threshold in mice (Noel *et al.*, 2009). Even though this thesis focused on understanding how MA ion channels are used to sense external force in DRG neurons these ion channels have importance to cells beyond external force detection and the MA channels discussed could play roles in other sensory or regulatory processes.



## 1.2 Somatosensory neurons of the dorsal root ganglion

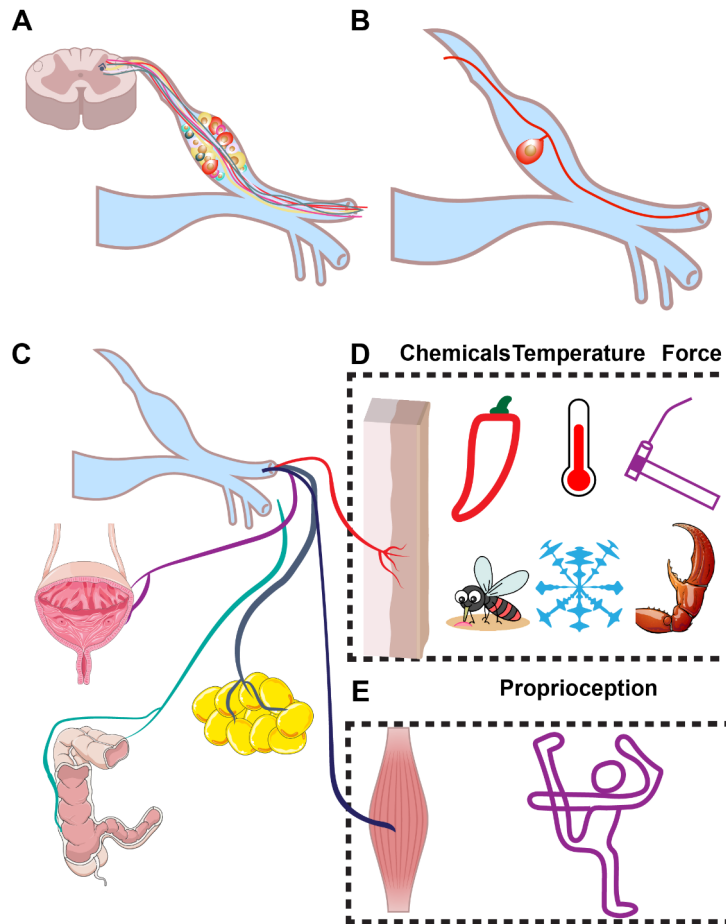


**Figure 1.2: Dorsal root ganglion anatomy and function.** **A:** The dorsal root ganglion (DRG) is composed of many neurons that send axons, which synapse on interneurons in the spinal cord. **B:** Neurons within the DRG have a T-shaped axon that sprouts from the cell body, one end projects to the spinal cord and the other to the periphery. **C:** The targets of DRG neurons include, but not limited to, bladder, colon, adipose tissue, skin, and muscle. **D:** The role of DRG neurons in the skin is to sense chemicals from plants and animals, temperature, and force. **E:** DRG neurons in the muscle sense stretch giving rise to proprioception. Cartoons made by: DBCLS spinal-cord, DBCLS sensory neuron, Servier bladder, Servier, adipocyte, Servier colon, Attendance Cute Mosquito, Kehan Thermometer, Namu Lobster.

DRG neurons serve as sensors for the peripheral nervous system and respond to various stimuli due to the expression of distinct molecular sensors—including ion channels—which are activated by chemicals, temperature, and mechanical force (**Figure 1.2D**). Their activation gives rise to explicit sensations like warmth or implicit phenomena like proprioception. DRG neurons are pseudo-unipolar; their cell bodies reside in the ganglia and they grow a T-shaped axon with one end of the axon projecting to a sensory target like skin, gut, bladder, or adipose tissue and the other end to the spinal cord (**Figure 1.2A-C**). (Stoney, 1990; Marshall *et al.*, 2020; Meltzer *et al.*, 2021; Wang *et al.*, 2022; Servin-Vences *et al.*, 2023). This thesis will focus on DRG neurons that target the skin or structures in the skin, like hair follicles, and examines how these neurons can encode mechanical stimuli (Li *et al.*, 2011; Abaira & Ginty, 2013b).

The way molecular sensors function in the somatosensory system is well illustrated by TRP ion channels, which serve as polymodal temperature and chemical sensors. When a neuron reaches a certain temperature, TRP channels activate, depolarizing the neuron and inducing action potentials. These TRP channel-initiated signals are how animals sense thermal stimuli, and the loss of a single TRP channel alters a mouse's preference for floor temperature (Caterina *et al.*, 1997; Lee *et al.*, 2005). TRP channels are activated by temperatures ranging from 17-52°C (Vay *et al.*, 2012). Instead of each member of the TRP channel family having a unique activation temperature, many TRP channels share the same activation range (Tominaga, 2007), suggesting redundancy and presenting a challenge for understanding how the nervous system deploys TRPs to encode a spectrum of temperatures. An example of redundancy is that three different TRP channels, TRPA1, TRPV1, and TRPV3, are independently necessary and sufficient to sense noxious burns (45°C) (Vandewauw *et al.*, 2018); however, sensations like warmth (42°C) are not carried by a single sensor. Warmth is mediated by the activation of DRG neurons expressing warm/hot TRP channels and the suppression of DRG neurons expressing the cool activated *Trpm8* (Paricio-Montesinos *et al.*, 2020). So, rather than simple channel dynamics, some sensations are brought about by the combination of responses from different subtypes of DRG neurons.

### ***1.2.1 High-threshold and low-threshold mechanoreceptors (HTMRs and LTMRs)***

One prominent feature shared by many, but not all, DRG neurons is the ability to respond to force. As with thermosensory neurons, mechanoreceptors have unique characteristics that limit what they encode. A major distinction between types of mechanoreceptors is the intensity of force that causes their activation. Neurons that respond to high threshold force encode painful stimuli like pinch and these neurons are called nociceptors (Delmas *et al.*, 2011b; Abraira &

Ginty, 2013a). Within these nociceptors are molecular and cellular distinctions that differentiate the information they relay to the spinal cord. This form of engineered redundancy also supplies spatiotemporal information to the central nervous system. The A-delta neurons are myelinated high-threshold mechanoreceptors (HTMRs), and C-fiber-HTMRs are unmyelinated (Basbaum *et al.*, 2009). The fast conduction allows A-delta-HTMRs to send rapid sharp sensations of pain and the slow-C-HTMRs send dull aching pain. The other major class of mechanoreceptors respond to low threshold force. There are more types of low-threshold mechanoreceptors (LTMRs) compared to HTMRs, so most research in the somatosensory field has focused on characterizing the functional and morphological differences between LTMR subtypes.

Early recordings and immunostaining experiments led to the identification of unique properties that differentiated the LTMR neuronal subtypes (Horch *et al.*, 1977). Researchers classified mechanoreceptor subtypes based on their conduction velocity, distinct axonal morphology or nerve ending patterns, action potential pattern, and preferred type of physical stimulus. These functional studies, paired with immunohistology, revealed how underlying cellular features give rise to unique response properties. For example, the extent of myelination governs the speed of action potential propagation, and neuronal ending morphologies govern distinct neuronal receptive fields and determine the type of physical stimulus encoded (Burgess *et al.*, 1968). Early research characterized the response profiles based on ending morphology, like finding that neurons that interact with Pacinian corpuscles respond to vibration (Sato, 1961). However, researchers lacked a true molecular understanding of LTMR subtypes, which prevented them from determining how molecular differences within these subtypes led to their unique development and function.

Researchers in the 2000's began to parse the relationship between molecular differences, and development and function by using *Cre*-lines. This allowed them to visualize receptive fields and probe molecules crucial for developmental signaling. With the advent of *Cre*-lines and inducible *Cre*<sup>ERT2</sup> researchers could use expression pattern throughout development to identify certain subpopulations (Feil *et al.*, 1997). One such study showed that early *Ret* expressing neurons comprised multiple types of mechanoreceptors that projected to specialized end organs in skin, Meissner corpuscles, Pacinian corpuscles and lanceolate endings (Luo *et al.*, 2009). Generating a cKO within these neurons showed *Ret* signaling was required for proper development of axonal projections to Pacinian corpuscles, in the skin as well as targets in the spinal cord. A similar study focusing on C-fibers that formed lanceolate ending on hairs found that Runx-1 signaling was needed for proper development of these ending morphologies (Lou *et al.*, 2013). These studies demonstrated that the *Cre-lox* system was crucial for understanding how certain proteins function within specific subtypes of DRG neurons.

*Cre*-lines, in combination with a GFP knock-in line, allowed researchers to perform a detailed characterization LTMRs like C-LTMRs, A $\delta$ -LTMRs, and A $\beta$  RA-LTMR, leading to a complete catalog of the innervation pattern of hair follicles in mouse hairy skin (Li *et al.*, 2011). This study was able to distinguish neurons that formed circumferential endings that wrap around hairs from lanceolate endings neuronal protrusions up the hair. The sparse labeling using *Cre*<sup>ERT2</sup> allowed for visualization of an individual neuron's receptive field, which became a standard in the field. The characterization of these LTMR subtypes was instrumental in demonstrating the receptive field of these neuronal subtypes and guided research into what these subtypes encoded.

Single cell RNA sequencing accelerated the ability to identify molecular markers for all DRG subtypes and lead to the development of transgenic *Cre* mouse lines, designed to label each

DRG subtype (Usoskin *et al.*, 2015; Sharma *et al.*, 2020). The work of Qi *et al.*, 2024, used 14 *Cre*-lines, guided by single cell sequencing data, to represent non-overlapping molecular subtypes. These *Cre* lines enabled Qi *et al.*, 2024 to catalog each subtype's axon, the ending morphology in the skin, and which lamina the efferent targets in the spinal cord. They imaged *in vivo* calcium ( $\text{Ca}^{2+}$ ) activity to record responses to punctate stimuli at discrete forces, mechanical stimuli like pinching or brushing, and a range of temperatures.

Experiments previously mentioned had done these studies to some extent, but the ability to compare each subtype's response profile allowed for a more complete interpretation. One example is the neurons labeled by Mas-related G-protein coupled receptors (*Mrgprd*), which were one of the first subtypes to be the focus of an *in vivo* calcium imaging study (Vrontou *et al.*, 2013). In Vrontou *et al.*, 2013 researchers noted that these C-fibers had dense bushy arbors on hairy skin and claimed that these neurons were responsive to paint brush stroking. They concluded that these C-fibers were analogous to CT neurons in humans that are responsible for the affective feeling of gentle stroking (Loken *et al.*, 2009). In Qi *et al.*, 2024 they found that MRGPRD+ neurons indeed have dense bushy arbors in the skin, but their response to stroking is muted compared to other neurons such as C-LTMRs, which are now accepted as the analogous subtype to human CT cells. It is still possible that the MRGPRD+ neurons could convey affective information to the downstream spinal cord neurons, but based on the response profile in Qi *et al.*, 2024 these neurons would be less reliable compared to C-LTMRs. The data set in Qi *et al.*, 2024 allows for at least two avenues of research. First is understanding how the responses characterized in Qi *et al.*, 2024 are encoded by the downstream neurons in the spinal cord. Second, which this thesis aims to do, is to investigate the molecules that generate diversity in function, including activation in response to force.

### 1.3 Mechanically activated ion channels in DRG neurons: the search

Attempts to identify molecular sensor(s) of force occurred in parallel to the subtype characterization studies described in the previous section. How DRG neurons generate action potentials in response to force was a research question many labs have attempted to answer. A primary question was: do the neurons have MA ion channels like thermosensory neurons have TRP channels, or do the neurons form synapses onto specialized mechanosensory cells in the skin as is the case in hair cells in the ear? In the inner ear the neurons are not responsible for transducing the mechanical signal into electrical impulses. Instead, the mechanosensitive hair cells, mentioned previously, convert sound waves into electrical activity to drive neurotransmitter release on to spiral ganglion neurons (Glowatzki & Fuchs, 2002). It is possible a similar mechanism could exist for touch where specialized skin cells stimulate DRG neurons. Another question was how do ion channels open in response to mechanical stimulation in the skin? As mentioned before, TMC1/2 in hair cells require auxiliary proteins to form the MET complex that connect to tip links to pull open the ion channel. Is this mechanism conserved in the skin, or do touch MA ion channels operate alone?

To answer if neurons in the DRG are inherently mechanosensitive, recordings of indentation-induced currents were done on the cell bodies of dissociated DRG neuronal cultures (**Figure 1.3A**). These recordings demonstrated for the first time that DRG neurons themselves are intrinsically mechanosensitive, and likely express an unknown MA ion channel (McCarter *et al.*, 1999). In an effort to further characterize the MA currents of DRG neurons a follow-up study recorded from 110 MA DRG neurons and found that the inactivation of the MA current could be classified into four categories based on the Tau of their inactivation kinetics,  $\tau < 10\text{ms}$  rapidly adapting (RA),  $10\text{ms} < \tau < 30\text{ms}$  intermediately adapting (IA),  $30\text{ms} < \tau < 100\text{ms}$  slowly adapting (SA), and  $> 100\text{ms}$   $\tau$  ultra slowly adapting (UA) (**Figure 1.3B**) (Hao & Delmas, 2010). At the

time no known MA ion channels were identified in these neurons, so hypotheses emerged that these distinct MA currents were the result of distinct MA ion channels or unique combinations of MA ion channels.

### 1.3.1 PIEZO ion channel family: *PIEZO2*, the low-threshold mechanosensor.

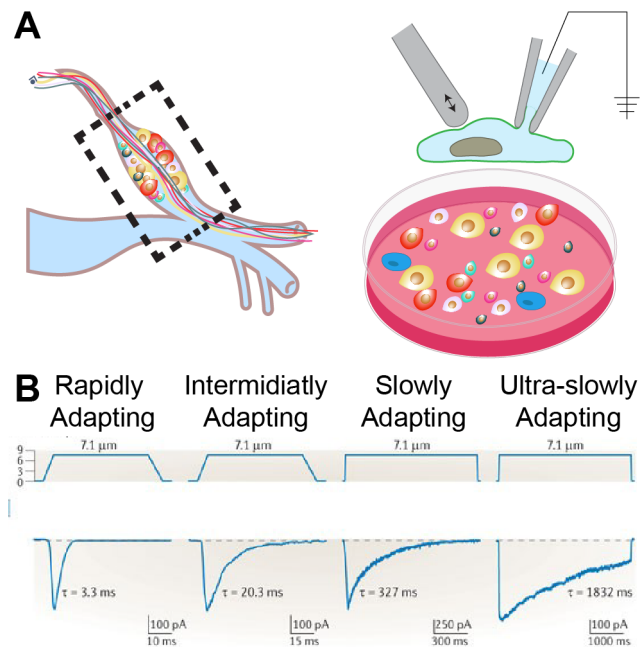


**Figure 1.3: Dissociated DRG neurons produce indentation-induced MA currents with distinct inactivation times.**

**A:** DRG neurons are dissected out of mice and the cell bodies are dissociated and cultured for the purpose of whole cell patch-clamp indentation recordings. **B:** Whole cell indentation recordings produce four different types of currents based on the inactivation kinetics. Figure adapted from Delmas *et al.*, 2011. Cartoons made by Dr. Swetha Murthy, DBCLS spinal-cord, DBCLS sensory neuron, Marcel Tisch Stem cell.

The molecular sensor for touch in mammals remained a mystery until the discovery of the PIEZO ion channel family. Upon the discovery of MA current in DRG neurons, researchers examined known ion channels from the DEG/ENaC, TRP, and KCNK families, but none of these channels served as a molecular sensor for touch in mammals (Basbaum *et al.*, 2009). To identify the PIEZO family, two screens were performed. First, mouse and rat cell lines (Neuro2A, C2C12, NIH/3T3, Min-6, 50B11, F11, and PC12) were screened to identify a cell line with indentation-induced MA current that matched DRG neuronal MA currents. Among the cell lines tested, Neuro2A cells had consistent MA currents with fast inactivation (called adaptation at the time). Using an Affymetrix microarray to identify genes upregulated in Neuro2A cells, a list of genes was developed. These genes encoded for proteins that were predicted to have

multiple transmembrane helices. To screen for the gene that was responsible for the endogenous MA current in Neuro2A cells, each candidate gene was systematically knocked down using siRNA and indentation-induced MA currents were recorded to determine a reduction in MA currents. One hit resulted from the screen in Neuro2A cells, *Fam38a*, later named *Piezo1*. Identification of the *Piezo1* gene lead researchers to its only other family member in mammals, *Piezo2* (*Fam38b*). Overexpression of *Piezo1* or *Piezo2* in non-mechanosensitive Human Embryonic Kidney 293T cells produced robust indentation-induced currents, making them *bona fide* MA ion channels.

The primary goal shifted to investigate if a member of the PIEZO family was a molecular sensor for touch by examining their contribution to MA currents in DRG neurons (Coste *et al.*, 2010). Initial studies showed that *Piezo2* is broadly expressed across many types of DRG neurons, and *Piezo1* is limited to a small percentage of DRG neurons initially dismissed as background in *in situ* hybridization (ISH) staining (Coste *et al.*, 2010; Ranade *et al.*, 2014). A later study revisited *Piezo1*, showing it is expressed in a subtype of DRG neurons and is only responsible for mechanical itch (Hill *et al.*, 2022). To understand PIEZO2's contribution to MA currents in DRG neurons, Coste *et al.*, 2010 and Ranade *et al.*, 2014 recorded MA currents from DRG neurons with either a knocked down (KD) or a conditional knock out (cKO) of *Piezo2* using siRNA and the *Cre-lox* system, respectively. These studies yielded complementary results: more DRG neurons had no MA currents, and fewer DRG neurons had RA currents, suggesting that PIEZO2 was responsible for RA currents in DRG neurons. Later, a study used *Hoxb8-Cre* to drive a more complete cKO of *Piezo2* (Murthy *et al.*, 2018b). *Hoxb8* is a patterning gene that turns on early in embryo development and drives *Cre* expression in the thoracic and lumbar segments of the embryo (Witschi *et al.*, 2010). Complete *Piezo2* cKO within lumbar DRG



showed that IA and RA currents were reduced (Murthy *et al.*, 2018b). These studies established that PIEZO2 is responsible for the RA and some IA currents in cultured neurons but were blind to important subtype information that would have hinted at what types of external forces PIEZO2 responds to. To understand PIEZO2's role in somatosensation, researchers have used behavioral assays of touch.

### **1.3.2 PIEZO2's role in touch, interoception, and proprioception**

The von Frey assay was the first method that showed PIEZO2 is the molecular sensory for low threshold touch (Ranade *et al.*, 2014). The assay asks what the is the minimum amount of force required to stimulate the conscious sensation of touch. The original von Frey assay used hair from different animals that would be woven together and recalibrated before each trial. The assay was adapted and standardized by Semmes and Weinstein (the first prototype was kept in an *El paso Cigars: The Cowboy's Payday Smoke box*) (Weinstein, 1993; Bradman *et al.*, 2015). The modern version uses a set of 20 nylon monofilaments; each filament can apply a discrete amount of force to the skin (in the case of the mouse a resting hind paw is the target). When a von Frey filament reaches its force target it bends preventing more force from being applied and informing the researcher that trial is complete. Ranade *et al.*, 2014 was the first study to deploy this test on *Piezo2* cKO mouse. Researchers showed that wildtype (WT) mice started responding to 1g of force, but *Piezo2* cKO mice did not respond until the 2.5g filament (Ranade *et al.*, 2014). This experiment demonstrated that in addition to PIEZO2 changing currents in cultured DRGs, PIEZO2 was a molecular sensor for low-threshold external force *in vivo*. This small change in threshold was a monumental step forward in somatosensory neuroscience as it was the first indication of a molecular sensor for touch in mice.

It was not known if PIEZO2 was a sensor for touch in humans until researchers identified rare cases of people who have loss-of-function (LOF) mutations in the *PIEZO2* gene, which results in diminished PIEZO2 activity. Chesler *et al.*, 2016 was the first study to identify humans with LOF mutations in *PIEZO2*. Two unrelated patients had undiagnosed disorders that were categorized as neuromuscular, but their phenotypes were similar and matched predicted PIEZO2 deficits. For this reason, the patients underwent whole exome sequencing, which revealed LOF mutations in the *PIEZO2* gene. These patients then volunteered for mechanosensory-specific assays that showed they had a loss in perception of low-threshold mechanical force on the skin, replicating the mouse findings. The individuals have a high threshold for punctate force and cannot feel vibrations of any frequency (Chesler *et al.*, 2016). Patients with LOF mutations in *PIEZO2* were given the diagnosis of PIEZO2-deficiency syndrome, and phenotyping confirmed that PIEZO2 is the sensor for low threshold force in mice and humans.

Furthermore, PIEZO2 is a pain sensor in mice and humans only in the case of mechanical allodynia (Murthy *et al.*, 2018b; Szczot *et al.*, 2018). Mechanical allodynia is when light touch is perceived as painful and occurs when the skin is inflamed by damage from an injury or sunburn, or after chemical irritants are applied to the skin like capsaicin. Murthy *et al.*, 2018b showed that nerve injury or application of capsaicin to the skin lowered the mechanical response threshold for WT mice but not *Piezo2* cKO mice. In patients with PIEZO2-deficiency syndrome capsaicin applied to a small section of their forearm elicited an inflammation response, measured by elevated skin temperature, but did not result in increased sensitivity to touch in that area (Szczot *et al.*, 2018). This showed that PIEZO2 is the sensor for mechanical allodynia in mice and humans and provided further evidence that painful sensations are mediated by multiple intersecting mechanical sensors.

Because DRG neurons also innervate certain internal organs, loss of PIEZO2 causes deficits in interoception, the sensations brought about by internal organs (**Figure 1.2C**). People with PIEZO2-deficiency syndrome could not sense bladder fullness and therefore set timers for urination. Staining in mice showed that both the DRG neurons that innervate the bladder and urothelial cells of the bladder express *Piezo2* (Marshall *et al.*, 2020). cKO of *Piezo2* in DRG neurons innervating the bladder led to altered urination behavior in mice. The cKO mice had less coordinated bladder contractions when a balloon inserted into the bladder was filled, simulating bladder fullness (Marshall *et al.*, 2020). PIEZO2 also functions as a sensor for interoception in the gut. PIEZO2-deficiency syndrome patients have sensory and gastrointestinal-related symptoms, meaning that PIEZO2 provides sensory feedback before and during bowel movements and supports proper gut function (Servin-Vences *et al.*, 2023). Mice with *Piezo2* cKO in DRG neurons had more frequent and smaller stools. cKO of *Piezo2* in other cell types involved in digestion like the nodose ganglion, peripheral neurons that innervate the gut, and gastrointestinal epithelial cells did not affect gut motility in any way (Servin-Vences *et al.*, 2023). These studies demonstrate that DRG neurons use PIEZO2 for interoception in the bladder and gut. These discoveries moved the field to focus more on the DRG's role in interoception, in addition to studying DRG's role in encoding external stimuli.

Proprioceptors are a subtype of DRG neuron that project to the skeletal muscle of the body and provide implicit signals to the central nervous system that give rise to proprioception, the ability to sense one's limbs in space (**Figure 1.2E**) (Tuthill & Azim, 2018). Mice and humans with LOF of PIEZO2 lose proprioception because PIEZO2 acts as the sensor for muscle stretching in proprioceptor neurons (Woo *et al.*, 2015; Chesler *et al.*, 2016). People learn to compensate with their vision, but they cannot walk in a balanced straight line if they close their

eyes. In cases of gain-of-function mutations in PIEZO2, the channel's overactivity within proprioceptor neurons accounted for the patients' skeletal symptoms of scoliosis and arthrogryposis (Coste *et al.*, 2013; Chesler *et al.*, 2016; Delle Vedove *et al.*, 2016; Ma *et al.*, 2023). PIEZO2 is a keystone protein for many functions in somatosensation and interoception, but these studies also revealed somatosensory phenomena that are independent of PIEZO2.

### ***1.3.3 What is beyond PIEZO2?***

Not all sensations are lost in patients with PIEZO2 deficiency or in *Piezo2* cKO mice. Perception of temperature and chemicals endure, which may seem obvious because these require other molecular sensors, but it demonstrates that DRG neurons are intact and functional in the absence of PIEZO2 (Ranade *et al.*, 2014; Chesler *et al.*, 2016). Notably, some mechanosensation remains in the absence of PIEZO2. Patients still sense deep pressure and painful high-threshold mechanical stimuli, which aligns with electrophysiological recordings of cultured DRG neurons that show roughly 50% of MA currents were unaffected by cKO of *Piezo2*. This indicates that there are additional MA ion channel(s) responsible for sensing noxious touch. My goal is to try to find a population of neurons with a non-PIEZO2 dependent response to force and test if a known MA ion channel TMEM63B initiates that response to force.

#### ***1.3.3.1 MA currents of specific subtypes in culture.***

Other research has attempted to identify non-PIEZO MA ion channels in DRG neurons. One group used a patch-sequencing approach whereby researchers recorded MA currents from individual cultured DRG neurons, to measure the neuron's type of inactivation. Then they collected the cytoplasmic content of those neurons to sequence the mRNA (Parpaite *et al.*, 2021). They repeated this for 56 neurons. By using the expression profile of molecular markers within a neuron they identified the subtype of a neuron and then matched that with the type of current

inactivation. A limitation in the Parpaite *et al.*, 2021 study is that DRG subtypes are not evenly represented. For example, only two C-LTMRs were reported, making it unlikely any relevant data can be extracted from that subtype. An unresolved question is whether sequencing the genes from all these MA neurons revealed any unidentified MA ion channels. The authors of Parpaite *et al.*, 2021 highlighted a list of protein candidates that were enriched in MA neurons and had no known function. However, there have been no publications so far showing any of these proteins are MA ion channels. Regarding known MA ion channels, no MA ion channel besides PIEZO2 was enriched in any neurons with specific inactivation properties. This analysis also showed that PIEZO2 is expressed in cells with non-RA currents (note that expressed and enriched are different). This study reaffirmed that PIEZO2 is enriched in RA neurons. However no other MA ion channel including TMEM63B was enriched in the cells they recorded from and sequenced, so this data set did not identify a subtype to focus on.

Studies that record MA current in cultured DRG neurons rarely identify the subtypes that were recorded, leading to a lack of information about how every subtype responds to mechanical force. Another study identifying subtypes with MA currents used *Cre*-lines to mark subtypes specifically (Zheng *et al.*, 2019). This design limited the scope of the study to established *Cre*-lines at the time of the experiments, and most of the neuronal subtypes in Zheng *et al.*, 2019 have high *Piezo2* expression according to single cell RNA sequencing (Sharma *et al.*, 2020). The MA current recordings showed all LTMR subtypes besides C-LTMRs have rapidly inactivating MA responses, which could indicate something unique about the C-LTMR population (Zheng *et al.*, 2019). It should be noted that this experiment also recorded other properties like AP width and rheobase, but because they did not record from a broad range of cell types, future research cannot

rely on these properties alone to identify cells. Specific *Cre*-lines are still needed to focus on certain DRG subtypes.

#### ***1.3.3.2 Population recordings from DRG neurons.***

By recording responses from many neurons simultaneously, identifying subtypes that have PIEZO2 independent responses to force became feasible. These experiments were made possible by advances in *in vivo* recording technology such as silicone probes with high density multielectrode arrays for extracellular recordings, or advances in GCaMP for Ca<sup>2+</sup> imaging (Royer *et al.*, 2010; Chen *et al.*, 2013). Neuronexus probes placed in the spinal cord of a mouse recorded the responses of dorsal horn neurons encoding poke or pinch stimuli *in vivo* (Chirila *et al.*, 2022). Many spinal cord neurons encode poke at low and high threshold forces. When *Piezo2* was cKO in all DRG neurons, the dorsal horn spinal cord neurons no longer responded to poke stimuli but responded to pinch, showing that some DRG neurons can still respond to high-threshold stimuli. However, in this study they only recorded the downstream neurons in the spinal cord, which means it is unknown what DRG neuronal subtypes carry that pinch stimulation into the spinal cord. Studies have used Neuronexus probes or other high density silicone probes to record many DRG neurons *in vivo*, by placing the probe into the ganglia or leaving it on the surface. (Kashkoush *et al.*, 2019). However, *in vivo* electrophysiology in the DRG yields 30-40 neurons per animal, and the identification of subtypes requires *Cre*-dependent optogenetic manipulation or *post-hoc* analysis of functional characteristics (Kashkoush *et al.*, 2019; Chirila *et al.*, 2022). Suggesting that many of the neurons recorded are not the subtype of interest. These limitations make multi-electrode electrophysiology a poor method for identifying subtypes with PIEZO2 independent activity but is a useful method for recording DRG activity *in vivo*.

*In vivo* imaging using GCaMP can record the activity of hundreds of sensory neurons at once and allows for *post-hoc* identification of subtypes (Chen *et al.*, 2013; Ghitani *et al.*, 2017). Imaging neurons generates a picture of where each neuron is in space and can be aligned with images that are stained post-mortem for molecular subtype markers using *in situ* hybridization (ISH) (Nguyen *et al.*, 2021; Von Buchholtz *et al.*, 2021). The most impactful imaging experiments that guided the work in this thesis were conducted on the trigeminal ganglion (TG) where researchers identified subtypes that retain their response to mechanical stimuli in the absence of PIEZO2 (Von Buchholtz *et al.*, 2021). TG neurons and DRG neurons share the same breakdown of functional/molecular subtypes, with the only major difference being that TG exclusively sends projections to the head and face, whereas projections from DRG neurons innervate skin all over the body (Le Pichon & Chesler, 2014; Bhuiyan *et al.*, 2023). TG neurons present advantages for imaging studies compared to DRG neurons. TG has a greater number of neurons and can be imaged more easily because it is in the skull underneath the brain, and the skull is relatively easy to stabilize compared to DRGs located near the spine. Researchers in Von Buchholtz *et al.*, 2021 recorded TG neurons in WT mice and *Piezo2* cKO mice and stimulated the face of these mice with gentle vibration and brush stimuli, and noxious stimuli like pinch or hair pull. After recording the neuronal activity, they identified each neuron's molecular identity with ISH, which allowed them to look at all the subtype responses to force with and without PIEZO2. C-LTMRs stood out as a subtype that had responses to gentle and noxious stimuli in WT mice, but only response to noxious stimuli in *Piezo2* cKO mice.

C-LTMRs have presented as an outlier in a few experiments discussed above and could be a subtype that utilizes TMEM63B and PIEZO2 to respond to force. In culture, C-LTMRs have a slowly inactivating MA response (Zheng *et al.*, 2019). Because there were only two C-

LTMRs in the patch-sequencing experiment the lack of *Tmem63b* enrichment in these neurons can be dismissed because of insufficient data (Parpaite *et al.*, 2021). The most impactful result was from von Buchholtz *et al.*, 2023, in *Piezo2* cKO mice, C-LTMRs lost their response to gentle vibration, but still responded to noxious stimuli. Thus, C-LTMRs have additional mechanisms by which they respond to noxious force, and are a good candidate to look for the noxious MA ion channel.

#### 1.4 TMEM63B in C-LTMRs

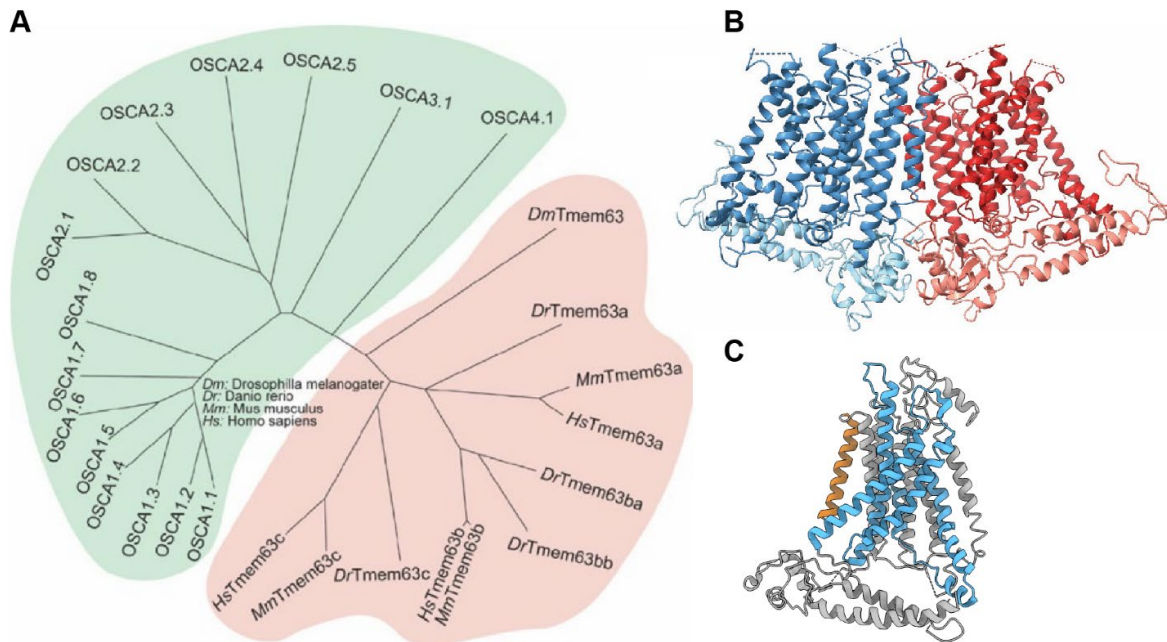


**Figure 1.4: The OSCA/TMEM63 are a family of MA ion channels.** **A:** Phylogenetic tree demonstrating sequence relationships of OSCA and TMEM63 family members. Sequences were aligned using MegAlign Pro and DrawTree created the plot. **B:** OSCA1.2 structure displayed with both subunits highlighted, PDB: 6MGV (Jojoa-Cruz *et al.*, 2018). **C:** Human TMEM63A transmembrane pore helices highlighted in blue, PDB 8GRS(Zhang *et al.*, 2023).

This thesis aims to test whether TMEM63B is the MA ion channel that responds to noxious force in C-LTMRs. TMEM63B is a member of the OSCA/TMEM63 family, a family of ion channels recently shown to be MA (Murthy *et al.*, 2018a). OSCAs are plant ion channels that



are homo-dimers, and each subunit contains an ion permeation pathway (**Figure 1.4B**) (Jojoa-Cruz *et al.*, 2018; Zhang *et al.*, 2018). Multiple OSCA homologs have poke- and stretch-activated currents in heterologous overexpression in HEK293 *Piezo1* KO cells (HEK P1KO) and MA currents in proteoliposomes that contain no auxiliary proteins. OSCA proteins alone open in response to force applied to a membrane, which is the basic definition of a MA ion channel. TMEM63's are the animal orthologs of OSCA channels. Mammalian TMEM63's have one subunit and the ion permeation pathway (Orange) is homologous to the OSCA channels (**Figure 1.4C**) (Zheng *et al.*, 2023). Different TMEM63A and B channels produce stretch activated current when they are overexpressed in HEK P1KO cells, but not poke activated current (Murthy *et al.*, 2018a).

TMEM63 orthologs can function as a molecular sensor for external forces, and TMEM63B in mammals plays a role in cellular responses to mechanical force. In *Drosophila*, TMEM63 is utilized for sensing humidity and helps to distinguish food texture, and has fundamental role in lysosomal function (Li & Montell, 2021; Li *et al.*, 2022; Li *et al.*, 2024). There is no known sensory role for TMEM63B in mammals, but certain cells require the channel. Research in lung alveolar cells showed TMEM63A and B work together to secrete surfactant (Chen *et al.*, 2024). This publication showed that TMEM63B's role in alveolar cells is likely why global *Tmem63b* KO mice do not survive past P0, as they showed cKO of just *Tmem63b* in alveolar cells recreates a similar survival pattern. Chen et al. 2024 recorded stretch currents that are dependent on TMEM63B. This is the first and only study to show endogenous MA currents that depend on TMEM63B (Chen *et al.*, 2024). *Tmem63b* cKO in mice results in hearing loss because outer hair cells require TMEM63B to survive (Du *et al.*, 2020), hypothesizing that TMEM63B serves as a pressure release valve in outer hair cells. As pressure

builds, TMEM63B is activated, causing  $\text{Ca}^{2+}$  to enter the cell and activate BK channels, resulting in ions and water flowing out of the outer hair cell. These are the most concrete studies of TMEM63B in mammals. Humans who have suspected loss of function mutations in *TMEM63B* have severe developmental encephalopathies, indicating TMEM63B could play a role in basic neuronal development or maintaining proper neuronal function (Vetro *et al.*, 2023). This paper did not fully characterize the *TMEM63b* mutations, and because cognitive symptoms were severe, these patients did not undergo voluntary experiments to test hearing, somatosensation, and other hypotheses for TMEM63B's function. So far, studies have not tested TMEM63B function in somatosensation, even though it is expressed in many subtypes of mouse DRG (Sharma *et al.*, 2020).

According to single-cell RNA sequencing, *Piezo2* and *Tmem63b* are the only known MA ion channels in C-LTMRs. **Table 1.1** shows relevant comparisons between the two channels that guided experiments to untangle their contribution to MA currents in C-LTMRs. Each channel is a MA ion channel, but PIEZO2 opens in response to poke and stretch, and TMEM63B responds to only stretch (Coste *et al.*, 2010; Murthy *et al.*, 2018a; Murthy, 2023). The hypothesis is that poke and stretch apply different types of force to the membrane (Young *et al.*, 2022). PIEZO2 has a rapidly inactivating response in poke recordings and a non-inactivating response in stretch recordings. TMEM63B has a non-inactivating response to stretch stimulation. These channels are both non-selective cation channels, but they have different conductance properties; PIEZO2 is 15-20pS and TMEM63B is <1pS (Murthy *et al.*, 2018a; Murthy, 2023). Our goal was to generate a cKO of *Tmem63b* to understand if the channel contributes to any MA currents in C-LTMR neurons, indicating a role as the noxious mechanosensor in these neurons. Evidence of

TMEM63B contribution to MA currents in C-LTMRs would be a steppingstone for future research to build on.

**Table 1.1: Comparison of PIEZO2 and TMEM63B properties relevant for this thesis.**

Ion channel	PIEZO2	TMEM63B
Indentation	Fast inactivation $\tau < 10\text{ms}$	No response in HEK P1KO cells
Stretch	Non-inactivating	Non-inactivating
Ions	Non-selective cation	Non-selective cation
Conductance	15-20 pS	$< 1\text{pS}$
Mouse Tools	Flox line	HA Tagged and Flox line

(Murthy *et al.*, 2018a; Murthy, 2023)

## Chapter 2 Exploring the Landscape of Mechanosensors in C-LTMRs

This text is an adaptation from the manuscript:

### **Exploring the Landscape of Mechanosensors in C- fiber Low Threshold Mechanoreceptors.**

By: Daniel J. Orlin, Antonio Munoz, Aidan Berryman, Destinee Semidey, Swetha E. Murthy

#### **2.1 Introduction: Untangling PIEZO2 and TMEM63B's contributions to MA currents in C-LTMRs**

DRG neurons are primary peripheral sensory neurons that innervate skin and internal organs and detect physical, thermal, and chemical stimuli. DRG neurons are classified into at least 15 distinct subtypes by their transcriptomic profiles and axonal morphology, which underlies their remarkable functional diversity (Usoskin *et al.*, 2015; Sharma *et al.*, 2020; Qi *et al.*, 2024). One such function is mechanosensation, the process by which neurons are activated by physical forces, giving rise to the sensation of a phone's vibration or a sibling's pinch on the arm.

DRG neurons that encode physical stimuli are intrinsically mechanosensitive because they express MA ion channels (McCarter *et al.*, 1999). DRG neurons have been classically sorted into discrete categories based on the inactivation kinetics of their MA currents, ranging between \) (Hao & Delmas, 2010). The hypothesis was that each category represents a certain MA ion channel's activity. Discovery of the PIEZO family of MA ion channels revealed that almost all RA currents, and some IA currents are mediated by PIEZO2 (Coste *et al.*, 2010; Murthy *et al.*, 2018b). Subsequent studies have demonstrated that PIEZO2 is the ion channel that initiates the neuronal response to light touch and gives rise to proprioception in both mice and

humans (Ranade *et al.*, 2014; Woo *et al.*, 2015; Chesler *et al.*, 2016). However, patients and mice are still able to sense noxious force and deep pressure. Thus, the MA ion channel(s) that detect high-threshold mechanical forces and acute mechanical pain remain unknown.

One strategy to identify the MA channel that responds to high-threshold mechanical force is to isolate DRG neurons with non-RA current, likely not dependent on PIEZO2, and sequence their mRNAs to find candidate genes that encode for putative MA channels. Indeed, an in-depth patch-sequencing approach that paired transcriptomics with electrophysiological recordings generated a list of candidates that are enriched in non-RA neurons to be used as a resource in future screens (Parpaite *et al.*, 2021). Another approach is to identify DRG subtypes that respond to noxious mechanosensation in the absence of PIEZO2. *In vivo* Ca<sup>2+</sup> imaging in mouse trigeminal ganglion demonstrated that the DRG neuronal subtype C-LTMRs respond to gentle and noxious stimuli. However, C-LTMRs only retain the response to noxious stimuli in *Piezo2* conditional knockout mice (Von Buchholtz *et al.*, 2021). Therefore, C-LTMRs express a MA ion channel that responds to high-threshold mechanical stimuli, making them sensitive to noxious force.

C-LTMRs have historically been classified in humans by their ability to respond to gentle stroking and to generate a pleasurable sensation (Loken *et al.*, 2009; Middleton *et al.*, 2022). In addition to encoding affective touch, in mice, studies have also unveiled C-LTMRs' role in acute mechanical nociception and allodynia (a condition where, due to injury or inflammation, light touch evokes pain) (Seal *et al.*, 2009; Nagi *et al.*, 2011; Delfini *et al.*, 2013; Larsson & Nagi, 2022). Although it is now known that PIEZO2 is the primary transducer for mechanical allodynia, its contribution to this phenomenon in C-LTMRs is ambiguous (Murthy *et al.*, 2018b; Szczot *et al.*, 2018). Furthermore, at the physiological level, MA currents in C-LTMRs are

slowly adapting, which is uncharacteristic of what has been described for PIEZO2 (Delfini *et al.*, 2013; Zheng *et al.*, 2019). Thus, the identity and contribution of the different MA ion channels that underlie C-LTMR properties, which make them sensitive to noxious mechanical forces, remain unknown.

This chapter evaluates TMEM63B, a monomeric non-selective MA cation channel, as a primary sensor for noxious force in C-LTMRs (Murthy *et al.*, 2018b; Zheng *et al.*, 2023). In mice, TMEM63B is responsible for osmotic regulation in outer hair cells, and *TMEM63B* mutations in humans lead to developmental encephalopathies in the central nervous system (Du *et al.*, 2020; Vetro *et al.*, 2023). The homolog in *Drosophila*, TMEM63, is crucial for sensory stimuli like humidity sensation and food texture discrimination as well as lysosomal function (Li & Montell, 2021; Li *et al.*, 2022; Li *et al.*, 2024). Interestingly, a single-cell RNA sequencing database from DRGs indicates that *Tmem63b* is expressed in C-LTMRs, along with *Piezo2* (Sharma *et al.*, 2020). While these studies raise the possibility that TMEM63B could function as a sensor for external mechanical stimuli, its role in mammalian mechanosensation remains unknown. Here, using a C-LTMR-specific *Cre* line we sought to examine whether TMEM63B contributes to C-LTMR function.

## **2.2 Results:**

### ***2.2.1 Validation of Cre-mediated recombination in a Vglut3-IRES-Cre mouse line***

To better understand the molecular properties of C-LTMRs and determine the underlying MA ion channels that contribute to their mechanosensation, we sought to identify a mouse line that would label and drive *Cre* expression in C-LTMRs. Among the previously known molecular markers for C-LTMRs like tyrosine hydroxylase (TH), Tafa4, and IB4-GNIP, we chose *Vglut3<sup>Cre</sup>* (Seal *et al.*, 2009; Li *et al.*, 2011; Delfini *et al.*, 2013; Urien *et al.*, 2017). We crossed

*Vglut3<sup>Cre</sup>* mice to the *Cre*-dependent tdTomato reporter line *Ai9* (referred to as *Vglut3<sup>Cre</sup>;Ai9* when pertinent) and determined the specificity and efficiency of the *Cre*-mediated recombination using immunohistochemistry (IHC) by measuring the overlap between tdTomato and DRG neuronal subtypes including medium/large diameter myelinated neurons (neurofilament-200; Nf-200), proprioceptors (Parvalbumin; PV), and C-LTMRs (Tyrosine Hydroxylase; TH). We calculated total percentages of labeled neurons with the pan-neuronal label ubiquitin carboxy-terminal hydrolase L1 (UCH-L1) (**Figure 2.1** and **Table 2.1**). Additionally, we evaluated the distribution of both tdTomato<sup>+</sup> neurons and the DRG subtypes of interest along the rostral-caudal axis.

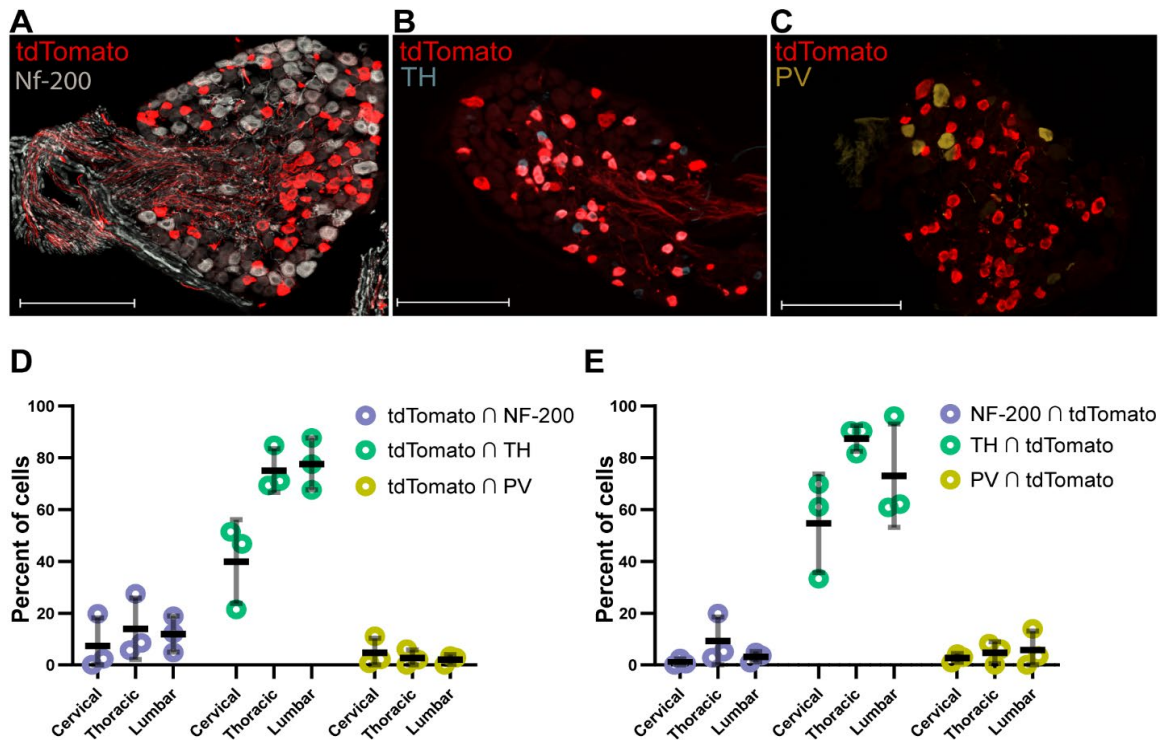


**Figure 2.1: *Vglut3<sup>cre</sup>* is specific and efficient in genetically labeling C-LTMRs.**

**A-C:** Immunostaining of neuronal cell bodies from *Vglut3<sup>Cre</sup>;Ai9* mice for tdTomato and DRG subtype markers. **A:** Neurofilament-200 (Nf-200), **B:** Tyrosine Hydroxylase (TH), and **C:** Parvalbumin (PV) (scale bar: 200μm). **D:** Measure of *Cre* specificity by percent of tdTomato<sup>+</sup> neurons overlapping with each DRG subtype marker (N=3 animals) **E:** Measure of *Cre* efficiency by percent of neurons with a DRG subtype marker overlapping with tdTomato (N=3 animals). Bars represent mean ± S.D.

To measure the specificity of the *Cre*-mediated recombination we calculated the percentage of tdTomato<sup>+</sup> neurons that were also labelled by a DRG subtype marker. In lumbar DRGs, we found that  $77.6 \pm 10.0$  % (mean  $\pm$  SD, N=3 animals) of tdTomato<sup>+</sup> neurons were putative C-LTMRs that co-labelled for TH,  $11.9 \pm 7.0$  % were putative myelinated neurons that stained for Nf-200, and  $2.09 \pm 1.84$  % were putative proprioceptors, which stained for PV (**Figure 2.1D** and **Table 2.1**). This result varied along the rostral-caudal axis with a decrease in C-LTMR staining in cervical DRGs ( $39.9 \pm 16.2$  %), compared to thoracic ( $75.0 \pm 8.5$  %) and lumbar ( $77.6 \pm 10.0$  %) DRGs (**Figure 2.1D** and **Table 2.1**). To gauge the efficiency of the *Cre*-mediated recombination, we calculated the percentage of neurons with a specific subtype marker that were tdTomato<sup>+</sup>. In lumbar DRGs,  $3.13 \pm 2.02$  % of Nf-200<sup>+</sup> neurons were tdTomato<sup>+</sup> and a small fraction of PV<sup>+</sup> neurons were tdTomato<sup>+</sup> ( $5.8 \pm 7.27$  %), whereas majority of TH<sup>+</sup> neurons were tdTomato<sup>+</sup> ( $73.1 \pm 20.0$  %); similar values were observed in cervical and thoracic DRGs (**Figure 2.1E** and **Table 2.1**). The high degree of overlap between tdTomato and TH suggests that *Vglut3<sup>Cre</sup>;Ai9* efficiently labels C-LTMRs.

To rigorously compare the *Cre*-mediated recombination in DRG neurons we analyzed the percentage of tdTomato<sup>+</sup> neurons across experiments. We found the percentage of tdTomato<sup>+</sup> neurons remained similar across experiments, suggesting that the *Cre* specificity and efficiency observed accurately represents *Slc17a8* (VGLUT3) expression (**Figure 2.2A,B** and **Table 2.1**). We observed some variability in labelling along the rostral-caudal axis with each experimental group (**Figure 2.2B**); tdTomato staining was the highest in thoracic DRGs ( $24.0 \pm 1.5$  %) compared to cervical ( $8.10 \pm 2.36$  %) and lumbar ( $14.8 \pm 2.0$  %) regions, suggesting that the percentage of C-LTMRs is higher in this region (**Figure 2.2B** and **Table 2.1**). We confirmed this by analyzing the percentage of neurons with subtype markers and observed that TH<sup>+</sup> neurons



were most abundant in thoracic DRGs (**Figure 2.2C** and **Table 2.1**). The percentage of TH+ and PV+ neurons we observed matched previous reports, but we noticed variability in Nf-200 staining along the rostral-caudal axis. Overall, tdTomato staining in the *Vglut3<sup>Cre</sup>; Ai9* line is consistent across staining procedures, experimental trials, and animals, and our reported percentages for each DRG subtype marker agree with previously published data.

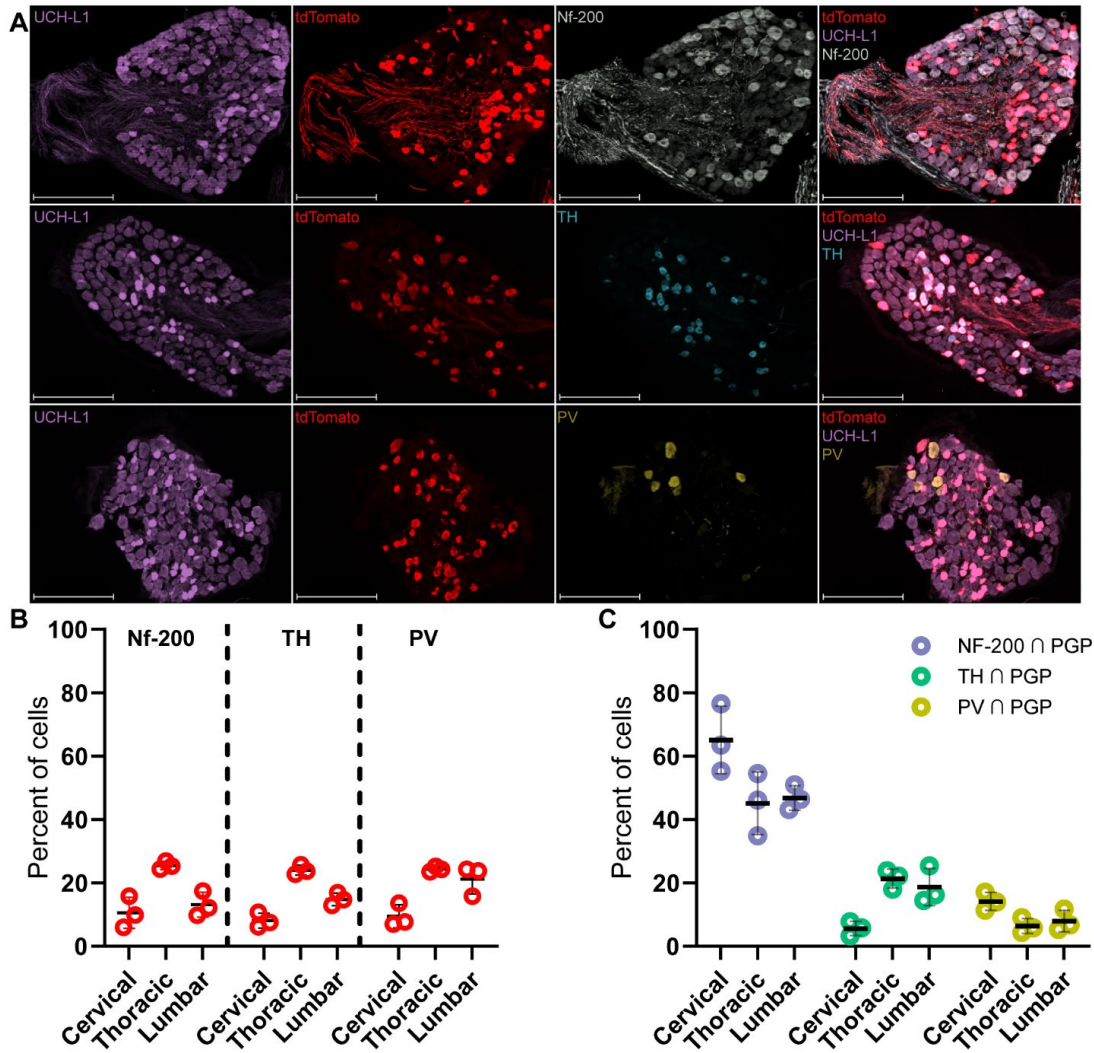


**Figure 2.2: Staining of subtype markers and tdTomato is consistent across animals and experiments** **A:** Immunostaining of neuronal cell bodies from *Vglut3<sup>Cre</sup>; Ai9* mice stained for UCH-L1, tdTomato, and Nf-200 (top), TH (middle), or PV (bottom); overlap of all channels are also indicated (scale bar: 200  $\mu$ m). **B:** Percent of tdTomato+ neurons represented as UCH-L1positive neurons that overlap with tdTomato separated by DRG subtype marker staining. **C:** Quantification of subtype abundance as a percent of UCH-L1 positive neurons that overlap with a DRG subtype marker. Bars represent mean  $\pm$  S.D.

**Table 2.1: DRG staining percentages for *Vglut3<sup>cre</sup>;Ai9* characterization.**

Type of DRG	Nf-200	TH	PV
<b>Specificity</b>			
Cervical	7.38±10.79	39.91±16.17	4.68±5.63
Thoracic	13.91±11.88	75.05±8.49	2.72±3.08
Lumbar	11.93±7.00	77.63±10.01	2.09±1.84
<b>Efficiency</b>			
Cervical	0.98±1.32	54.76±19.06	2.68±1.68
Thoracic	9.27±9.22	87.45±5.02	4.75±4.25
Lumbar	3.13±2.02	73.08±20.00	5.80±7.27
<b>Subtype distribution</b>			
Cervical	65.07±10.69	5.58±2.23	14.14±2.85
Thoracic	45.13±9.85	21.31±3.00	6.41±2.39
Lumbar	45.80±3.89	18.67±5.67	7.91±3.39
<b>tdTomato</b>			
Cervical	10.54±4.95	8.10±2.36	9.43±3.65
Thoracic	25.48±1.30	24.03±1.55	24.30±0.86
Lumbar	13.13±3.92	14.82±1.99	21.25±4.75

Note: Values indicate mean ± S.D. N = 3 animals and 3= images.

### 2.2.2 Expression of MA ion channels *Tmem63b* and *Piezo2* in C-LTMRs

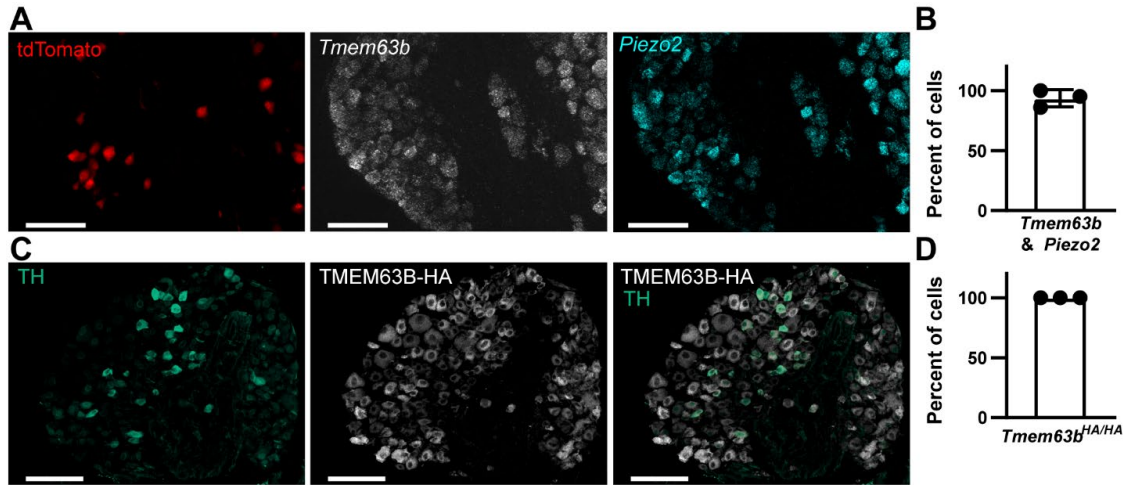


**Figure 2.3: *Tmem63b* and *Piezo2* expression in C-LTMRs.** A: Thoracic DRG somas from *Vglut3<sup>Cre</sup>;Ai9* mice with Cre-dependent tdTomato fluorescence, co-labeled with *in situ* probes against *Tmem63b* and *Piezo2*. B: Percent of tdTomato+ neurons that co-express both *Tmem63b* and *Piezo2* calculated by mean fluorescence above negative probes (N = 3 animals). C: Thoracic DRG somas from *Tmem63b<sup>HA/HA</sup>* mice stained for TH, HA-tag, and overlay of both channels. D: Percent of TH positive DRG neurons with HA staining (N=3 animals). Bars represent mean ± S.D. scale bars 100 µm.

RNA sequencing studies in mice have shown that C-LTMRs co-express *Tmem63b* and *Piezo2* (Usoskin *et al.*, 2015; Sharma *et al.*, 2020). We wanted to examine these observations in the *Vglut3<sup>Cre</sup>;Ai9* mice and further characterize the percentage of C-LTMRs that express both of these channels. To visualize expression, we used ISH to label DRG neurons for *Tmem63b* and *Piezo2* transcripts and compared against tdTomato fluorescence (**Figure 2.3A**). *In situ* images show broad expression for each gene in tdTomato+ and tdTomato- neurons. Within the tdTomato+ cells,  $93.7 \pm 7.1$  % of cells co-express *Tmem63b* and *Piezo2* (**Figure 2.3B**). We next evaluated TMEM63B protein presence in the DRG. For this we utilized a previously reported *Tmem63b<sup>HA/HA</sup>* mouse that has a haemagglutinin (HA) epitope fused to the N-terminal of TMEM63B in the endogenous locus of the gene, to perform IHC on DRG neurons and compare the expression profile against its localization with the C-LTMR marker, TH (Li *et al.*, 2011; Du *et al.*, 2020). 100 % of TH+ neurons were TMEM63B+ (**Figure 2.3C-D**). These results indicate that TMEM63B is present in C-LTMRs and support previously reported RNA sequencing studies, demonstrating that C-LTMRs co-express *Tmem63b* and *Piezo2*.

### 2.2.3 Characterization of indentation- and stretch-activated currents in C-LTMRs

To reveal TMEM63B's contribution to C-LTMR MA currents, we crossed *Vglut3<sup>Cre</sup>;Ai9* mice to *Tmem63b<sup>fl/fl</sup>* to generate *Tmem63b* cKO animals. For simplicity, we will refer to the wildtype *Vglut3<sup>Cre</sup>;Ai9;Tmem63b<sup>wt/wt</sup>* mice as *Tmem63b<sup>wt</sup>* and the *Tmem63b* cKO *Vglut3<sup>Cre</sup>;Ai9;Tmem63b<sup>fl/fl</sup>* mice as *Tmem63b<sup>fl</sup>*. In dissociated DRG neurons from *Tmem63b<sup>fl</sup>* animals we were able to distinguish tdTomato+ C-LTMRs from the 13% of non-C-LTMR neurons based on small soma size and observed action potentials with wide half-width of  $2.84 \pm 0.81$  ms (N=18), characteristic of C-LTMRs (**Figure 2.4A, C**). Analysis of electrical properties

of tdTomato<sup>+</sup> neurons from *Tmem63b<sup>wt</sup>* and *Tmem63b<sup>fl</sup>* showed no differences in rheobase or membrane resistance (**Table 2.2**).

**Table 2.2: Electrical properties of C-LTMRs.**

Electrophysiological Properties	<i>Tmem63b<sup>wt</sup></i>	<i>Tmem63b<sup>fl</sup></i>
Rheobase	181.4 ± 88.8	164.2 ± 68.2
Membrane Resistance	372.8 ± 151.2	381.0 ± 142.6
Half-width	3.07 ± 0.63	2.83 ± 0.80

Note: Values indicate mean ± S.D. *Tmem63b<sup>wt</sup>*; 4 animals and 18 cells and *Tmem63b<sup>fl</sup>*; 5 animals and 19 cells. Data collected and analyzed by Antonio Munoz.

We used two distinct methods to activate MA currents in dissociated C-LTMR neurons. In the first method, the soma membrane is indented with a blunt glass probe in whole-cell patch-clamp mode and in the second, a patch of soma membrane is excised and stretched in the outside-out patch-clamp mode. Each of these techniques represents different modes of mechanical stimulation and activation of MA ion channels (Young *et al.*, 2022). In DRG neurons, PIEZO2 elicits RA or IA currents in response to indentation and non-inactivating currents in response to membrane stretch (Ranade *et al.*, 2014; Murthy, 2023). All cells had a whole-cell indentation response higher than 15 pA, with a mean maximum peak current of 244.1 ± 200.4 pA (N = 33 cells) (**Figure 2.4B, D**). We further characterized the indentation MA currents by their inactivation kinetics and steady state current (% current remaining after the current has relaxed to steady state). We measured the tau for inactivation by fitting an exponential from peak to steady state current of one of the near-saturating traces (**Figure 2.4E**). Based on the historical categorization of MA currents by their inactivation kinetics, almost all cells had slowly adapting to ultra-slowly adapting MA currents (Hao & Delmas, 2010). We also observed a steady state current of 34.4 ± 25.8 % of peak current (**Figure 2.4F**). Overall, our observations are consistent with previous reports of MA currents from C-LTMRs that were identified using a *TH<sup>2A-CreER</sup>* mouse line (Zheng *et al.*, 2019). Indentation-induced MA currents

from *Tmem63b<sup>fl</sup>* animals showed similar mean maximum peak currents of  $218.7 \pm 197.8$  pA (N = 32 cells), and inactivation time constants compared to *Tmem63b<sup>wt</sup>* (Figure 2.4B, D-F).

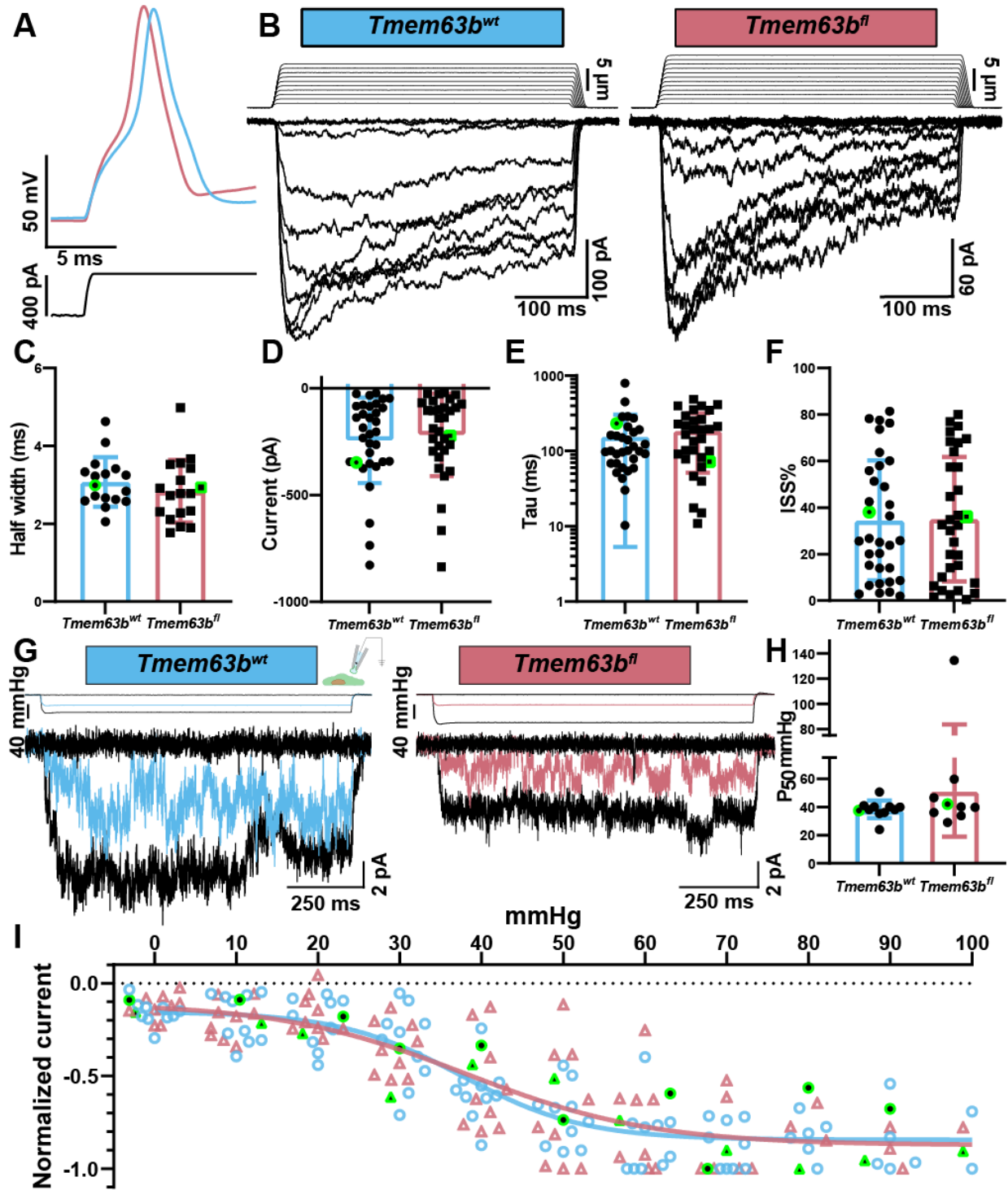


**Figure 2.4: Cultured C-LTMRs have MA currents in response to both indentation and stretch stimuli.** **A:** Representative trace of action potential of a tdTomato+ positive DRG neuron from *Tmem63b<sup>wt</sup>* (blue) vs *Tmem63b<sup>fl</sup>* (red) mice. **B:** Representative trace of indentation-induced whole-cell MA currents from *Tmem63b<sup>wt</sup>* and *Tmem63<sup>fl</sup>* C-LTMRs. **C:** Half-width of action potentials within 0-4 pA of rheobase. Green indicates the example trace's corresponding measurement (*Tmem63b<sup>wt</sup>*;  $3.07 \pm 0.63$  ms, cells = 17 and animals = 4, *Tmem63b<sup>fl</sup>*;  $2.84 \pm .80$  ms, cells= 18 and animals= 4; unpaired t-test  $p = 0.34$ ). **D:** Maximum peak current . Green indicates the example trace's corresponding measurement (*Tmem63b<sup>wt</sup>*;  $-244.1 \pm 200.4$  pA, cells= 33 and animals= 6, *Tmem63b<sup>fl</sup>*;  $-218.7 \pm 193.7$  pA, cells = 32 and animals = 6, unpaired t-test  $p = 0.61$ ). **E:** Inactivation kinetics plotted on log<sub>10</sub> axis (*Tmem63b<sup>wt</sup>*;  $154.7 \pm 149.4$  ms, cells = 32 and animals = 6, *Tmem63b<sup>fl</sup>*;  $183.9 \pm 132.3$  ms, cells = 31 and animals = 6, unpaired t-test  $p = 0.42$ ). **F:** Steady state current taken as a percentage of the peak current (*Tmem63b<sup>wt</sup>*;  $34.42 \pm 25.82$ , cells = 33 and animals = 6, *Tmem63b<sup>fl</sup>*;  $34.96 \pm 26.75$ , cells = 33 and animals = 6, unpaired t-test  $p = 0.93$ ). **G:** Representative traces of outside-out stretch currents from *Tmem63b<sup>wt</sup>* and *Tmem63b<sup>fl</sup>*. **H:** P<sub>50</sub> of stretch response fit to a Boltzmann curve (*Tmem63b<sup>wt</sup>*;  $38.28 \pm 6.24$  mmHg, cells = 11 and animals = 3, *Tmem63b<sup>fl</sup>*;  $51.32 \pm 32.39$  mmHg, cells = 9 and animals = 3, unpaired t test  $p = 0.21$ ). **I:** Current vs pressure relationship, current normalized to maximum response. Shown is a Boltzmann fit of the average values for each group , green indicates the representative trace's corresponding measurement (*Tmem63b<sup>wt</sup>*; cells = 11 and animals = 5, *Tmem63b<sup>fl</sup>*; cells = 10 and animals = 4, Boltzmann fit is not different  $p = 0.80$ ). Bars represent mean  $\pm$  S.D. For all quantifications, green data points indicate the example trace's corresponding measurement.

In dissociated DRG neurons, we induced stretch-activated currents in the outside-out patch clamp configuration by applying positive pressure to excised patches at 10 mmHg increments (**Figure 2.4G**). We observed non-inactivating macroscopic currents from tdTomato+ neurons of *Tmem63b<sup>wt</sup>* and *Tmem63b<sup>fl</sup>*. To obtain P<sub>50</sub>, we normalized stretch-activated currents from individual cells to the maximum response of that patch and fit with a Boltzmann curve. We observed similar P<sub>50</sub> values of stretch-activated currents from cells of *Tmem63b<sup>wt</sup>* and *Tmem63b<sup>fl</sup>* mice,  $38.28 \pm 6.24$  mmHg (N = 11) and  $51.32 \pm 32.39$  mmHg (N = 9), respectively (**Figure 2.4H, I**). Together, the detailed electrophysiological characterization of C-LTMR current properties and indentation-induced and stretch-activated MA currents indicated no difference between *Tmem63b<sup>wt</sup>* and *Tmem63b<sup>fl</sup>* animals.

#### 2.2.4 In situ hybridization reveals that the *Vglut3<sup>Cre</sup>* line does not delete *Tmem63b* within C-LTMRs

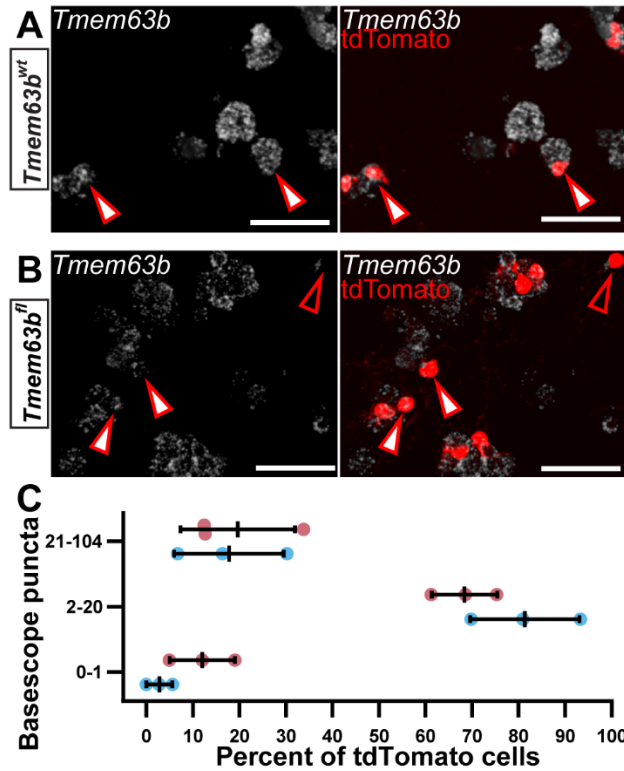


**Figure 2.5: *Tmem63b* expression persists in *tdTomato*+ neurons from *Tmem63b*<sup>fl</sup> mice.**

**A:** *In situ* hybridization and immunostaining of dissociated DRG neurons from *Tmem63b*<sup>wt</sup> for probe against *Tmem63b*-exon 5 (white) and *tdTomato* (red), respectively. Closed arrows denote *tdTomato* positive neurons with *Tmem63b* puncta. **B:** Same as **A**, but neurons are from *Tmem63b*<sup>fl</sup> mouse. Open arrows denote *tdTomato*+ neurons without *Tmem63b* puncta. scale bars 50  $\mu$ m. **C:** *Tmem63b* expression measured by the percentage of *tdTomato*+ cells with a defined number of *in situ* hybridization puncta. Groups binned by the following levels, 0-1 puncta no expression (mean  $\pm$  SD %), 2-20 puncta medium expression (mean  $\pm$  SD %), 21-104 puncta high expression (mean  $\pm$  SD %). N = 3 animals per group. Chi-Square ( $p < 0.0001$   $\chi^2 = 22.76$ , df = 2).

To gauge the extent of *Tmem63b* deletion in *Tmem63b*<sup>fl</sup> mouse, we used ISH with a probe that recognizes exon 5 in *Tmem63b*, the region flanked by *loxP* sites in the *Tmem63b*<sup>fl</sup> mice. We performed these experiments in dissociated DRG neurons to recapitulate the conditions used for the electrophysiology experiments. To correlate loss of *Tmem63b* transcript with *Cre* expression, we combined ISH with IHC to stain for *Cre*-dependent *tdTomato*. Surprisingly, we observed *Tmem63b* puncta in a majority of *tdTomato*+ neurons in *Tmem63b*<sup>wt</sup> and *Tmem63b*<sup>fl</sup> mice (Figure 2.5A, B). To quantify these observations, we generated 3D regions of interests (ROIs) within all *tdTomato* cells and counted the *in situ* puncta for each ROI. We binned *tdTomato* cells by 0-1 puncta for no transcript expression, 2-20 puncta for medium transcript expression, and 21-104 puncta for high transcript expression. 2.8  $\pm$  2.8 % of *tdTomato*+ neurons in *Tmem63b*<sup>wt</sup> mice had 0-1 *Tmem63b* puncta compared to 12.0  $\pm$  7.0 % of *tdTomato*+ neurons in *Tmem63b*<sup>fl</sup> mice (Figure 2.5C). 81.3  $\pm$  11.7 % of *tdTomato*+ neurons in *Tmem63b*<sup>wt</sup> mice had 2-21 *Tmem63b* puncta compared to 68.4  $\pm$  7.0 % of *tdTomato*+ neurons in *Tmem63b*<sup>fl</sup> mice. Both



groups had similar amounts of high-expressing tdTomato+ neurons (21-104 puncta). Although we see some tdTomato+ neurons in *Tmem63b<sup>fl</sup>* mice without any *Tmem63b* puncta, a majority of cells have medium to high transcript levels. These results suggest that although the *Vglut3<sup>Cre</sup>;Ai9* line reliably labelled the C-LTMR positive population by driving recombination of the tdTomato gene, the efficiency in deleting *Tmem63b* is poor.

## 2.3 Discussion

In this study we aimed to evaluate whether TMEM63B could act as a sensor for noxious mechanical force by examining C-LTMR neurons. We demonstrated that the *Vglut3<sup>Cre</sup>;Ai9* mouse specifically and efficiently labels C-LTMRs (**Figure 2.1** and **Figure 2.2**). We confirmed that the two known MA ion channels, *Tmem63b* and *Piezo2*, are co-expressed in C-LTMRs (**Figure 2.3**). Additionally, we performed an in-depth characterization of two types of MA currents from dissociated C-LTMRs neurons (**Figure 2.4**). We observed robust indentation-induced whole-cell MA currents with slowly or ultra-slowly adapting properties. To our knowledge, we also report for the first time stretch-activated currents from C-LTMRs. These stretch-activated currents are non-inactivating and resemble PIEZO2 and TMEM63B stretch-activated currents in heterologous expression systems (Murthy, 2023). Despite the robust and consistent nature of C-LTMR MA currents we did not observe any differences between the *Tmem63b<sup>wt</sup>* and *Tmem63b<sup>fl</sup>* animals. Upon further analysis, we found that the *Tmem63b<sup>fl</sup>* animals had only a small reduction in *Tmem63b* expression, which might explain the lack of effect in the *Tmem63b<sup>fl</sup>* animals (**Figure 2.5**).

Using the *Vglut3<sup>Cre</sup>* mouse line to conditionally delete *Tmem63b* in C-LTMRs was the most direct approach to test its role as noxious mechanosensor in these cells, given that *Tmem63b* global knockout animals are embryonically lethal and TMEM63B-specific channel



blockers do not yet exist (Chen *et al.*, 2024). Our results highlight the underlying complexity of using *Cre-Lox* systems to generate cKO animals. Although the *Vglut3<sup>Cre</sup>;Ai9* mouse line genetically labelled C-LTMRs by turning on tdTomato expression, it was inefficient at deleting *Tmem63b*. The reason for this inefficient deletion is unclear. In some conditional lines, the *loxP* sites are too far apart for efficient recombination, but this is not the case in the *Tmem63b<sup>fl/fl</sup>* animal (Zheng *et al.*, 2000). The *loxP* sites that flank *Tmem63b*-exon 5 are 756 base pairs (bp) apart, which is closer than the *Ai9* reporter strain used in this study, 837 bp (Madisen *et al.*, 2010). Beside this circumstantial evidence, another study successfully used the *Tmem63b<sup>fl/fl</sup>* line to generate *Tmem63b* conditional knockout and showed that the post birth lethality of *Tmem63b* global KO mice is likely due to its role in lung alveolar epithelial cell function (Chen *et al.*, 2024). Therefore, the inefficient deletion of *Tmem63b* in C-LTMRs may be specific to the *Vglut3<sup>Cre</sup>* line used in this study. Using the *Vglut3<sup>Cre</sup>* line to cKO floxed alleles should only be done following rigorous controls. Future investigations with other Cre lines or viral strategies that can selectively delete *Tmem63b* in C-LTMRs will be needed to conclusively determine TMEM63B's contribution to noxious mechanosensation in C-LTMRs.

A major outstanding question in the somatosensory field is the identity of the MA channel responsible for slowly adapting currents. MA currents from DRG neurons fall into four categories based on their inactivation kinetics, and so far, it is thought that RA and some IA currents are PIEZO2 dependent (Ranade *et al.*, 2014; Murthy *et al.*, 2018b). Our data demonstrates that C-LTMR neurons are an ideal candidate subtype to screen for the underlying ion channel that elicits slowly adapting currents in DRG neurons. First, all C-LTMRs have robust MA currents in response to indentation and second, a majority of the MA currents are slowly adapting. These two properties are uncommon when recording from dissociated DRG

neurons. Most subtypes typically have at least 20% non-responders and the MA currents have heterogeneous inactivation properties (Murthy *et al.*, 2018b). It should be noted that while the C-LTMRs MA currents having slow inactivation agree with Zheng *et al.*, 2019 our results conflict with Lou *et al.*, 2013 that found C-LTMRs had a mix of inactivation kinetics, using a different *Vglut3-IRES-Cre* mouse line to mark the C-LTMRs study (Lou *et al.*, 2013; Zheng *et al.*, 2019). Regardless, all studies including ours, report slowly adapting currents in the C-LTMR population, which has high *Piezo2* expression. Therefore, further studies are needed to assess if PIEZO2 indeed accounts for only RA and IA MA currents. This notion is also supported by evidence from patch-sequencing data that reveal neurons across the four inactivation groups express *Piezo2* (Parpaite *et al.*, 2021). Together, these data imply that PIEZO2 might induce RA as well as SA currents.

PIEZO2 MA currents in C-LTMRs might be modulated by auxiliary proteins like TMC7, resulting in the slowly adapting MA current property. In DRG neurons, *Tmc7* deletion leads to a reduction in non-RA currents, and co-expression of *Tmc7* with *Piezo2* in a heterologous expression system recapitulates the breadth of DRG neuron MA current inactivation properties (Zhang *et al.*, 2024). Similarly, TMEM63B could modulate PIEZO2 MA current properties and the slowly adapting currents in C-LTMRs could be a product of both channels. Conversely, conformational changes in PIEZO2 could influence TMEM63B function, as has been demonstrated for PIEZO1-dependent modulation for K<sub>2</sub>P channels (Glogowska *et al.*, 2021; Lewis *et al.*, 2024). In this context it is noteworthy that the *in situ* results in **Figure 2.3** indicate *Piezo2* and *Tmem63b* are co-expressed in other DRG neuronal populations beyond C-LTMRs. Furthermore, the two channels are co-expressed in non-neuronal cells like bladder endothelial cells (Marshall *et al.*, 2020) and outer hair cells (Wu *et al.*, 2017; Du *et al.*, 2020; Lee *et al.*,

2024). This co-expression pattern elicits the question of whether the presence of two channels with distinct responses to mechanical stimuli might confer cells with their mechanosensitive properties. Finally, the possibility exists that beyond *Piezo2* and *Tmem63b*, C-LTMRs express other MA ion channels that are yet to be discovered. These PIEZO2-, TMEM63B- dependent and independent possibilities will have to be tested in the future using combinations of *Piezo2* and *Tmem63b* tissue-specific cKO mice.

Our data shows that *Tmem63b* is expressed in many DRG neurons, but its role in mechanosensation beyond C-LTMR function and somatosensory neurons remain largely unknown. In the central nervous system, *Tmem63b* is broadly expressed in different neuronal cell types in certain brain regions like the cerebellum(Saunders *et al.*, 2018). Unexplored *TMEM63B* mutations in humans lead to developmental epileptic encephalopathy, which implies that TMEM63B plays a crucial role in these neurons, but the underlying mechanism is yet to be determined (Vetro *et al.*, 2023). Recent studies are beginning to unravel mechanistic details of the structure and function of TMEM63B and the OSCA/TMEM63 family as MA channels (Zhang *et al.*, 2018; Zheng *et al.*, 2023; Han *et al.*, 2024; Lowry *et al.*, 2024; Niloy *et al.*, 2024). But as *in vivo* mechanosensors, in outer hair cells TMEM63B activation couples with BK ( $\text{Ca}^{2+}$ -activated  $\text{K}^{+}$  channels) channels to reduce cell swelling, which could be a ubiquitous mechanism utilized by cell types outside the auditory system (Du *et al.*, 2020). These studies and the embryonic lethality of global *Tmem63b* KO mice suggest that TMEM63B could be important for proper cellular function and neuronal development (Chen *et al.*, 2024). Together they stress the importance of future studies to better understand TMEM63B's role as a mechanosensor.

## **2.4 Methods**

### **2.4.1 Animals**

All animal procedures were approved by the Institutional Animal Care and Use Committee of Oregon Health and Science University. The *Vglut3-IRES-Cre* mouse was purchased from Jax (028534, RRID:IMSR JAX:028534). The *Ai9* mouse was a generous gift by Dr. Kevin Wright (Pomaville & Wright, 2023). *Tmem63b<sup>HA/HA</sup>* was a generous gift by Dr. Yun Stone Shi and previously published (Du *et al.*, 2020). The *Tmem63b<sup>fl/fl</sup>* mouse was acquired from EMMA (EM:07650) as frozen embryos and rederived at the Scripps Research. First generation mice were crossed to *Flp* (flippase) mice to excise the *LacZ* cassette but to retain the *loxP* sites that flank Exon 5 of *Tmem63b*. Genotyping with PCR detects the first *LoxP* site; forward primer: 5'-GTTCTTCATATTTTCAGGCTTCCTTGCTC, reverse primer: 5'-TGCAGTTCCAAAGATGACCAGCAG.

#### **2.4.2 Whole DRG dissections**

For ISH: Animals were perfused with phosphate buffered saline (PBS) followed by 4% Paraformaldehyde (PFA), and after extracting the spine DRGs were dissected and collected in PBS. After all DRGs were removed, the PBS was replaced with 4% PFA for overnight post-fix. After post-fix DRGs were washed with PBS and placed in 30% sucrose until they sunk or for at least 3 days. After cryoprotection in sucrose, DRGs were frozen in blocks of optimal cutting temperature (OCT) compound and sectioned in a Leica CM3050 S cryostat. 12-20  $\mu$ m sections were placed directly on slides that had been washed with RNAase-away.

For IHC: Dissections were conducted as described above, but DRGs were post-fixed for 30-45 minutes. Following sectioning, sections were placed directly on TOMO slides that were untreated and processed for staining (see below).

#### **2.4.3 Dissociated DRG cultures**

All mice were between the ages of 9-14 weeks old. For electrophysiology and basescope ISH, cervical, thoracic, and lumbar DRGs were extracted and collected into 1ml DMEM/F-12 media. After collection, 1 ml of 12.5mg/ml of collagenase IV (Gibco fisher scientific 17-104-019) predissolved in DMEM/F-12 was added. The DRGs were incubated for 1 hour and then were digested in papain (Worthington) at 10 units/ml for 30 minutes. DRGs were then mechanically dissociated with a fire polished glass Pasteur pipette. The DRG-containing solution was layered above a denser 1.5 mg/ml Bovine serum albumin (BSA) solution, which was made in DMEM/F-12 media with 10% serum. The DRG-BSA layered solution was centrifuged at 80 g for 10 minutes, the supernatant was removed, and the neurons were resuspended in DMEM/F-12 media with 10% serum growth medium supplemented with 100 ng/ml nerve growth factor (NGF), 50 ng/ml Glial cell line-derived neurotrophic factor (GDNF), 50 ng/ml Brain-derived neurotrophic factor (BDNF), 50 ng/ml Neurotrophin-3 (NT-3), 50 ng/ml Neurotrophin-4 (NT-4) and plated on coverslips for electrophysiology experiments or on Lab-Tek II chamber slide that have been treated with laminin.

#### ***2.4.4 In situ hybridization***

ISH on DRG cryosection was done following the RNAscope multiplex fluorescent assay kit user manual methods from ACDbio, using the 431531 probe for *Tmem63b* and the 400191-c2 probe for *Piezo2*. For each animal the same tissue was used on different slides to run the 3-plex negative control probes and matched by the opal channels used for our experimental probes. For *in situ* analysis of cultured DRGs, the BaseScope Detection Reagent Kit v2-Red user manual was used. Cultured cells were stained with either the positive, negative, or 1039041-C1 *Tmem63b* BaseScope probe. Immediately after BaseScope staining was completed, slides were

treated with blocking solution with PBS, 0.1% triton, and 10% donkey serum for 1 hour. Then IHC was performed with the Goat-tdTomato antibody and corresponding secondary antibody.

#### ***2.4.5 IHC***

Using a Pap Pen, a barrier was drawn around all DRG sections. Slides were incubated for 1 hour in permeabilization and blocking buffer (PBS, 0.2% triton, and 5% donkey serum). Primary antibodies were diluted in the same permeabilization and blocking buffer and added to incubate overnight at 4°C. The next day primary antibodies were removed, and slides were washed 3 times in PBS for 10 minutes or longer. Secondary antibodies diluted in permeabilization and blocking buffer and were added for 45 minutes at room temperature. After the secondary antibody solution was removed, the slides were washed 5 times with PBS, with the 2<sup>nd</sup> wash containing 1:5000 DAPI. Slides rested at room temperature until they were dry (1-2 hours), and then coverslips were mounted with Fluoromount-G with DAPI (Fisher 50-112-8966).

#### ***2.4.6 Primary antibodies***

**HA/TH staining:** Rabbit anti-HA Cell Signaling Technology #3724 1:250, sheep anti-tyrosine hydroxylase Sigma AB1542 1:1000.

**UCH-L1/tdTomato/DRGmarker:** Guinea pig anti UCH-L1 from Neuromics inc GP 1410450UL at 1:400, goat anti tdTomato OriGene Technologies AB8181-200 1:500, rabbit anti PV GeneTex GTX132759 1:150, rabbit anti TH 1:500 Sigma AB 152, and rabbit anti NF-200 1:1000 EMD Milipore ABN76.

#### ***Secondaries antibodies***

**HA/TH staining:** anti-rabbit IgG-Alexa Fluor 555 Biotium 20038 1:500, and anti-sheep Alexa Fluor 647 Jackson ImmunoResearch 713-605-003 1:500.

**UCH-L1/tdTomato/DRG-marker:** Anti-Guinea pig-cy3 Jackson ImmunoResearch 706-165-148 1:500, Anti-Goat IgG-Alexa Fluor 647 Jackson ImmunoResearch 705-605-003 1:500, and anti-Rabbit IgG-Alexa Fluor 488 Thermo Scientific R37118 2 drops per 1mL of permeabilization and blocking buffer (as per the manufacturer's instructions).

#### ***2.4.7 Imaging and analysis***

##### ***2.4.7.1 Tmem63b and tdTomato ISH and IHC***

**Imaging:** Images were taken on a BC43 Andor Spinning Disk Confocal using a 20X objective to obtain a montage of images and z-stacks of almost the entire culture of DRG neurons.

**Processing:** The montage of images was loaded into Imaris stitching software to make a single stitched image. That image was converted into an arivis file. An arivis pipeline was developed to process and analyze the image. Steps include denoising for all channels, and a background correction for the basescope channel with method: morphology, filter: Preserve bright objects: and radius 1.24  $\mu\text{m}$ . **Segmentation:** Part of the arivis pipeline uses a 'machine learning segmenter' that was trained by Aidan Berryman with previous images to generate 3-dimensional Regions of Interests (ROI) within tdTomato neurons. Then a blob finder is used to capture ROIs for the Basescope puncta. **Thresholding:** All blobs with 35% of their area in a tdTomato+ cell were counted as puncta. Before the final tally all blobs in the negative control stain within tdTomato neurons were measured for their mean fluorescence and a threshold was made using the 99<sup>th</sup> percentile of these negative blobs. That threshold was applied to the experimental blobs and any blob with a mean fluorescence below that threshold was discounted. Then each tdTomato+ cell had their blobs recorded and binned by the number of blobs.

### 2.4.7.2 *Tmem63b* and *Piezo2* ISH

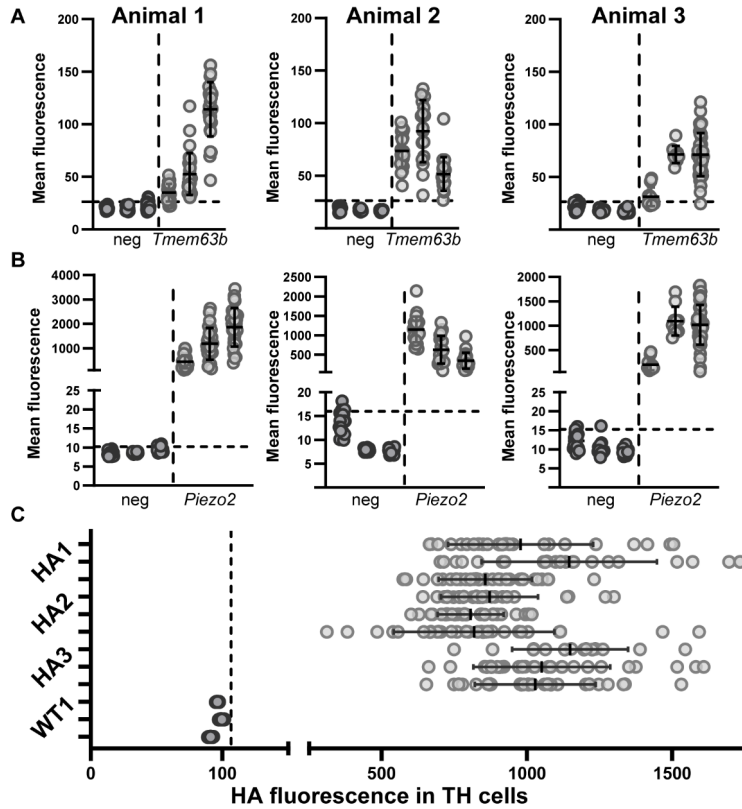


**Figure 2.6: Negative controls used to create threshold for ISH and IHC experiments.** **A:** Each tdTomato positive neuron's mean fluorescence from the *in situ* probes against *Tmem63b* and negative control probes across each section of DRG imaged for all three animals in the cohort. **B:** Same as above but *in situ* probe is for *Piezo2*. **C:** Mean fluorescence of HA antibody staining of TH positive DRG neurons in *Tmem63b*<sup>HA/HA</sup> vs *Tmem63b*<sup>WT/WT</sup>. Threshold made from the 99<sup>th</sup> percentile of mean fluorescence of HA staining from *Tmem63b*<sup>WT/WT</sup> DRG used as a cut off for *Tmem63b*<sup>HA/HA</sup> HA staining. Bars represent mean  $\pm$  S.D.

**Imaging:** Following RNAscope, Z-stack images were taken on a ApoTome2 Zeiss Microscope, tdTomato was imaged using its natural fluorescence. **Processing:** Images were processed in Zen Lite by clicking on the ApoTome tab and creating a new image using optical sectioning. The stack was then opened in Fiji where a central z-slice was selected for analysis. **Segmentation:** ROIs were created by using the wand tool (mode set to legacy, tolerance set to 331), and clicking on tdTomato+ cells. Within each ROI the mean intensity of pixels in the ISH channels was recorded. This analysis was the same for all RNAscope images including the negative controls. **Thresholding:** The mean fluorescence from the negative controls was used to create a threshold to determine if a cell expresses *Tmem63b* or *Piezo2*. For each animal all the tdTomato+ cells' mean fluorescence in the negative control c1 and c2 channels was recorded to calculate the 95<sup>th</sup> percentile. The 95<sup>th</sup> percentile calculated for each animal was used as threshold for the



corresponding channel from that animal i.e. if the 95 percentile for the c1 channel in animal 1 was 22 any cells from that corresponding channel, *Tmem63b*, in the experimental group that falls below 22 were determined not to express *Tmem63b* (**Figure 2.6A-B**).

#### **2.4.7.3 HA and TH IHC**

**Imaging:** Images were taken on a BC43 Andor Spinning Disk Confocal with a 20X objective with z-stacks encompassing the entire slice. Each animal had 3 image stacks recorded.

**Segmentation:** Analysis was done in Imaris where surfaces were created in the TH channel that represented each TH positive cell. **Thresholding:** The mean fluorescence of TMEM63B-HA within each surface was exported to excel. In prism the 99<sup>th</sup> percentile was calculated using all the values for the mean fluorescence of the TMEM63B-HA channel within TH positives cells from a *Tmem63b*<sup>WT/WT</sup> animal. That 99<sup>th</sup> percentile was used as a threshold for TMEM63B-HA staining. If a TH cell had a mean fluorescence above that threshold it was counted as TMEM63B-HA positive cell (**Figure 2.6.C**).

#### **2.4.7.4 *Vglut3<sup>cre</sup>;Ai9* IHC**

**Imaging:** Images were taken on a ApoTome2 Zeiss Microscope. **Processing:** Images were processed in Zen Lite by clicking on the ApoTome tab and creating a new image using optical sectioning. Images were then imported into Imaris. **Segmentation:** Using the surface function and some customization, a unique surface program was created for each stain (*i.e.*, the TH stain and NF stain had different parameters). Parameters remained constant within an animal but were adjusted slightly between animals. The UCH-L1 surfaces were generated first for every image, and then those surfaces were deleted by hand if they did not correspond to a cell. Then the surfaces for the other markers were generated and any surface that did not overlay with the UCH-L1 surfaces was deleted by hand. **Thresholding:** Using the coloc function a new channel

was created that consisted of the overlap between tdTomato and the DRG subtype marker used, with the intensity for each channel staying consistent within animals. A surface was created for that channel as the overlap between the two. Surfaces were then tallied and recorded for analysis in GraphPad (**Figure 2.4C**).

#### **2.4.8 Electrophysiology**

Extracellular Solution: NaCl 133 mM, KCl 3 mM, CaCl<sub>2</sub> 2.5 mM, MgCl<sub>2</sub> 1 mM, HEPES 10 mM, Glucose 10 mM, pH adjusted to 7.3 with NaOH, then osmolarity adjusted, if necessary, with Mannitol solution to 310 mOsm. Intracellular solution: KCl 133 mM, EGTA 5 mM, CaCl<sub>2</sub> 1 mM, MgCl<sub>2</sub> 1 mM, HEPES 10 mM, pH adjusted to 7.3 with KOH, then osmolarity adjusted, if necessary, with Mannitol solution to 300 mOsm. Prior to use, Mg-ATP is added at 4 mM and Na-GTP is added at 0.4 mM. Patch pipettes were made from borosilicate glass O.D.:1.5 mm I.D.:0.86 mm pulled on a Sutter P-97 puller and polished with a microforge MF-830.

To identify C-LTMRs in dissociated DRG neuronal cultures we used tdTomato and small cell soma size. Soma size allowed us to distinguish C-LTMRs from the ~13% of larger diameter non-CLTMR neurons labelled by tdTomato in the *Vglut3<sup>Cre</sup>;Ai9* line (Seal *et al.*, 2009). To confirm that we could reliably identify C-LTMRs based on their small soma size, we turned to the inherent electrical properties of C-LTMRs defined by their wide action potential. Most DRG neurons have action potentials with sub-millisecond half-widths, whereas C-LTMRs have action potentials with a half-width wider than 1.5 ms (Zheng *et al.*, 2019). Indeed, the mean half-width of an action potential recorded from the tdTomato+ neurons was  $3.07 \pm 0.63$  ms (N= 17) as reported in **Figure 2.4A and C**.

Whole-cell patch clamp: Currents were recorded in whole-cell voltage clamp mode using Axopatch 200b amplifier (Molecular devices) sampled at 10 Hz and filtered at 2 kHz. Pipettes

used were between 1.7-4.5 M $\Omega$ . Cells for patching were chosen based on their tdTomato fluorescence and small soma size. Cells were held at -60mV and were stimulated by a blunt glass probe positioned at an angle  $\sim 80^\circ$  with a piezo-electric crystal microstage (E625 LVPZT Controller/Amplifier; Physik Instrumente). The probe was typically positioned  $\sim 1$ -2  $\mu\text{m}$  from the cell body, stimulus duration was 400 ms and steps were applied at an increment of 1  $\mu\text{m}$  per sweep.

Outside-out patch clamp: Set up for outside-out recording was same as whole-cell patch clamp recordings. Stretch-activated currents in the outside-out patch was induced by applying positive pressure to the excised membrane patch with a High-Speed Pressure Clamp 2-SB by ALA science. Pressure stimulus duration was for 1 sec, and steps were applied at increments of 10 mmHg per sweep.

Current clamp experiments: Currents were recorded in whole-cell current-clamp mode using Axopatch 200b amplifier (Molecular devices) sampled at 10 Hz and filtered at 2 kHz. Neurons were recorded in the extracellular bath solution. Pipettes used were between 3-6 M $\Omega$ . After a giga-ohm seal was formed, pipette capacitance was offset. Current was injected into the soma to maintain a membrane potential of 60  $\pm$  5 mV. In rheobase recordings, a 20 pA step stimulus was applied for 200 ms, every 10 seconds until a cell fired an action potential. Membrane resistance was calculated using Ohm's law with data from the rheobase recordings. The amount of injected current, average resting membrane potential prior to the current stimulus, and average change in membrane voltage during current stimulus were recorded and these values were used to calculate membrane resistance. Half width was measured from action potentials elicited at a saturating stimulus of 400 pA for 200 ms. Cells were excluded from analysis if, after forming a giga-ohm seal the break-in resting membrane potential of a cell was above -40 mV, or

if during rheobase recordings the cells failed to elicit an action potential past 0 mV after applying more than 400 pA of current, or if more than 100 pA of current was injected during recordings to maintain membrane potential of  $60 \pm 5$  mV.

All electrophysiology data was analyzed in Clampfit11.1 and GraphPad Prism.

## Chapter 3 Investigating MA currents of cells over expressing of *Piezo2* and *Tmem63b*

### 3.1 Introduction:

MA ion channels may have a unique relationship with one another because they use the same substrate for activation. As mentioned in Chapter 1, channels that can open in the force-from-lipid model directly interact with lipids to transfer energy felt on the membrane into protein movements (Kefauver *et al.*, 2020). That transfer of energy could affect how mechanical stimuli are felt by other MA ion channels by dissipating the force on the membrane. Voltage gated channels are similar and exert miniscule but measurable voltage change to the membrane during activation (Bezanilla, 2018). PIEZO1/2 have the most transmembrane domains of any protein, and their effect on the membrane generates a footprint of 100-250 nm in area depending on the environment (Haselwandter *et al.*, 2022). It was hypothesized that PIEZO channels' large domed structure flattens during activation easing pressure on other PIEZO ion channels (Guo & MacKinnon, 2017; Lin *et al.*, 2019). However, one experiment showed that no matter how densely PIEZO1 ion channels were packed, there was no change to their responses to force (Lewis & Grandl, 2021). This experiment suggests PIEZO1 is more like voltage sensing channels in that their activation movements generate an opposite force that is much smaller than the force that activated them.

The large size and dome of PIEZO ion channels present the opportunity for smaller MA ion channels to be affected by PIEZO activation. Recent experiments showed that PIEZOs can increase the magnitude of MA currents from TREK1 (Glogowska *et al.*, 2021). This study co-expressed *Kcnk2* (TREK1) with *Piezo1* and showed TREK1 MA currents increased substantially (Glogowska *et al.*, 2021). Follow-up studies investigated the mechanism by which PIEZO1 causes this effect by using a mutant *Piezo1*<sub>RE-CC</sub> that could be locked in a closed confirmation by

cystine-cystine interactions (Lewis *et al.*, 2024). This closed mutant PIEZO1 did not increase TREK1 currents until the addition of reducing agent dithiothreitol (DTT) that allowed Piezo1<sub>RE-CC</sub> to open demonstrating that PIEZO1 opening was responsible for potentiating TREK1. One possibility is that PIEZO1 physically interacts with TREK1 however, the study found no evidence of a direct interaction between PIEZO1 and TREK1. This suggests that PIEZO1 could be signaling through an intermediary protein or the TREK1 channel can sense changes in the large membrane footprint of the PIEZO1 ion channel. Whether PIEZO2 alters the currents of other MA ion channels remains an open question. My goal was to test if PIEZO2 could alter TMEM63B activation.

Given the expression patterns and electrophysiological results we observed in C-LTMRs, it seemed likely that, if a PIEZO protein was altering TMEM63b, it was PIEZO2. HA staining in the *Tmem63b*<sup>HA/HA</sup> mouse showed that TMEM63B is present in many DRG neurons, and ISH demonstrated that *Piezo2* and *Tmem63b* are co-expressed in not just in C-LTMRs, but in other DRG neurons as well (**Figure 2.3**). DRG neurons are not the only cells in the body that co-express these channels; bladder endothelial cells, and outer hair cells have PIEZO2 and TMEM63B (Wu *et al.*, 2017; Du *et al.*, 2020; Marshall *et al.*, 2020; Lee *et al.*, 2024). Understanding whether these two proteins function independently or together will have implications for cell types outside of DRG neurons, and it is possible their synergy confers a cell with a unique response to force.

### **3.2 Results: Indentation currents of cells co-expressing of *Piezo2* and *Tmem63b***

To examine the MA currents of cells that co-express *Piezo2* and *Tmem63b*, I used HEK P1KO. I transfected the HEK P1KO cells with plasmids that encoded each MA ion channel followed by an *IRES*-sequence then a sequence that encodes the fluorescent proteins eGFP or

mCherry; in the case of PIEZO2 only controls, the *Tmem63b* plasmid was substituted for one with a fluorescent reporter alone. By patching cells with eGFP and mCherry and indenting cells while in whole cell patch clamp-mode, I recorded MA currents from cells overexpressing either *Piezo2* alone or co-expressing *Piezo2* and *Tmem63b* (**Figure 3.1A**). I ran two different protocols, one where I increased the poke stimulation by 1 micron each sweep, or I repeated the same stimulation multiple times (**Figure 3.1A, Figure 3.2A**). Furthermore, because PIEZO2 inactivation is slowed by high membrane voltage, I poked cells during 20 mV steps to examine if TMEM63B altered this effect on PIEZO2.

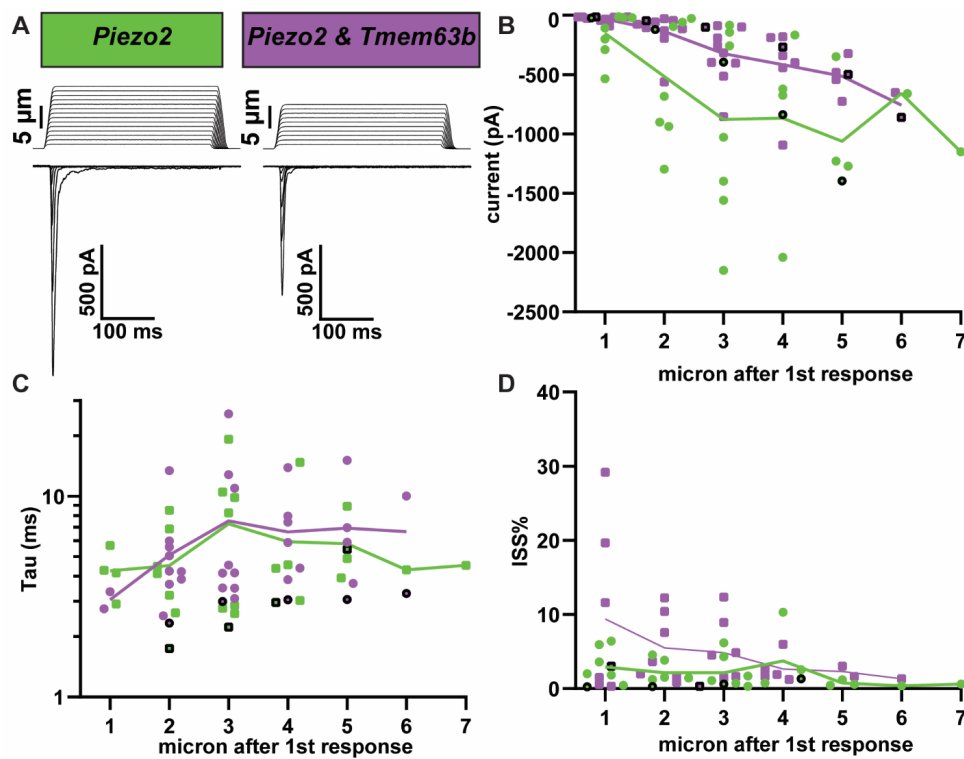


**Figure 3.1: Indentation responses of HEK P1KO cells expressing *Piezo2* alone or alongside *Tmem63b*.** **A:** Representative trace of indentation-induced currents at increasing forces in HEK P1KO cells overexpressing *Piezo2* (green) alone or co-expressing *Piezo2* and *Tmem63b* (purple). Black dots indicate the example trace's corresponding measurement. **B:** Maximum current response of increasing stimulation steps starting at the 1<sup>st</sup> responses until the cell popped, line mean response for each group (*Piezo2*; N=8, Co-express; N=10). **C:** Inactivation kinetics plotted on log<sub>10</sub> axis, line mean response for each group (*Piezo2*; N=8, Co-express; N=10). **D:** Steady state current taken as a percentage of the peak current, line mean response for each group (*Piezo2*; N=7, Co-express; N=9). Multiple unpaired t-test with Welch's correction.

**Table 3.1: Multiple t-test for each micron after threshold for maximum current.**

Significance	Micron	P value	Mean of Piezo2	Mean of Piezo2 & Tmem63b	Difference	SE of difference	t ratio	df	q value
No	1	0.109419	-150.5	-29.72	-120.7	66.10	1.826	7.185	0.138142
No	2	0.072308	-514.7	-135.5	-379.2	183.7	2.065	8.125	0.138142
No	3	0.085160	-876.9	-321.9	-554.9	282.9	1.962	8.066	0.138142
No	4	0.234420	-867.4	-415.9	-451.5	335.5	1.346	5.166	0.236764
No	5	0.103407	-1061	-513.2	-547.8	248.6	2.204	3.434	0.138142
	6		-660.0	-756.1	96.14				
	7		-1150						

**Table 3.2: Multiple t-test for each micron after threshold for tau of inactivation.**

Significance	Micron	P value	Mean of Piezo2	Mean of Piezo2 & Tmem63b	Difference	SE of difference	t ratio	df	q value
No	1	0.134644	4.257	3.052	1.205	0.6428	1.875	3.971	0.67995
No	2	0.675152	4.513	5.09	-0.5773	1.35	0.4275	14.82	0.946579
No	3	0.937207	7.292	7.541	-0.2495	3.118	0.0800	15.98	0.946579
No	4	0.796319	5.931	6.635	-0.7037	2.625	0.2681	7.02	0.946579
No	5	0.652117	5.795	6.943	-1.148	2.417	0.4751	5.786	0.946579
	6		4.297	6.661	-2.364				
	7		4.536						

**Table 3.3: Multiple t-test for each micron after threshold for steady state percentage.**

Significance	Micron	P value	Mean of Piezo2	Mean of Piezo2 & Tmem63b	Difference	SE of difference	t ratio	df	q value
No	1	0.184689	2.930	9.405	-6.475	4.371	1.481	6.582	0.295981
No	2	0.111158	2.156	5.494	-3.337	1.857	1.797	7.759	0.295981
No	3	0.176808	2.142	4.865	-2.723	1.857	1.467	8.919	0.295981
No	4	0.672260	3.751	2.666	1.086	2.377	0.4566	3.890	0.678982
No	5	0.234440	0.7452	2.335	-1.590	0.7234	2.198	1.220	0.295981
	6		0.3959	1.330	-0.9338				
	7		0.6316						

PIEZO2 currents are still present in HEK P1KO cells co-expressing *Tmem63b* (**Figure 3.1A**). When these currents are aligned by the first response there was no difference between the maximum currents (**Figure 3.1B**). The response properties are unaltered in the co-expressing cells. The tau of inactivation and the percentage of steady state current compared to the max current is the same in *Piezo2* and co-expressing cells at each micron after the first response (**Figure 3.1C-D**). These results suggest that PIEZO2 is not modulated by TMEM63B at different indentation steps. When I ran the repeated stimulation protocol, there were no changes in the



inactivation time or the amount of steady state current (**Figure 3.2C-D**). Co-expression of *Piezo2* and *Tmem63b* did not alter MA currents in HEK P1KO cells.

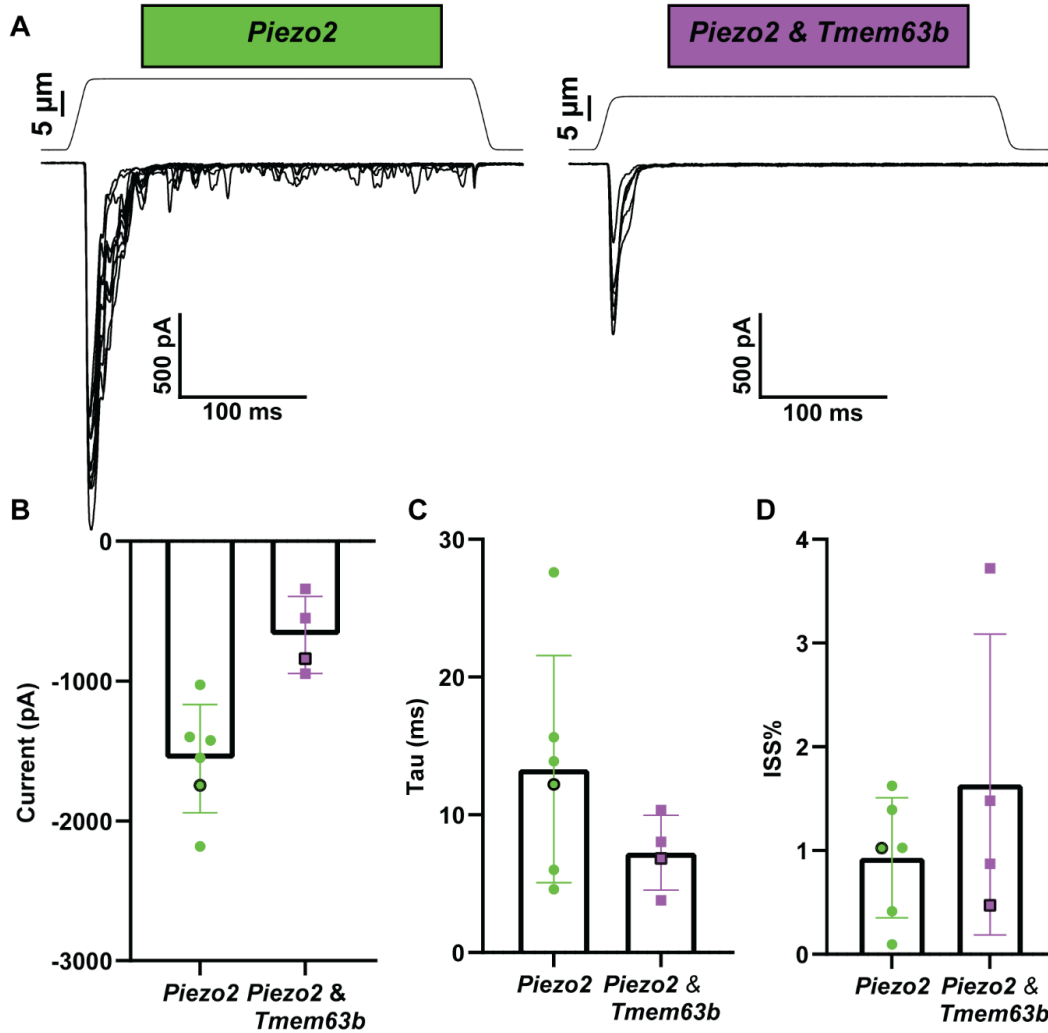


**Figure 3.2: Repeated stimulation of HEK P1KO cells expressing *Piezo2* alone or alongside *Tmem63b*.** **A:** Representative trace of repeated indentation-induced currents in HEK P1KO cells overexpressing *Piezo2* (green) alone or co-expressing *Piezo2* and *Tmem63b* (Purple). Black outlines indicate the example trace's corresponding measurement. **B:** Maximum current response of the mean response after repeating the same indentation force (*Piezo2*;  $-1555 \pm 387.4$  pA, N=6, *Piezo2 & Tmem63b*;  $-670.1 \pm 276.4$  pA, N=4, Unpaired t-test  $p = 0.004$ ). **C:** Inactivation kinetics plotted (*Piezo2*;  $13.3 \pm 8.2$  ms, N=6, *Piezo2 & Tmem63b*;  $7.2 \pm 2.7$  ms, N=4, Unpaired t-test  $p = 0.2$ ). **D:** Steady state current taken as a percentage of the peak current (*Piezo2*;  $0.93 \pm 0.58$  %, N=6, *Piezo2 & Tmem63b*;  $1.6 \pm 1.4$  %, N=4, Unpaired t-test  $p = 0.3$ ). Mean  $\pm$  S.D.

Because PIEZO2's MA currents are modulated by voltage, I repeated these co-expression experiments at different voltages (Coste *et al.*, 2010). I found no changes in reversal potential, an expected result given both channels are non-selective cation channels (**Figure 3.3B-C**) (Coste *et al.*, 2010; Murthy *et al.*, 2018a). Co-expressing cells had slower inactivation at positive voltages that were similar in speed to cells expressing *Piezo2* alone (**Figure 3.3D**). Expression of *Tmem63b* alongside *Piezo2* in HEK P1 KO cells does not alter MA currents.

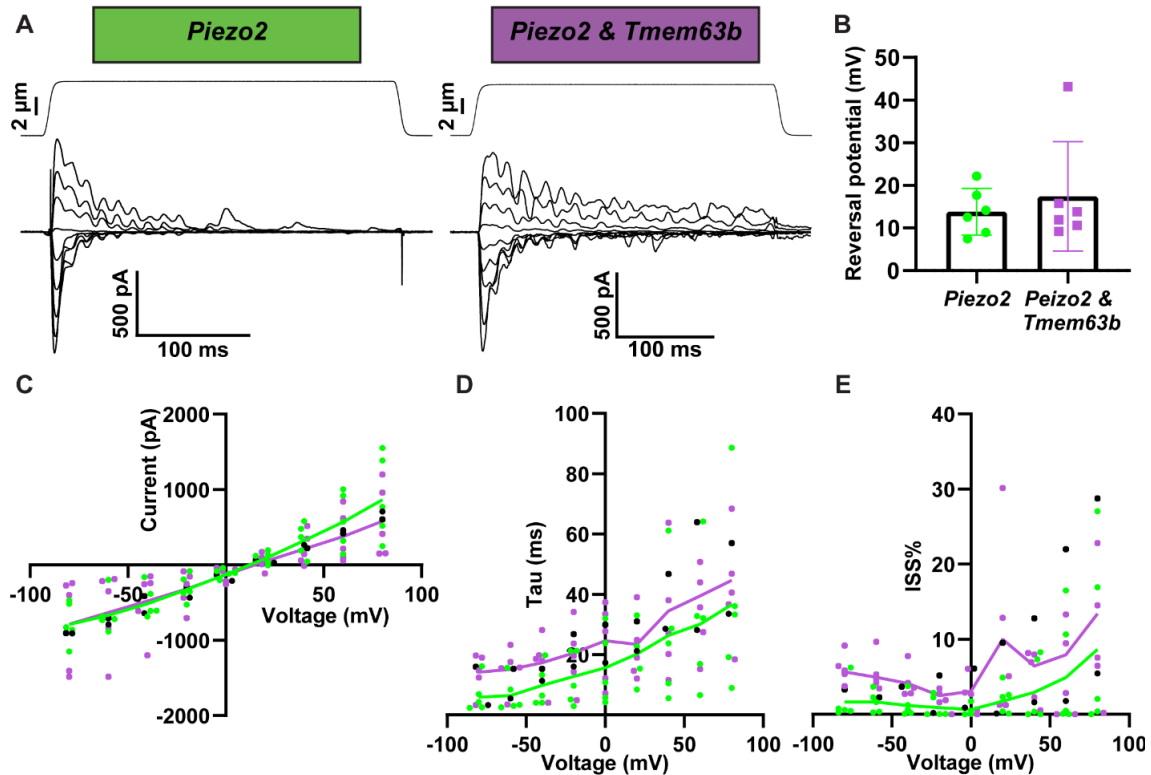


**Figure 3.3: Indentation responses of HEK P1KO cells expressing *Piezo2* alone or with *Tmem63b* at different voltages.** **A:** Representative trace of indentation-induced currents in HEK P1KO cells overexpressing *Piezo2* alone or co-expressing *Piezo2* and *Tmem63b* with voltage steps of 20 mV starting at -80 mV. **B:** Reversal potential calculated by a linear regression using the maximum current of the two sweeps where the polarity of the current flips (*Piezo2*;  $13.8 \pm 5.5$  pA N=6, *Piezo2* & *Tmem63b*;  $17.4 \pm 12.8$  pA, N=6, Unpaired t-test  $p = 0.5$ ). **C:** Maximum current response at each voltage step, line mean response for each group (*Piezo2*; N=6, *Piezo2* & *Tmem63b*; N=7). **D:** Inactivation kinetics plotted on log<sub>10</sub> axis, line mean response for each group (*Piezo2*; N=6, *Piezo2* & *Tmem63b*; N=7). **E:** Steady state current taken as a percentage of the peak current, line mean response for each group (*Piezo2*; N=6, *Piezo2* & *Tmem63b*; N=7). Mean  $\pm$  S.D.

**Table 3.4: Multiple t-test for each volage step for maximum current.**

Significance	mV	P value	Mean of Piezo2	Mean of Piezo2 & Tmem63b	Difference	SE of difference	t ratio	df	q value
No	-80	0.029857	5.898	14.16	-8.261	3.256	2.537	9.834	0.135701
No	-60	0.026807	6.384	15.11	-8.726	3.330	2.620	9.420	0.135701
No	-40	0.096531	9.773	17.28	-7.509	4.072	1.844	9.496	0.292490
No	-20	0.172015	12.73	20.54	-7.812	5.287	1.478	9.464	0.374316
No	0	0.205894	15.62	24.62	-9.000	6.647	1.354	9.880	0.374316
No	20	0.590954	20.16	23.43	-3.269	5.864	0.5574	8.938	0.596864
No	40	0.479850	26.34	34.52	-8.172	11.13	0.7339	9.992	0.596864
No	60	0.399244	30.09	39.47	-9.378	10.64	0.8811	9.854	0.596864
No	80	0.561599	36.61	44.63	-8.021	13.27	0.6043	8.400	0.596864

**Table 3.5: Multiple t-test for each volage step for tau of inactivation.**

Significance	mV	P value	Mean of Piezo2	Mean of Piezo2 & Tmem63b	Difference	SE of difference	t ratio	df	q value
No	-80	0.029502	5.898	14.16	-8.261	3.256	2.537	10.00	0.134089
No	-60	0.025586	6.384	15.11	-8.726	3.330	2.620	10.00	0.134089
No	-40	0.094948	9.773	17.28	-7.509	4.072	1.844	10.00	0.287694
No	-20	0.170316	12.73	20.54	-7.812	5.287	1.478	10.00	0.373676
No	0	0.205542	15.62	24.62	-9.000	6.647	1.354	10.00	0.373676
No	20	0.595229	20.16	23.43	-3.269	5.935	0.5507	9.000	0.601182
No	40	0.479837	26.34	34.52	-8.172	11.13	0.7339	10.00	0.601182
No	60	0.398945	30.09	39.47	-9.378	10.64	0.8811	10.00	0.601182
No	80	0.559095	36.61	44.63	-8.021	13.27	0.6043	10.00	0.601182

**Table 3.6: Multiple t-test for each volage step for tau of inactivation.**

Significance	mV	P value	Mean of Piezo2	Mean of Piezo2 & Tmem63b	Difference	SE of difference	t ratio	df	q value
No	-80	0.019422	1.660	5.649	-3.989	1.405	2.839	9.000	0.088272
No	-60	0.029973	1.641	4.952	-3.312	1.286	2.574	9.000	0.090819
No	-40	0.019301	1.179	4.123	-2.944	1.035	2.843	9.000	0.088272
No	-20	0.107759	0.9018	2.484	-1.582	0.8954	1.767	10.00	0.163255
No	0	0.074240	0.6388	3.072	-2.434	1.205	2.019	9.000	0.163255
No	20	0.096590	1.749	10.02	-8.267	4.509	1.834	10.00	0.163255
No	40	0.173048	2.932	6.442	-3.510	2.392	1.467	10.00	0.224715
No	60	0.523133	4.915	7.930	-3.016	4.558	0.6617	10.00	0.528364
No	80	0.468103	8.646	13.39	-4.739	6.283	0.7542	10.00	0.528364

### 3.3 Discussion:

Whole-cell indentation responses of TMEM63B and PIEZO2 currents were unchanged by co-expression. If either channel had an increase in open probability, conductance, or altered kinetics, when co-expressed with the other, there would be a difference in one of the electrophysiological metrics between groups. The current I recorded in both groups was similar

to PIEZO2 currents in overexpressed cells, and because TMEM63B does not produce indentation-induced currents on its own, it is unlikely that TMEM63B was contributing to currents in the co-expressing cells (Coste *et al.*, 2010; Murthy *et al.*, 2018a). If PIEZO2 did cause TMEM63B to respond to indentation it would be hard to separate the TMEM63B currents from the PIEZO2 currents.

If TMEM63B and PIEZO2 were both contributing the MA currents, using a non-conducting PIEZO2 protein would be the only way to isolate TMEM63B currents. Changing the holding potential (voltage) to isolate current from different ions, a method used in studies with TREK1 and PIEZO1, does not work in the present experiments because both channels are non-selective cation currents (Glogowska *et al.*, 2021). There are no specific blockers for TMEM63B or PIEZO2 and known blockers like ruthenium red block both channels. Generating a non-conducting PIEZO2-mutant could reveal any currents PIEZO2 is masking. However, it is hard to disentangle if a protein is non-conducting a still opening vs no longer moving into an open state. For example the Piezo1<sub>RE-CC</sub> mutant does not conduct because it cannot move into an open conformation (Lewis *et al.*, 2024). If the hypothetical non-conducting PIEZO2 does not move into an open conformation, but an open conformation is required to signal to TMEM63B, similar to the TREK1-PIEZO1 affect, then it would not be a useful tool (Lewis & Grandl, 2020; Lewis *et al.*, 2024). The Piezo1<sub>RE-CC</sub> mutant has two residues mutated to cysteine that are strategically placed on PIEZO1 to form disulfide bonds to prevent PIEZO1 from opening unless a reducing agent is present. Lewis *et al.*, 2024 used Piezo1<sub>RE-CC</sub> to show that TREK1 was not modulated by the mere presence of PIEZO1 but by the conformational changes that PIEZO1 undergoes during opening. Lewis *et al.*, 2024 recorded TREK1 currents in the presence and absence of the reducing agent dithiothreitol (DTT) and found only when Piezo1<sub>RE-CC</sub> could move were TREK1

currents increased. If TMEM63B and PIEZO2 have a similar relationship, then a non-conducting PIEZO2 ion channel will only be a useful tool if PIEZO2 still opens in response to force. Even though my experiments did not reveal a unique MA current in cells co-expressing *Piezo2* and *Tmem63b*, it is possible that in endogenous cells that co-express these channels there are proteins or lipid environments that facilitate a unique interaction that I was unable to recreate in HEK P1KO cells.

### **3.4 Methods:**

#### **3.4.1 Cell culture**

HEK P1KO cells were acquired from Ardem Patapoutian's lab at Scripps Institute (Dubin *et al.*, 2017). Splitting cells: Old media was aspirate out of the flask and then warm (37C°) PBS was added, 10 mL for T-75, 5 ml for T-25. After a 2–3-minute incubation the PBS was aspirated then 0.05% Trypsin-EDTA was added, 1 mL for T-75, 500 uL for T-25. Trypsin-EDTA incubated for 5 minutes and then then flask is rocked gently to monitor cell detachment. Gibco Dulbecco's Modified Eagle Medium (DMEM) media to flask along the bottom to remove cells 9 mL for T-75, 4.5 ml for T-25. The media/cell/trypsin solution was then pipetted into new flasks and diluted with more fresh media to achieve required cell dilution or confluency.

Coverslip coating with poly-D-Lysine: Done primarily by Aidan Berryman (AB) in the lab the following is a paragraph adapted from her protocol: 5 mg of poly-lysine was dissolved in 50 mL of sterile tissue culture grade water. Then one VWR 12mm circle No. 2 coverslip is added to each well of a 24-well plate. Each coverslip is coated with the poly-lysine solution ~100µL. After 5 minutes, the solution is removed by aspirating. Each cover slip is rinsed with 100µL of sterile water three times. The plate is then left in the tissue culture hood for 2 hours before introducing cells and medium. Once coated with PDL store coverslips at 4° C.

Transfection: 50  $\mu$ L of OptiMEM was mixed with .5  $\mu$ L of Lipofectamine 2000 per-well in test tube. Then another 50  $\mu$ L of OptiMEM was mixed 1000 ng of DNA plasmid per-well. Both reactions were incubated for 5 minutes and then mixed. The new mixture was incubated for 20 minutes. During that incubation coverslips coated in poly-D-Lysine were added to a 24 plate and each well was filled with 1 mL of fresh DMEM media. Then cells were split and 15-25  $\mu$ L of concentrated cells were added to wells with media. At the end of the transfection mix incubation 100  $\mu$ L is added to each well. All cells were transfected with a total of 1000 ng of DNA. Co-expressing cells were transfected with two plasmids one encoding *Piezo2* (500ng) and GFP and the other for *Tmem63b* (500 ng) and mCherry.

### ***3.4.2 Electrophysiology***

**Increasing stimulation:** Cells were held at -80mV, and indentation steps were applied at an increment of 1  $\mu$ m per sweep for 300 ms

**Repeated stimulation:** Cells were held at -80mV, and indentation steps were applied at an increment of 1  $\mu$ m per sweep. Once the cell responded for 3-6 sweeps the increasing protocol was stopped. Then a repeated protocol was started by repeatedly indenting the cell at furthest micron from the previous recording for 4-5 sweeps.

**Voltage Steps:** Cells were held at 0 mV. During the recording protocol there was a 1 second voltage step, the first step was to -80 mV and increased 20 mV each sweep. 400ms into the voltage step the blunt glass probe indented the cell for 300 ms. The distance of the probe was determined by a previous 'increasing stimulation' protocol that stopped at the first response above 50 pA. 3 microns were added to that distance and used for that cell; each cells distance of indentation was unique.

Analysis: All electrophysiology data was analyzed in Clampfit11.1 and GraphPad Prism.

Extracellular Solution: NaCl 133 mM, KCl 3 mM, CaCl<sub>2</sub> 2.5 mM, MgCl<sub>2</sub> 1 mM, HEPES 10 mM, Glucose 10 mM, pH adjusted to 7.3 with NaOH, then osmolarity adjusted, if necessary, with Mannitol solution to 310 mOsm.

Intracellular solution: CsCl 133 mM, EGTA 5 mM, CaCl<sub>2</sub> 1 mM, MgCl<sub>2</sub> 1 mM, HEPES 10 mM, pH adjusted to 7.3 with CsOH, then osmolarity adjusted, if necessary, with Mannitol solution to 300 mOsm. Prior to use, Mg-ATP was added at 4mM and Na-GTP was added at 0.4mM. Patch pipettes were made from borosilicate glass O.D.:1.5mm I.D.:0.86mm pulled on a Sutter P-97 puller and polished with a microforge MF-830.

Whole-cell patch clamp: Currents were recorded in whole-cell voltage clamp mode using Axopatch 200b amplifier (Molecular devices) sampled at 10 Hz and filtered at 2 kHz. Pipettes used were between 1.7-4.5 MΩ. Cells for patching were chosen based on fluorescence of both plasmid reporter fluorophores GFP and mCherry. Indentation stimulation was done using a blunt glass probe positioned at an angle ~80° with a piezo-electric crystal microstage (E625 LVPZT Controller/Amplifier; Physik Instrumente). The probe was typically positioned ~1-2 μm from the cell body stimulus duration was 400ms.

## Chapter 4 Discussion

A major aim of my thesis was to characterize TMEM63B's role in C-LTMRs. *Tmem63b* and *Piezo2* are co-expressed in C-LTMRs and other neuronal subtypes in the DRG that remain undefined (**Figure 2.3A**). I used the *Vglut3<sup>Cre</sup>* mouse line to drive *Cre* expression in C-LTMRs. Using *Cre* dependent tdTomato I showed that *Cre* was expressed specifically and efficiently in the C-LTMR population (**Figure 2.1**). The *Vglut3<sup>Cre</sup>; Ai9* line allowed me to patch tdTomato+ C-LTMRs in culture where I recorded indentation and stretch activated MA currents. All C-LTMRs labeled by *Vglut3<sup>Cre</sup>; Ai9* had indentation currents; the inactivation constants of these currents were above 30 ms, which is considered an SA current (**Figure 2.4B-F**). Stretch induced currents were non-inactivating and had a mean P<sub>50</sub> of 38.28 mmHg (**Figure 2.4G-I**). Together, these results show that C-LTMRs have active MA ion channels in culture, but I was unable to tease apart the identity of the ion channel(s) contributing to these currents. I bred *Vglut3<sup>Cre</sup>; Ai9; Tmem63b<sup>fl</sup>* mice to generate cKO *Tmem63b* in C-LTMRs. However, staining experiments showed that *Vglut3<sup>Cre</sup>; Ai9; Tmem63b<sup>fl</sup>* mice had only a small reduction in *Tmem63b* transcript within tdTomato+ neurons compared to *Tmem63b<sup>wt</sup>* mice (**Figure 2.5C**). In separate experiments, I attempted to generate *Piezo2* cKO mice, by crossing *Vglut3<sup>Cre</sup>; Ai9* line with *Piezo2<sup>fl/fl</sup>* line (*Piezo2<sup>fl</sup>*) and double cKO of *Piezo2* and *Tmem63b* by combining *Piezo2<sup>fl</sup>* and *Tmem63b<sup>fl</sup>* (dbl-cKO). The *Piezo2<sup>fl</sup>* had intact *Piezo2* transcript in all but one tdTomato+ neuron, and thus recording indentation currents in cells from these cKO mice showed no differences



compared to currents from WT *Vglut3<sup>Cre</sup>; Ai9* mice (**Figure 4.4**). The *Vglut3<sup>Cre</sup>; Ai9* labeled the C-LTMR population well, but it failed to generate cKO mice.

To understand if TMEM63B is modulated by PIEZO2 like TREK1 is modulated by PIEZO1 I tested the effect of co-expression of *Piezo2* and *Tmem63b* in HEK P1KO cells. In chapter 3, I recorded from HEK P1KO cells transfected with *Piezo2* alone or co-expressed with *Tmem63b*. Indentation currents from both groups were large, inactivated quickly, and had a small steady state (**Figure 3.1**). These currents were like PIEZO2-indentation currents reported in previous studies (Coste *et al.*, 2010). In the repeated stimulus protocol, there was no difference in the MA currents between the *Piezo2* expressing cells and *Tmem63b* and *Piezo2* co-expressing cells (**Figure 3.2**). To determine whether co-expression caused a voltage dependent effect, I changed the holding potential while using the repeated stimulus protocol, but the current in both groups retained their PIEZO2-like shape (**Figure 3.3**). Thus, in HEK P1KO cells, combined heterologous expression of *Piezo2* and *Tmem63b* does not change the indentation MA current responses of TMEM63B or PIEZO2.

#### 4.1 MA currents in cultured DRG neurons.

A long-standing hypothesis in somatosensation is that multiple MA ion channels are responsible for the MA currents in cultured DRG neurons. MA currents from DRG neurons can be binned by their inactivation kinetics as RA, IA, and SA. Using *Cre*-lines to cKO of *Piezo2* in all subtypes of DRG neurons supported this hypothesis because researchers found a significant reduction in the percentage of neurons with RA and IA currents (Ranade *et al.*, 2014; Murthy *et al.*, 2018b). One limitation of these recordings was that they were conducted on the entire DRG population with no way to identify subtypes. Experiments like Zheng *et al.*, 2019 examined the MA currents of distinct LTMRs subtypes, all of which express *Piezo2*, and they found these

subtypes predominantly have RA currents (Zheng *et al.*, 2019; Sharma *et al.*, 2020). The only exception was C-LTMRs, which had slowly inactivating currents, aligning with my indentation recordings (**Figure 2.4E**). C-LTMRs have both a high level of *Piezo2* expression, and SA currents indicating that there could be a role for PIEZO2 in SA currents. Another explanation could be that a different MA ion channel(s) is driving the MA current in C-LTMRs. It could be the same MA ion channel(s) that initiates  $\text{Ca}^{2+}$  responses to noxious stimuli, which persist in *Piezo2* cKO mice (Von Buchholtz *et al.*, 2021).

#### 4.1.1 Further studies on SA currents in C-LTMRs.

To address how C-LTMRs have SA currents I tested whether PIEZO2 modulated TMEM63B or whether TMEM63B and PIEZO2 function independently as MA channels in C-LTMRs, with the hypothesis that either option could explain the SA MA currents observed in C-LTMRs. For these experiments I needed a tool to identify C-LTMRs in dissociated cultures of DRG neurons. We chose to use a mouse with specific expression of *Cre* in C-LTMRs. However, the *Vglut3<sup>Cre</sup>* line could not delete the channels of interest with *Cre* recombination. There are other mouse lines used to drive *Cre* recombination specifically in C-LTMRs, like the *TH<sup>2A-CreER</sup>*, which could be used to cKO *Tmem63b* and/or *Piezo2* in future experiments. However, most studies use this line for sparse labeling that would not generate a strong phenotype for future behavioral analysis and increasing the dose of tamoxifen might lead to off target effects (Li *et al.*, 2011). Because this mouse line may present problems for behavioral experiments in addition to being time consuming to breed it would be worth utilizing viral transduction to induce transgene expression as an alternative.

Using virus to induce *Cre* expression within C-LTMRs requires tool development to preserve specific expression within C-LTMRs. Viral transduction without a specific promoter

occurs stochastically across all cells in a DRG culture leading to *Cre* expression in non-C-LTMRs and C-LTMRs. Because I used *Cre* to identify tdTomato<sup>+</sup> neurons and cKO genes of interest broad expression of the *Cre* makes it hard to identify C-LTMRs (Nieuwenhuis *et al.*, 2021). Designing a virus with a C-LTMR specific promoter like *Th* or *Slc17a8*, or proper enhancers to induce transduction could facilitate the use of virus to drive *Cre* expression in C-LTMRs. To use commercially available viruses, one could use fluorescence flow cytometry to sort tdTomato<sup>+</sup> neurons from dissociated DRG neurons extracted from *Vglut3<sup>Cre</sup>; Ai9* mice, and culture those neurons. All the neurons in that culture would be C-LTMRs, so commercially available viruses with broad promoters would not cause a problem. Investigating the MA currents in C-LTMRs could show that TMEM63B contributes to SA currents, or could show that PIEZO2 is responsible for MA currents beyond RA or IA.

#### **4.1.2 Reexamining PIEZO2's role in MA currents in cultured DRG neurons**

Focusing on C-LTMRs ignored the fact that *Piezo2* and *Tmem63B* are co-expressed in many other subtypes of DRG neurons. Many of the LTMRs tested in Zheng *et al.*, 2019 express both channels yet these neurons have RA currents (Sharma *et al.*, 2020). It is possible that the cellular composition in C-LTMRs is unique and promotes special interaction between these proteins leading to the SA current. If there is something that makes C-LTMRs different from other LTMRs, focusing on *Piezo2* and *Tmem63b* could get at the root cause of SA currents, but logistical hurdles prevented me from investigating the contribution of PIEZO2 or TMEM63B to the SA currents in C-LTMRs specifically. Understanding the contradicting data that PIEZO2 does not produce SA currents, but C-LTMRs produce SA currents could alter how the field thinks of PIEZO2's function and generate new theories about SA currents.

Reexamining the studies that concluded PIEZO2 contributes to only RA and IA currents is important to understand how to examine PIEZO2's role in SA currents. To generate the most complete cKO of *Piezo2*, researchers used a *Hoxb8-Cre* that caused a reduction of RA and IA responses (Murthy *et al.*, 2018b). Summary data reported in Murthy *et al.*, 2018 show that in WT mice ~80% of DRG neurons have MA currents compared to 45% of neurons in the cKO mice, but closer to 70% of DRG neurons express *Piezo2* (Sharma *et al.*, 2020). One explanation for why the percentage of neurons with MA currents does not match *Piezo2* expression is that a subset of neurons co-express *Piezo2* with the mystery MA ion channel(s). There is evidence for unidentified MA ion channel(s) from single channel recordings that found multiple conductance states, one of which belongs to PIEZO2, within a single DRG neuron (Murthy, 2023). The unknown MA ion channel(s) is hypothesized to induce the SA current. However, patching from every neuron without knowledge of their subtypes could lead to an under representation of certain subtypes, and result in errors when attributing roles to certain ion channels.

I hypothesized that there are multiple mechanisms by which SA currents are generated, and under sampling of DRG subtypes could obscure PIEZO2's role in SA currents. Parpaite *et al.*, 2021 highlighted that 24/52 DRG neurons had MA currents consisting of two inactivation speeds, and Murthy, 2023 also notes cell with currents that required bi-exponential fits. These MA currents are likely caused by an active PIEZO2 population in addition to other MA ion channel(s). However, data sets from Coste *et al.*, 2010, Ranade *et al.*, 2014, and Murthy *et al.*, 2018b likely lumped these cells into one of three categories, RA, IA, or SA. When the fast PIEZO2 component was eliminated, the slower component should have remained and caused an increase in SA currents, but the only changes were decreases in the RA and IA populations (Murthy *et al.*, 2018b). One hypothesis is that some subtypes lose their SA currents in PIEZO2

cKO, but other subtypes that have MA currents driven by both PIEZO2 and an unknown MA ion channel(s) become SA currents when *Piezo2* is absent. This balance beam effect might have been missed by Coste *et al.*, 2010, Ranade *et al.* 2014, and Murthy *et al.*, 2018b because of two limitations in their experiments. First was the inability to identify neuronal subtypes. There are approximately 14 DRG neuron subtypes identified by single cell RNA sequencing experiments; thus, recording 50-60 neurons will not detect small changes that only occur in one or two subtypes (Sharma *et al.*, 2020). Second was the lack of tools to identify active PIEZO2 protein on the membrane as well as the inability to manipulate PIEZO2 pharmacologically in a specific and reversible manner. Overcoming these two obstacles would be a monumental leap forward for the somatosensory field and would impact experiments beyond MA currents on DRG neurons.

Examining MA currents within specific neuronal subtypes could provide insights into molecular mechanisms of MA currents in cultured DRG neurons. The ISH data in **Figure 2.3** showed that *Piezo2* is expressed in C-LTMRs, and my electrophysiological experiments demonstrated that C-LTMRs have exclusively SA currents (**Figure 2.4**). This is not the only experiment to show *Piezo2* expression in non-RA or IA cells. Parpaite *et al.*, 2021, found *Piezo2* expression in cells with each type of inactivation kinetics. Although only neurons with RA currents were enriched for *Piezo2*, there could be an under sampling in this study of certain subtypes with PIEZO2 dependent SA currents. Enrichment was calculated by pooling the sequencing data of cells with similar inactivation kinetics, regardless of molecular subtype, and comparing a gene's expression within that group compared to other groups. One interpretation could be that PIEZO2 mainly induces RA currents, but plays a limited role in SA currents, possibly depending on the neuronal subtype.

To address this hypothesis, researchers could catalog how each subtype of DRG neuron responds to indentation stimulation. Zheng *et al.*, 2019 got started on this question by characterizing MA currents from LTMR subtypes, proprioceptors, and petidergic nociceptors by using *Cre* lines. Another study could mirror the Qi *et al.*, 2024 study to analyze the MA currents of the remaining DRG subtypes that have established *Cre* lines. A survey of this nature could identify other subtypes like C-LTMRs that have *Piezo2* expression and SA currents. Researchers could then use *Cre* lines to cKO *Piezo2* to test if it is necessary for these SA current, and then search for proteins that are uniquely expressed within these subtypes that might modulate PIEZO2.

#### **4.2 Tools to study PIEZO2 in DRG neurons.**

As of now there is no tool that allows researchers to acutely and reversibly manipulate the PIEZO2 ion channel. A specific agonist or antagonist for PIEZO2 could be used to isolate PIEZO2 currents by reversibly activating the channel in the absence of force or blocking the channel during force application. For example, perfusing a specific antagonist for PIEZO2 during MA current recordings of C-LTMR and finding no changes would quickly confirm PIEZO2 is not responsible for SA currents in C-LTMRs. If the MA currents changes when the antagonist is applied, it would reveal PIEZO2's contribution to SA currents in C-LTMRs. In addition to this hypothetical drug's impact on basic research it could be developed into a therapy to prevent pain in cases of extreme mechanical allodynia. Generating specific drugs for PIEZO2 would have a lasting impact on basic research and in the clinic.

Demonstrating PIEZO2 is active in C-LTMRs would be the first evidence that SA currents are brought about by PIEZO2. There are tools to identify cells with active PIEZO2 channel in cells. Currently there are no available antibodies, but the FM-143 dye permeates

active PIEZO2. Therefore, perfusing FM-143 on a DRG culture and stimulating the neurons mechanically would label all cells with active PIEZO2 on the membrane (Villarino *et al.*, 2023). One could indent DRG neurons to record MA currents then repeat the experiment in the presence of FM-143 to determine whether PIEZO2 contributes to the MA currents by imaging the dye at the end of the experiment. Identifying active PIEZO2 within a cell would allow researchers to know if the MA current was driven by PIEZO2.

Recording MA currents from cultured neurons is informative about what neurons have MA ion channels, but MA currents on the somas of DRG neurons is not how mechanical stimuli are encoded by DRG neurons. *In vivo* recordings with either  $\text{Ca}^{2+}$  imaging or extracellular electrophysiology allow experimenters to investigate how mutations, drugs, or injury alter DRG neuronal coding. Extensive recordings showed how WT neurons respond to basic mechanical stimuli building a wealth of knowledge about certain neuronal subtypes' response profiles (Ghitani *et al.*, 2017; Qi *et al.*, 2024). To uncover if a protein is integral for somatosensation one can use a virus to drive *Cre* expression in floxed animals to generate cKO of a protein of interest within a specific subtype and stimulate the skin while recording the activity of DRG neurons *in vivo*. Subtypes that lose activity in the cKO condition depend on that protein to sense a given stimulus. Conducting experiments *in vivo* evaluates how a protein functions within the intact DRG neuronal ending providing information on what types of stimuli a given protein responds guiding future behavioral tests.

### **4.3 TMEM63B, what does it do?**

#### **4.3.1 TMEM63B in humans.**

Although recording from TMEM63B is challenging, other methods have been used to understand what function TMEM63B has in biology. Phenotyping humans with mutations in

*TMEM63B* reveals that the channel is crucial for neurons of the central nervous system. Patients have developmental and epileptic encephalopathy (DEE), intellectual disability, and progressive neurodegenerative brain changes presented as motor and cortical visual impairments (Vetro *et al.*, 2023). The mutations have not been electrophysiologically characterized but have been hypothesized to be LOF based on where they occur within the protein sequence. This study will serve as the foundation for many experiments that will characterize how brain regions and cell types are affected throughout development by loss of *TMEM63B*. Once the field has a basic understanding of *TMEM63B*'s effect on neurons in the brain, functional studies can be tailored to measure *TMEM63B*'s role within neurons to understand how they fit into a cellular pathway that affects neuronal function.

#### **4.3.2 *TMEM63B* in mice**

Since the early description of the MA currents of the OSCA/*TMEM63* family, studies have uncovered cell types that need *TMEM63B* for survival, but studying how its MA currents or other functional roles could fit into cellular pathways are challenging (Murthy *et al.*, 2018a). In Du *et al.*, 2020, loss of *TMEM63B* leads to outer hair cell death. They found *TMEM63B*-dependent  $\text{Ca}^{2+}$  activity in outer hair cells by inducing swelling with osmotic shock (switching the bath from 300 to 200 mOsm/L). A limitation is that osmotic shock is an exaggerated MA stimulus much larger than what would be experienced by the cell. In lung alveolar cells, researchers record MA currents that depend on both *TMEM63B* and *TMEM63A* and demonstrated without these channels surfactant release is inhibited (Chen *et al.*, 2024). These are the only two examples in literature that record *TMEM63B* currents or activity in endogenous cell types.



In all cell types recorded so far, TMEM63B only has stretch- but not indentation- activated currents. Cell-attached and outside-out are the only patch recording configurations where one can induce and record stretch activated currents. Both recording methods under sample the membrane because only a small patch of membrane is recorded instead of the entire cell. This means enough ion channels need to be captured within that patch of membrane to produce a response. In the case of TMEM63B, a single channel produces less than 1 pA at -80 mV in physiological recording solutions. Thus, many channels are needed to detect and confidently measure a response. Even more channels are needed if there is another MA ion channel co-expressed like *Piezo2*. In my research of TMEM63B I struggled to record functional output from the channel, and it is not clear if I actually recorded TMEM63B currents. These hurdles for recording TMEM63B can be overcome, but also suggests that other methods like *in vivo* recordings should be deployed to study TMEM63B.

#### ***4.3.3 TMEM63B and the scramblase hypothesis.***

In addition to functioning as ion channels, researchers have proposed that the OSCA/TMEM63 family could function as scramblases with an unknown role. Scramblases are proteins that shuttle lipids between the outer and inner leaflet of the membrane in either direction (Sakuragi & Nagata, 2023). Due to the similarity of these channels with members of TMEM16 and TMC families, there is an emerging theory that OSCA/TMEM63s could function as MA scramblases in addition to being ion channel just like members of the TMEM16 and TMC families (Le *et al.*, 2021; Ballesteros & Swartz, 2022). The first piece of evidence for OSCA/TMEM63 being scramblases came from a recent structure of the OSCA1.2 protein that showed a potential open structure with the pore lined by amino acids and ordered lipids that spanned the inner and outer leaflet of the membrane (Han *et al.*, 2024). To test this model

researchers altered the lipid content of liposomes, like making point mutations, and recorded OSCA1.2 currents and demonstrated that lipids with certain properties altered currents in a way that suggested a pore partially made of lipids. The lipids of this pore could theoretically move from one side to the other of the membrane accomplishing the same biological function of a scramblase.

However, the field is not settled on the ability for the OSCA/TMEM63 proteins to function as scramblases. One study found certain mutations are required to confer OSCA/TMEM63 proteins with MA scramblases activity (Lowry *et al.*, 2024). In more recent papers researchers proposed that endogenous TMEM63B was constitutively active scramblase (Miyata *et al.*, 2024; Niu *et al.*, 2024). The disagreement between these studies highlights that it is unclear if TMEM63B has scramblase activity and what impact that might have on any cell.

#### **4.3.4 TMEM63B in DRG neurons and its role in touch**

Recording MA currents dependent on TMEM63B in DRG neurons is challenging, but characterizing the expression profile and trafficking is feasible and impactful. *Tmem63b* is broadly expressed in DRG neurons, and neurons that do not express *Tmem63b* tend to express *Tmem63a* (Sharma *et al.*, 2020). According to the HA antibody staining in the TMEM63B-HA mouse, the channel appears as a haze inside the soma (**Figure 2.3B**). This haze is typical for DRG staining even for membrane proteins like TMEM63B or TRPV1 (Yu *et al.*, 2008). Speculating on the broad expression pattern, it is possible that *Tmem63b* plays a fundamental role in neurons, either helping them grow and develop or maintain cell health during periods of high activity.

I stained neurons in the skin to study TMEM63B localization to nerve terminals. Neuronal terminals in the skin are where external stimuli activate sensory neurons by opening

ion channels; thus, if TMEM63B was present in the skin, the channel is in the right place to respond to mechanical stimuli. Other sensory ion channels like TRPV1, the channel that responds to high temperature and chili peppers, can be detected in the skin with antibody staining (Lee *et al.*, 2009). To identify PIEZO2 in the skin initially researchers used PIEZO2-GFP but staining for the GFP tag did not always yield consistent results (Ranade *et al.*, 2014; Woo *et al.*, 2014). The addition of a unique epitope consisting of 3FLAGs-GFP-3FLAGs-GFP-3FLAGs to C-terminus of PIEZO2 results in robust and distinct signal (Handler *et al.*, 2023). Staining for TRPV1 and PIEZO2 with a neuronal marker, neurofilament, reported regions of overlap between the ion channel of interest and the neuronal marker. For PIEZO2, the overlap of the two stains revealed lanceolate endings around hair follicles. These are specialized neuronal endings that wrap around the base of and have slender protrusions along the hair (Li & Ginty, 2014). For staining experiments in the skin to work there must be clear signal for the protein of interest and distinct overlap with neuronal stain, which reveals the filament like structures of the peripheral nerve fibers.

The staining experiments I performed used hairy skin from the back of mice because C-LTMRs exclusively form lanceolate endings around hairs (Rutlin *et al.*, 2014). However, I was limited by which antibodies worked for staining neurons and the HA tag, and I could not confidently demonstrate HA staining within the lanceolate endings. Using sections of skin, I saw no HA staining in structures that resemble nerve fibers and the HA antibody appeared to be bound to sebaceous glands in a non-specific manner (**Figure 4.1A-B**). I tried whole mount staining and obtained ambiguous results. A major issue was inconsistent TMEM63B-HA staining, some images had dim staining that overlapped with the neuronal TH staining (**Figure 4.3B**). Other images had non-specific staining that overlapped with TH, but also overlapped with

the mirrored TH channel that was created as a control. I used TH because of its specificity to C-LTMRs, and when I co-stained skin with the antibody for Beta-tubulin III the overlap showed that the TH does not penetrate in the lanceolate endings around hairs (**Figure 4.3D**). The Beta-tubulin III stained for many different types of lanceolate endings but was incompatible with HA antibodies (**Figure 4.3D**). Future staining studies in the skin could be aided by development of new TMEM63B specific antibodies that could be paired with Beta-tubulin III antibodies.

The most conclusive evidence for TMEM63B's role as a sensor for force will come from *in vivo* recordings. As mentioned in the introduction, researchers used *in vivo*  $\text{Ca}^{2+}$  imaging to characterize many peripheral neurons *in vivo*, revealing how 14 different DRG neuronal subtypes responded to various tactile stimuli, punctate force of increasing intensity, and temperature (Qi *et al.*, 2024). Imaging from TG neurons showed that responses to low threshold stimuli in all subtypes disappeared in *Piezo2* cKO peripheral somatosensory neurons, corroborating the behavioral studies on *Piezo2* cKO mice (Ranade *et al.*, 2014; Von Buchholtz *et al.*, 2021). An open question is how these neurons initiate their responses to noxious MA force. Future studies could utilize these techniques in conjunction with *Tmem63b* and *Piezo2* cKO in DRG neurons. cKO of *Piezo2* alongside *Tmem63b* is crucial because high-threshold stimuli like pinch will still activate neurons with PIEZO2 because these stimuli are above PIEZO2's threshold. In double cKO DRG neurons, imaging results will show whether high threshold mechanical stimuli are dependent on TMEM63B activation. This experiment would allow for subsequent staining to identify the sub-populations that use TMEM63B as a noxious force sensor.

Uncovering what a new protein like TMEM63B does in somatosensory neurons or other cells type will shed new insights into the biology of mechanosensors. Based on its structural homology with TMC's it could be that TMEM63B requires a complex to properly respond to

force. Another possibility is that TMEM63B has high threshold for force, and new methods are needed to study its response in culture. Established tools for *in vivo* recordings could help fill some of this gap, but fundamental improvements for assaying of mechanosensor are required for both somatosensory biology and for other cells that express these proteins.

## Appendix A: Skin Staining

The peripheral axons of DRG neurons are where external stimuli activates molecular sensors that initiate action potentials (Delmas *et al.*, 2011a). There is evidence that PIEZO2 is localized within these structures' based on IHC experiments (Ranade *et al.*, 2014; Handler *et al.*, 2023). Here I tried to demonstrate that TMEM63B was trafficked to DRG neuronal projections in the skin.

I stained fixed and frozen sections of hairy back skin from *Tmem63b*<sup>wt/wt</sup> and *Tmem63b*<sup>HA/HA</sup> mice (mice will be referred to as WT and HA for the rest of the Appendix). All methods except the exact antibodies followed Pomaville and Wright 2021 (Pomaville & Wright, 2021). In **Figure 4.1** there are striations around one of the hairs in the HA mouse. However, there was no counter stain to show what type of cells the HA antibody was bound to. To reveal neurons in skin sections I added a UCH-L1 antibody that labels DRG neurons in the ganglion (**Figure 2.2A**). Then I compared the overlap with the HA antibody. The UCH-L1 antibody stained something around the base of the hairs, but the staining resembles a blob and not a filament as would be expected from a neuron (**Figure 4.1B**). Comparing the HA staining from WT and HA skin showed each group has HA staining in the same place as UCH-L1 staining indicating that the HA antibody was labeling something non-specific (**Figure 4.1B**). To investigate what the UCH-L1 antibody is staining I co-stained with Beta-Tubulin III, another neuronal marker, that successfully labeled neurons in the skin (**Figure 4.1C**). This co-stain with the UCH-L1 and Beta-Tubulin III shows that UCH-L1 does not label neurons, and labels

something at the base of a subset of hair follicles (I would speculate these are sebaceous glands (Schneider & Paus, 2010)).

Two factors limited our ability to evaluate TMEM63B's presence in neuronal projections in the skin. First choosing the UCH-L1 antibody that did not label neurons, and second sectioning the skin cuts important neuronal features. We could not pair the Beta-Tubulin III and HA antibodies because they both come from rabbit, and alternatives from chicken species did not work. The Beta-Tubulin III staining in **Figure 4.2A** shows multiple hairs, but only a single hair has the specialized circumferential and lanceolate ending that are hypothesized to be involved in sensing mechanical stimuli (Rutlin *et al.*, 2014). Staining and imaging whole-mount skin showed the complete neuronal structures better because they are left intact, and can be image in their entirety (**Figure 4.2B**).

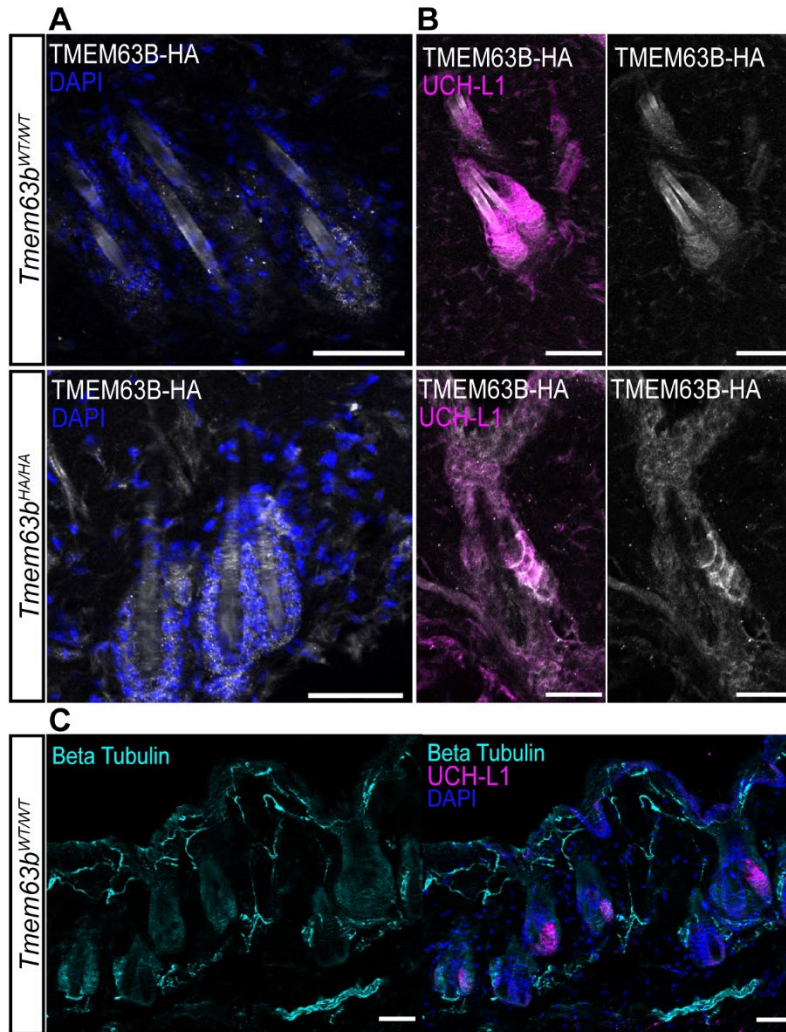


**Figure 4.1: Stained sections of mouse hairy skin for neurons and TMEM63B.** A: HA and DAPI staining in skin sections from *Tmem63b*<sup>WT</sup> and *Tmem63b*<sup>HA</sup>. B: UCH-L1 marks something around hair follicles that overlaps with HA staining in *Tmem63b*<sup>WT</sup> and *Tmem63b*<sup>HA</sup>. C: Beta-Tubulin III stains neurons in the skin whereas UCH-L1 aligns with a subset of hair follicles. All scale bars are 50 μm.



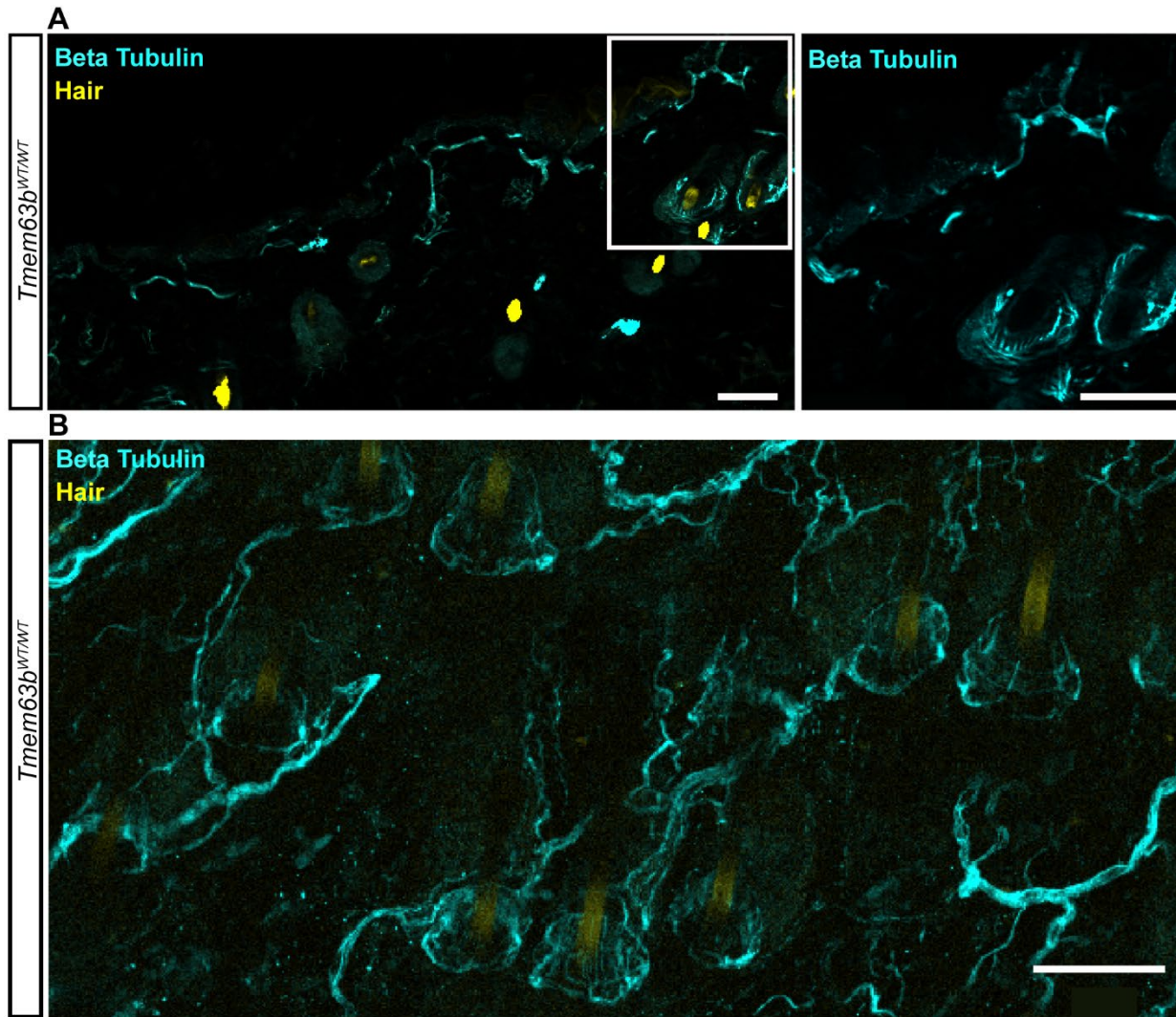


**Figure 4.2: Staining compared between skin sections and whole mount. A:** Skin sections with Beta-Tubulin III noted different in panel staining and auto-fluorescent hairs reveal neurons in the skin, Inset shows a lanceolate ending, specialized neuronal morphology that surround a hair. **B:** Same staining as **A** in whole mount skin shows each hair surrounded by multiple types of ending morphology in addition to free nerve endings. All scale bars 50µm.

In the whole-mount skin, I used the TH and HA antibodies in WT and HA animals to look for overlap between the neuronal marker and the TMEM63B-HA protein. In **A** the HA channel has off-target staining, but the TH marks filament structures that appear to be neurons.

To pull out HA staining within neurons I created an overlap channel using the coloc function in Imaris. To evaluate if the overlap between the HA and TH staining was genuine, I mirrored the TH channel in the Zen program. Using the mirrored TH channel and the original HA channel as inputs to the colocalization function I found a similar amount of overlap compared to output from the colocalization output of the original channel. The similarity is probably because the HA staining was non-specific. Although, in **Figure 4.3B** the HA staining did not cover most of the field of view, and as a result the HA co-localized with the real TH stain and not the flipped TH stain. In the WT animal there was also limited HA staining and a small amount of overlap in both the original and flipped images (**Figure 4.3C**). **Figure 4.3B-C** alone would indicate that the TMEM63B-HA protein is trafficked to the neurons in the skin, but the staining done in the HA animal gave conflicting results. Further refinement of the staining protocol is needed to attain more consistent results before we can make conclusions about the trafficking of TMEM63B.

One change that should be considered is using TH as a counterstain for neurons in the skin. In DRG neurons TH is specific for C-LTMRs, and C-LTMRs make lanceolate endings around hairs in the skin (Li *et al.*, 2011). There are no clear lanceolate endings in **Figure 4.3A-C**, and it is possible that without clear landmarks, the images were taken at the wrong depth. I co-stained the whole-mount skin for Beta-Tubulin III and TH (**Figure 4.3D**). By overlapping these stains, I found that TH stains for neurons, but the TH staining stops before neurons form a circle around a hair. This means that TH might not be the best for revealing TMEM63B trafficking into specialized structures. Another interpretation is that TMEM63B is not trafficked into these specialized structures. None of these images have clear HA staining for neurons in the skin, but refinement of the staining procedure or the use of a different tag is needed before a concrete conclusion is made.

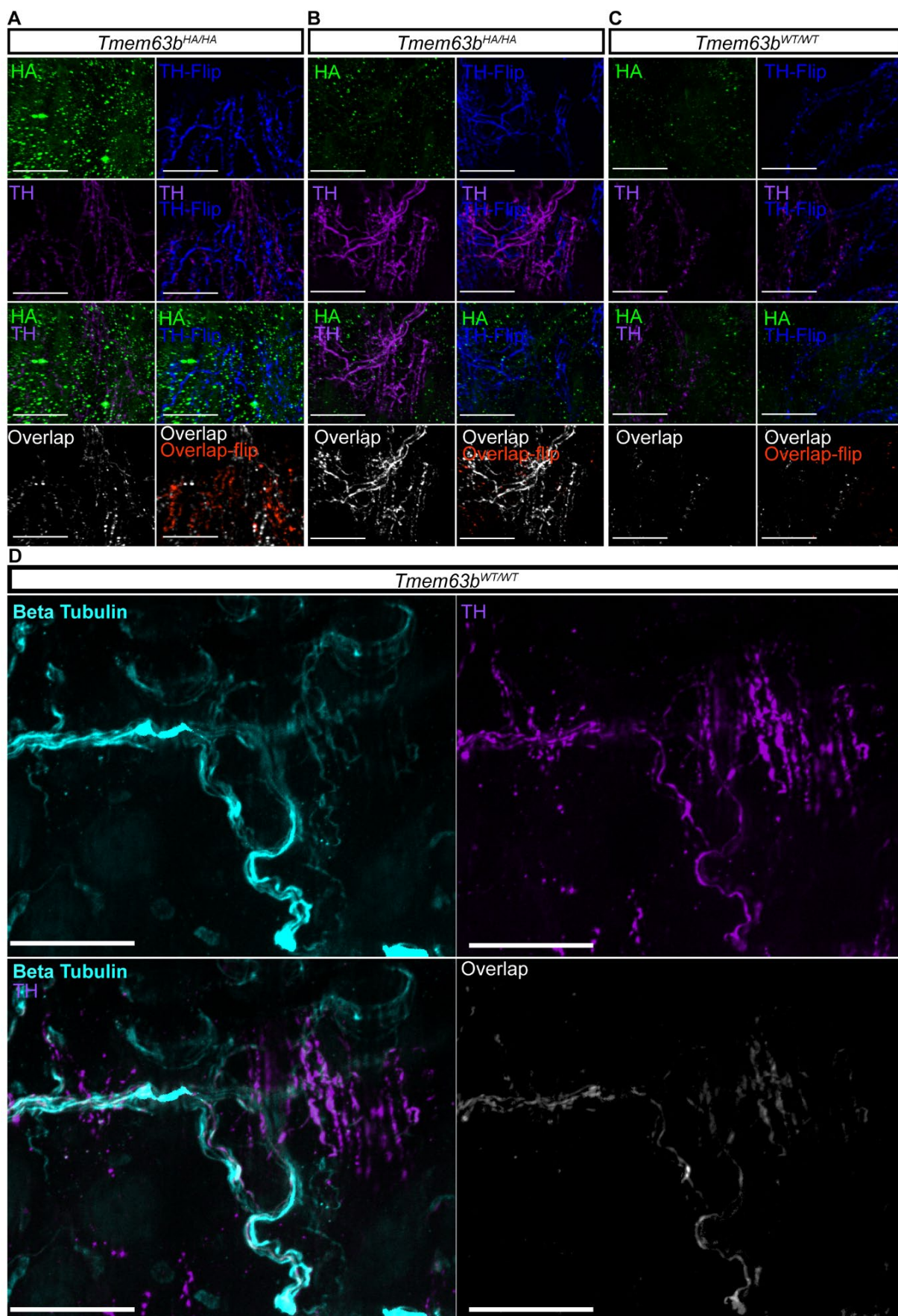


**Figure 4.3: Whole mount skin staining for TMEM63B-HA channels has mixed results. A-C:** Whole mount skin staining of mouse hairy skin. Left column: HA, TH, merged image of HA and TH channels, and overlap of HA and TH staining. Right column: TH-flip is a mirrored image of the TH channel, merged image of TH and TH-flip, merged image of HA and TH-Flip, and merge image of the overlap from the left column and the overlap-flip is the overlap of HA staining with the TH-flip channel. **A-B:** Representative images of whole mount skin from the same TMEM63B<sup>HA/HA</sup> mouse. **C:** Skin from a TMEM63B<sup>WT/WT</sup> mouse. **D:** Whole mount skin staining showing Top: Beta-TubulinIII staining and TH staining alone. Bottom: Merged image of Beta-Tubulin III and TH images, and the colocalization of the two antibody stains.

## Methods:

**Tissue processing:** All dissections, tissue processing, and staining followed protocols from Pomaville and Wright 2021.

**Imaging:** Images were taken on a ApoTome2 Zeiss Microscope with a 20X objective.

**Processing:** Images were processed in Zen Lite by clicking on the ApoTome tab and creating a new image using optical sectioning. Then the TH channel was mirrored a function in the zen processing tab. The files were then exported and converted into imaris files. TH and HA overlaps were made by creating a new channel with the coloc function. This process was repeated with the TH-flip and HA channel.

## Primary:

Rabbit anti-HA Cell Signaling Technology #3724 1:500, sheep anti-tyrosine hydroxylase Sigma AB1542 1:750, Guinea pig anti UCH-L1 from Neuromics inc GP 1410450UL at 1:400, and Rabbit anti-beta-TubulinIII Sigma-Aldrich T2200 1:1000

## Secondaries antibodies

anti-rabbit IgG-Alexa Fluor 555 Biotium 20038 1:500, and anti-sheep Alexa Fluor 647 Jackson ImmunoResearch 713-605-003 1:500. Anti-Guinea pig-cy3 Jackson ImmunoResearch 706-165-

148 1:500, Rabbit IgG-Alexa Fluor 488 Thermo Scientific R37118 2 drops per 1mL of permeabilization and blocking buffer (as per the manufacturer's instructions).

## Appendix B: *Piezo2* and *Tmem63b* double flox indentation induced currents in C-LTMRs.

I attempted to generate a *Piezo2* cKO and a double cKO by crossing the *Piezo2*<sup>fl/fl</sup> mice with the *Vglut3-IRES-Cre:Ai9* mice (*Piezo*<sup>fl</sup>), and the *Tmem63b*<sup>fl/fl</sup> (*Piezo*<sup>fl</sup> & *Tmem63b*<sup>fl</sup>). I recorded indentation responses from both these groups, and measured the same metrics, max current, Tau of inactivation and steady state current (**Figure 4.4A-F**). Currents remained in all cells, which prompted us to stop recording and examine the cKO of *Piezo2* with ISH. Because we only have recordings from one animal from each group, I did not run statistical analyses to compare the two experimental groups to the WT group (**Figure 4.4A-F**). For ISH I used probes for the exons in the *Piezo2* gene that are flanked by the loxp sites exon 43-45. I stained DRG cultures from *Vglut3-IRES-Cre:Ai9* mice and *Piezo2*<sup>fl</sup> mice and used the endogenous tdTomato fluorescence to identify cells of interest. The ISH images showed that *Piezo2-Exon43-45* staining could be found in most cells including tdTomato+ cells marked with a purple ROI surface generated in Imaris (**Figure 4.4E**). In **Figure 4.4F** I quantified the *Piezo2-Exon43-45* expression by asking if a cell was above a threshold I set using the negative stain fluorescence in the corresponding channel. I measured the mean fluorescence within each tdTomato+ cell in the *Piezo2-Exon43-45* channel, and I repeated this measurement in a separate culture of cells stained with negative control probes. tdTomato+ neurons counted as having *Piezo2* expression if the mean fluorescence for *Piezo2-Exon43-45* with an ROI was above the 99<sup>th</sup> percentile mean fluorescence of all tdTomato+ neurons of the negative stain.



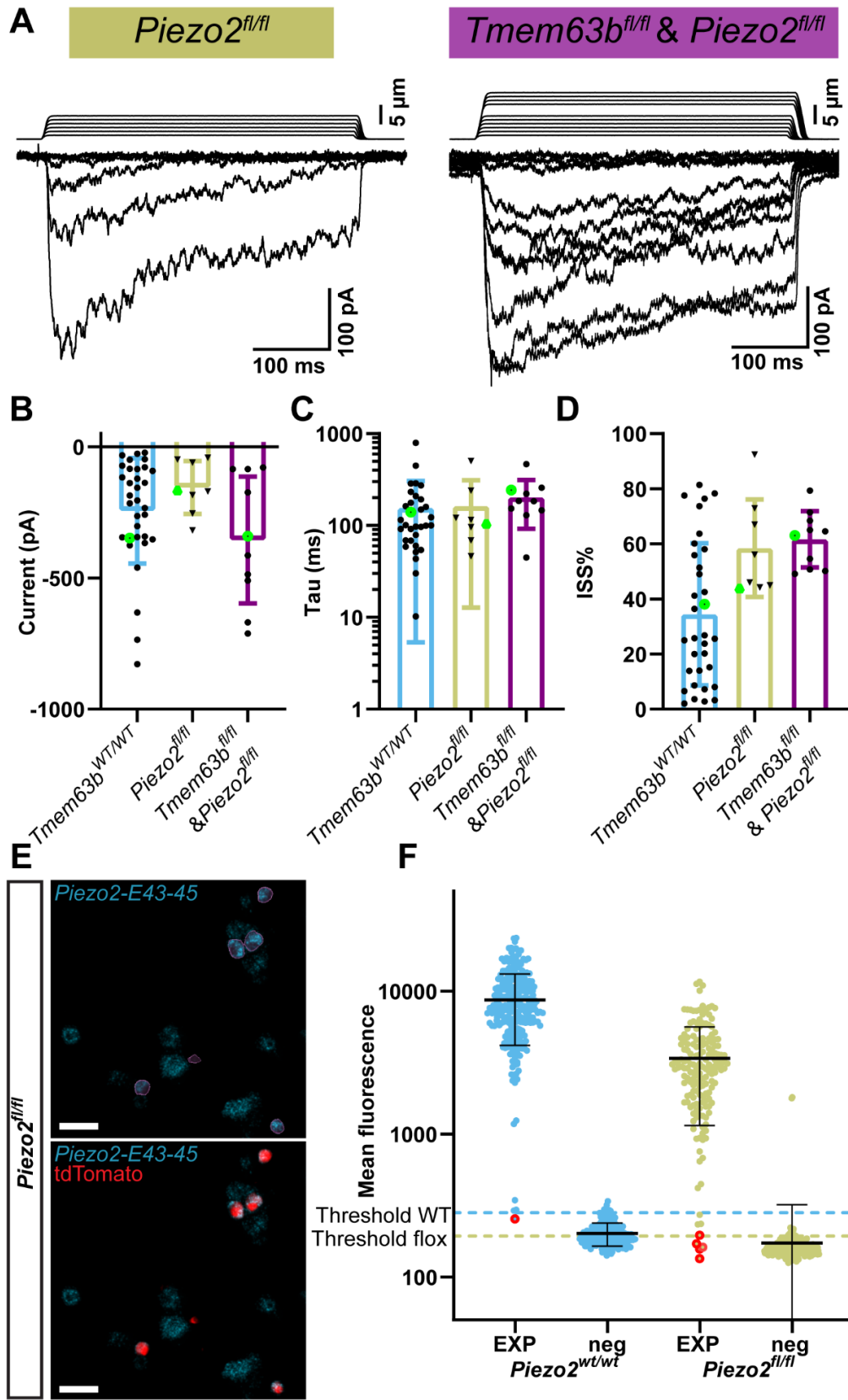


**Figure 4.4: Whole-cell indentation currents of C-LTMRs in *Piezo2<sup>fl</sup>* and *Tmem63b<sup>fl</sup>* & *Piezo2<sup>fl</sup>* and *in situ* hybridization showing *Piezo2<sup>fl</sup>*.** **A:** Representative trace of indentation-induced whole-cell MA currents from *Piezo2<sup>wt</sup>* and *Piezo2<sup>fl</sup>* C-LTMRs. **D:** Maximum peak current. Green indicates the example trace's corresponding measurement (*Tmem63b<sup>wt</sup>*;  $-244.1 \pm 200.4$  pA, cells= 33 and animals= 6, *Piezo2<sup>fl</sup>*;  $-155.3 \pm 100.6$  pA, cells = 8 and animals = 1, *Tmem63b<sup>fl</sup>* & *Piezo2<sup>fl</sup>*;  $-355.7 \pm 241.7$  pA, cells = 10 and animals = 1). **E:** Inactivation kinetics plotted on log<sub>10</sub> axis (*Tmem63b<sup>wt</sup>*;  $154.7 \pm 149.4$  ms, cells= 32 and animals= 6, *Piezo2<sup>fl</sup>*;  $162.1 \pm 149.4$  ms, cells = 8 and animals = 1, *Tmem63b<sup>fl</sup>* & *Piezo2<sup>fl</sup>*;  $203.1 \pm 111.1$  ms, cells = 10 and animals = 1). **F:** Steady state current taken as a percentage of the peak current (*Tmem63b<sup>wt</sup>*;  $34.42 \pm 25.82$ , cells = 33 and animals = 6, *Piezo2<sup>fl</sup>*;  $58.45 \pm 17.69$ , cells = 8 and animals = 1, *Tmem63b<sup>fl</sup>* & *Piezo2<sup>fl</sup>*;  $61.6 \pm 10.2$  ms, cells = 10 and animals = 1). **E.** *In situ* hybridization staining of cultured DRG neurons from *Piezo2<sup>fl</sup>* mice with a probe against *Piezo2-Exon43-45* (blue) and natural tdTomato fluorescence (red). **F.** Mean fluorescence plotted on a log<sub>10</sub> axis of the ISH probe of every tdTomato+ cell in a *Piezo2<sup>wt</sup>* and *Peizo2<sup>fl</sup>* mouse. Threshold for a cell expressing *Piezo2* was based on the 99<sup>th</sup> percentile of mean fluorescence of a negative probe within tdTomato+ cells.



## Bibliography

- Abraira VE & Ginty DD. (2013a). The sensory neurons of touch. *Neuron* **79**, 618-639.
- Abraira VE & Ginty DD. (2013b). The Sensory Neurons of Touch, pp. 618-639. NIH Public Access.
- Attendance, Cute Mosquito cartoon, <https://www.cleanpng.com/png-wings-bee-standing-with-long-antenna-holding-pills-8129133/>. 2024.
- Ballesteros A, Fenollar-Ferrer C & Swartz KJ. (2018). Structural relationship between the putative hair cell mechanotransduction channel TMC1 and TMEM16 proteins. *Elife* **7**.
- Ballesteros A & Swartz KJ. (2022). Regulation of membrane homeostasis by TMC1 mechanoelectrical transduction channels is essential for hearing. *Sci Adv* **8**, eabm5550.
- Basbaum AI, Bautista DM, Scherrer G & Julius D. (2009). Cellular and molecular mechanisms of pain. *Cell* **139**, 267-284.
- Berrier C, Besnard M, Ajouz B, Coulombe A & Ghazi A. (1996). Multiple mechanosensitive ion channels from Escherichia coli, activated at different thresholds of applied pressure. *J Membr Biol* **151**, 175-187.
- Bezanilla F. (2018). Gating currents. *J Gen Physiol* **150**, 911-932.
- Bhuiyan SA, Xu M, Yang L, Semizoglou E, Bhatia P, Pantaleo KI, Tochitsky I, Jain A, Erdogan B, Blair S, Cat V, Mwirigi JM, Sankaranarayanan I, Tavares-Ferreira D, Green U, McIlvried LA, Copits BA, Bertels Z, Del Rosario JS, Widman AJ, Slivicki RA, Yi J, Woolf CJ, Lennerz JK, Whited JL, Price TJ, Gereau RWt & Renthal W. (2023). Harmonized cross-species cell atlases of trigeminal and dorsal root ganglia. *bioRxiv*.
- Bradman MJ, Ferrini F, Salio C & Merighi A. (2015). Practical mechanical threshold estimation in rodents using von Frey hairs/Semmes-Weinstein monofilaments: Towards a rational method. *J Neurosci Methods* **255**, 92-103.
- Brohawn SG, Su Z & MacKinnon R. (2014). Mechanosensitivity is mediated directly by the lipid membrane in TRAAK and TREK1 K<sup>+</sup> channels. *Proc Natl Acad Sci U S A* **111**, 3614-3619.

- Brohawn SG, Wang W, Handler A, Campbell EB, Schwarz JR & MacKinnon R. (2019). The mechanosensitive ion channel TRAAK is localized to the mammalian node of Ranvier. *Elife* **8**.
- Burgess PR, Petit D & Warren RM. (1968). Receptor types in cat hairy skin supplied by myelinated fibers. *J Neurophysiol* **31**, 833-848.
- Caterina MJ, Schumacher MA, Tominaga M, Rosen TA, Levine JD & Julius D. (1997). The capsaicin receptor: a heat-activated ion channel in the pain pathway. *Nature* **389**, 816-824.
- Chen GL, Li JY, Chen X, Liu JW, Zhang Q, Liu JY, Wen J, Wang N, Lei M, Wei JP, Yi L, Li JJ, Ling YP, Yi HQ, Hu Z, Duan J, Zhang J & Zeng B. (2024). Mechanosensitive channels TMEM63A and TMEM63B mediate lung inflation-induced surfactant secretion. *J Clin Invest* **134**.
- Chen TW, Wardill TJ, Sun Y, Pulver SR, Renninger SL, Baohan A, Schreiter ER, Kerr RA, Orger MB, Jayaraman V, Looger LL, Svoboda K & Kim DS. (2013). Ultrasensitive fluorescent proteins for imaging neuronal activity. *Nature* **499**, 295-300.
- Chesler AT, Szczot M, Bharucha-Goebel D, Čeko M, Donkervoort S, Laubacher C, Hayes LH, Alter K, Zampieri C, Stanley C, Innes AM, Mah JK, Grosmann CM, Bradley N, Nguyen D, Foley AR, Le Pichon CE & Bönnemann CG. (2016). The role of PIEZO2 in human mechanosensation. *New England Journal of Medicine* **375**, 1355-1364.
- Chirila AM, Rankin G, Tseng SY, Emanuel AJ, Chavez-Martinez CL, Zhang D, Harvey CD & Ginty DD. (2022). Mechanoreceptor signal convergence and transformation in the dorsal horn flexibly shape a diversity of outputs to the brain. *Cell* **185**, 4541-4559 e4523.
- Coste B, Houge G, Murray MF, Stitzel N, Bandell M, Giovanni MA, Philippakis A, Hoischen A, Riemer G, Steen U, Steen VM, Mathur J, Cox J, Lebo M, Rehm H, Weiss ST, Wood JN, Maas RL, Sunyaev SR & Patapoutian A. (2013). Gain-of-function mutations in the mechanically activated ion channel PIEZO2 cause a subtype of Distal Arthrogryposis. *Proceedings of the National Academy of Sciences of the United States of America* **110**, 4667-4672.
- Coste B, Mathur J, Schmidt M, Earley TJ, Ranade S, Petrus MJ, Dubin AE & Patapoutian A. (2010). Piezo1 and Piezo2 Are Essential Components of Distinct Mechanically Activated Cation Channels Bertrand. *Science (New York, NY)* **330**, 7-12.
- Cox CD, Bavi N & Martinac B. (2019). Biophysical Principles of Ion-Channel-Mediated Mechanosensory Transduction, pp. 1-12. Elsevier Company.
- Cunningham CL & Muller U. (2019). Molecular Structure of the Hair Cell Mechanoelectrical Transduction Complex. *Cold Spring Harb Perspect Med* **9**.

DBCLS, spinal-cord\_anterior-horn-cells\_motor-nerves\_muscles icon, <https://togotv.dbcls.jp/en/pics.html> is licensed under CC-BY 4.0 Unported <https://creativecommons.org/licenses/by/4.0/>. 2024. Adapted by Daniel Orlin.

DBCLS, Sensory\_neuron icon and skin, <https://togotv.dbcls.jp/en/pics.html> is licensed under CC-BY 4.0 Unported <https://creativecommons.org/licenses/by/4.0/>. 2024. Adapted by Daniel Orlin.

Delfini MC, Mantilleri A, Gaillard S, Hao J, Reynders A, Malapert P, Alonso S, Francois A, Barrere C, Seal R, Landry M, Eschallier A, Alloui A, Bourinet E, Delmas P, Le Feuvre Y & Moqrich A. (2013). TFAA4, a chemokine-like protein, modulates injury-induced mechanical and chemical pain hypersensitivity in mice. *Cell Rep* **5**, 378-388.

Delle Vedove A, Storbeck M, Heller R, Holker I, Hebbar M, Shukla A, Magnusson O, Cirak S, Girisha KM, O'Driscoll M, Loeys B & Wirth B. (2016). Biallelic Loss of Proprioception-Related PIEZO2 Causes Muscular Atrophy with Perinatal Respiratory Distress, Arthrogryposis, and Scoliosis. *Am J Hum Genet* **99**, 1206-1216.

Delmas P, Hao J & Rodat-Despoix L. (2011a). Molecular mechanisms of mechanotransduction in mammalian sensory neurons. *Nature Reviews Neuroscience* **12**, 139-153.

Delmas P, Hao J & Rodat-Despoix L. (2011b). Molecular mechanisms of mechanotransduction in mammalian sensory neurons, pp. 139-153. Nature Publishing Group.

Du H, Ye C, Wu D, Zang YY, Zhang L, Chen C, He XY, Yang JJ, Hu P, Xu Z, Wan G & Shi YS. (2020). The Cation Channel TMEM63B Is an Osmosensor Required for Hearing. *Cell Reports* **31**, 107596.

Dubin AE, Murthy S, Lewis AH, Brosse L, Cahalan SM, Grandl J, Coste B & Patapoutian A. (2017). Endogenous Piezo1 Can Confound Mechanically Activated Channel Identification and Characterization. *Neuron* **94**, 266-270.e263.

Enyedi P & Czirjak G. (2010). Molecular background of leak K<sup>+</sup> currents: two-pore domain potassium channels. *Physiol Rev* **90**, 559-605.

Feil R, Wagner J, Metzger D & Chambon P. (1997). Regulation of Cre recombinase activity by mutated estrogen receptor ligand-binding domains. *Biochem Biophys Res Commun* **237**, 752-757.

Ghitani N, Barik A, Szczot M, Thompson JH, Li C, Le Pichon CE, Krashes MJ & Chesler AT. (2017). Specialized Mechanosensory Nociceptors Mediating Rapid Responses to Hair Pull. *Neuron* **95**, 944-954.e944.

Glogowska E, Arhatte M, Chatelain FC, Lesage F, Xu A, Grashoff C, Discher DE, Patel A & Honore E. (2021). Piezo1 and Piezo2 foster mechanical gating of K2P channels. *Cell Rep* **37**, 110070.

- Glowatzki E & Fuchs PA. (2002). Transmitter release at the hair cell ribbon synapse. *Nat Neurosci* **5**, 147-154.
- Guo YR & MacKinnon R. (2017). Structure-based membrane dome mechanism for Piezo mechanosensitivity. *Elife* **6**.
- Han Y, Zhou Z, Jin R, Dai F, Ge Y, Ju X, Ma X, He S, Yuan L, Wang Y, Yang W, Yue X, Chen Z, Sun Y, Corry B, Cox CD & Zhang Y. (2024). Mechanical activation opens a lipid-lined pore in OSCA ion channels. *Nature* **628**, 910-918.
- Handler A, Zhang Q, Pang S, Nguyen TM, Iskols M, Nolan-Tamariz M, Cattel S, Plumb R, Sanchez B, Ashjian K, Shotland A, Brown B, Kabeer M, Turecek J, Rankin G, Xiang W, Pavarino EC, Africawala N, Santiago C, Lee W-CA, Shan Xu C & Ginty DD. (2023). Three-dimensional reconstructions of mechanosensory end organs suggest a unifying mechanism underlying dynamic, light touch.
- Hao J & Delmas P. (2010). Multiple desensitization mechanisms of mechanotransducer channels shape firing of mechanosensory neurons. *Journal of Neuroscience* **30**, 13384-13395.
- Haselwandter CA, Guo YR, Fu Z & MacKinnon R. (2022). Quantitative prediction and measurement of Piezo's membrane footprint. *Proc Natl Acad Sci U S A* **119**, e2208027119.
- Haswell ES & Meyerowitz EM. (2006). MscS-like proteins control plastid size and shape in *Arabidopsis thaliana*. *Curr Biol* **16**, 1-11.
- Hill RZ, Loud MC, Dubin AE, Peet B & Patapoutian A. (2022). PIEZO1 transduces mechanical itch in mice. *Nature* **607**, 104-110.
- Honore E, Patel AJ, Chemin J, Suchyna T & Sachs F. (2006). Desensitization of mechano-gated K2P channels. *Proc Natl Acad Sci U S A* **103**, 6859-6864.
- Horch KW, Tuckett RP & Burgess PR. (1977). A Key to the Classification of Cutaneous Mechanoreceptors. *Journal of Investigative Dermatology* **69**, 75-82.
- Jojoa-Cruz S, Saotome K, Murthy SE, Tsui CCA, Sansom MSP, Patapoutian A & Ward AB. (2018). Cryo-EM structure of the mechanically activated ion channel OSCA1.2, pp. 1-17.
- Jojoa-Cruz S, Saotome K, Tsui CCA, Lee WH, Sansom MSP, Murthy SE, Patapoutian A & Ward AB. (2022). Structural insights into the Venus flytrap mechanosensitive ion channel Flycatcher1. *Nat Commun* **13**, 850.
- Kashkoush AI, Gaunt RA, Fisher LE, Bruns TM & Weber DJ. (2019). Recording single- and multi-unit neuronal action potentials from the surface of the dorsal root ganglion. *Sci Rep* **9**, 2786.

- Kefauver JM, Ward AB & Patapoutian A. (2020). Discoveries in structure and physiology of mechanically activated ion channels. *Nature* **587**, 567-576.
- Kehan, thermometer icon, <https://github.com/kehantan> is licensed under CC0 <https://creativecommons.org/publicdomain/zero/1.0/>. 2024.
- Kloda A & Martinac B. (2002). Common evolutionary origins of mechanosensitive ion channels in Archaea, Bacteria and cell-walled Eukarya. *Archaea* **1**, 35-44.
- Larsson M & Nagi SS. (2022). Role of C-tactile fibers in pain modulation: animal and human perspectives. *Current Opinion in Behavioral Sciences* **43**, 138-144.
- Le Pichon CE & Chesler AT. (2014). The functional and anatomical dissection of somatosensory subpopulations using mouse genetics. *Front Neuroanat* **8**, 21.
- Le SC, Liang P, Lowry AJ & Yang H. (2021). Gating and Regulatory Mechanisms of TMEM16 Ion Channels and Scramblases. *Front Physiol* **12**, 787773.
- Lee H, Iida T, Mizuno A, Suzuki M & Caterina MJ. (2005). Altered thermal selection behavior in mice lacking transient receptor potential vanilloid 4. *J Neurosci* **25**, 1304-1310.
- Lee JH, Perez-Flores MC, Park S, Kim HJ, Chen Y, Kang M, Kersigo J, Choi J, Thai PN, Woltz RL, Perez-Flores DC, Perkins G, Sihn CR, Trinh P, Zhang XD, Sirish P, Dong Y, Feng WW, Pessah IN, Dixon RE, Sokolowski B, Fritzsche B, Chiamvimonvat N & Yamoah EN. (2024). The Piezo channel is a mechano-sensitive complex component in the mammalian inner ear hair cell. *Nat Commun* **15**, 526.
- Lee YM, Kim YK & Chung JH. (2009). Increased expression of TRPV1 channel in intrinsically aged and photoaged human skin in vivo. *Experimental Dermatology* **18**, 431-436.
- Lewis AH, Cronin ME & Grandl J. (2024). Piezo1 ion channels are capable of conformational signaling. *Neuron*.
- Lewis AH & Grandl J. (2020). Inactivation Kinetics and Mechanical Gating of Piezo1 Ion Channels Depend on Subdomains within the Cap. *Cell Rep* **30**, 870-880 e872.
- Lewis AH & Grandl J. (2021). Piezo1 ion channels inherently function as independent mechanotransducers. eLife Sciences Publications Ltd.
- Li K, Guo Y, Wang Y, Zhu R, Chen W, Cheng T, Zhang X, Jia Y, Liu T, Zhang W, Jan LY & Jan YN. (2024). Drosophila TMEM63 and mouse TMEM63A are lysosomal mechanosensory ion channels. *Nat Cell Biol* **26**, 393-403.
- Li L & Ginty DD. (2014). The structure and organization of lanceolate mechanosensory complexes at mouse hair follicles, pp. 1-24.

- Li L, Rutlin M, Abaira VE, Cassidy C, Kus L, Gong S, Jankowski MP, Luo W, Heintz N, Koerber HR, Woodbury CJ & Ginty DD. (2011). The Functional Organization of Cutaneous Low-Threshold Mechanosensory Neurons. *Cell* **147**, 1615-1627.
- Li Q & Montell C. (2021). Mechanism for food texture preference based on grittiness  
Mechanism for food texture preference based on grittiness. *Current Biology* **31**, 1-12.
- Li S, Li B, Gao L, Wang J & Yan Z. (2022). Humidity response in *Drosophila* olfactory sensory neurons requires the mechanosensitive channel TMEM63. *Nat Commun* **13**, 3814.
- Lin Y-C, Guo YR, Miyagi A, Levring J, MacKinnon R & Scheuring S. (2019). Force-induced conformational changes in PIEZO1, pp. 230-234.
- Loken LS, Wessberg J, Morrison I, McGlone F & Olausson H. (2009). Coding of pleasant touch by unmyelinated afferents in humans. *Nat Neurosci* **12**, 547-548.
- Lou S, Duan B, Vong L, Lowell BB & Ma Q. (2013). Runx1 controls terminal morphology and mechanosensitivity of VGLUT3-expressing C-mechanoreceptors. *J Neurosci* **33**, 870-882.
- Lowry AJ, Liang P, Serena Wan YC, Pei Z-M, Yang H & Zhang Y. (2024). TMEM16 and TMEM63/OSCA proteins share a conserved potential to permeate ions and phospholipids. *Elife*.
- Luo W, Enomoto H, Rice FL, Milbrandt J & Ginty DD. (2009). Molecular identification of rapidly adapting mechanoreceptors and their developmental dependence on ret signaling. *Neuron* **64**, 841-856.
- Ma S, Dubin AE, Romero LO, Loud M, Salazar A, Chu S, Klier N, Masri S, Zhang Y, Wang Y, Chesler AT, Wilkinson KA, Vasquez V, Marshall KL & Patapoutian A. (2023). Excessive mechanotransduction in sensory neurons causes joint contractures. *Science* **379**, 201-206.
- Madisen L, Zwingman TA, Sunkin SM, Oh SW, Zariwala HA, Gu H, Ng LL, Palmiter RD, Hawrylycz MJ, Jones AR, Lein ES & Zeng H. (2010). A robust and high-throughput Cre reporting and characterization system for the whole mouse brain. *Nat Neurosci* **13**, 133-140.
- Marshall KL, Saade D, Ghitani N, Coombs AM, Szczot M, Keller J, Ogata T, Daou I, Stowers LT, Bönnemann CG, Chesler AT & Patapoutian A. (2020). PIEZO2 in sensory neurons and urothelial cells coordinates urination. *Nature* **588**, 290-295.
- McCarter GC, Reichling DB & Levine JD. (1999). Mechanical transduction by rat dorsal root ganglion neurons in vitro. *Neuroscience Letters* **273**, 179-182.

- Meltzer S, Santiago C, Sharma N & Ginty DD. (2021). The cellular and molecular basis of somatosensory neuron development, pp. 3736-3757. Cell Press.
- Middleton SJ, Perini I, Themistocleous AC, Weir GA, McCann K, Barry AM, Marshall A, Lee M, Mayo LM, Bohic M, Baskozos G, Morrison I, Loken LS, McIntyre S, Nagi SS, Staud R, Sehlstedt I, Johnson RD, Wessberg J, Wood JN, Woods CG, Moqrich A, Olausson H & Bennett DL. (2022). Nav1.7 is required for normal C-low threshold mechanoreceptor function in humans and mice. *Brain* **145**, 3637-3653.
- Miyata Y, Takahashi K, Lee Y, Sultan CS, Kuribayashi R, Takahashi M, Hata K, Bamba T, Izumi Y, Liu K, Uemura T, Nomura N, Iwata S, Nagata S, Nishizawa T & Segawa K. (2024). Membrane structure-responsive lipid scrambling by TMEM63B to control plasma membrane lipid distribution. *Nat Struct Mol Biol*.
- Murthy SE. (2023). Deciphering mechanically activated ion channels at the single-channel level in dorsal root ganglion neurons. *J Gen Physiol* **155**.
- Murthy SE, Dubin AE, Whitwam T, Jojoa-Cruz S, Cahalan SM, Mousavi SAR, Ward AB & Patapoutian A. (2018a). OSCA/TMEM63 are an evolutionarily conserved family of mechanically activated ion channels. *eLife* **7**, 1-17.
- Murthy SE, Loud MC, Daou I, Marshall KL, Schwaller F, Kühnemund J, Francisco AG, Keenan WT, Dubin AE, Lewin GR & Patapoutian A. (2018b). The mechanosensitive ion channel Piezo2 mediates sensitivity to mechanical pain in mice. *Science Translational Medicine* **10**.
- Nagi SS, Rubin TK, Chelvanayagam DK, Macefield VG & Mahns DA. (2011). Allodynia mediated by C-tactile afferents in human hairy skin. *J Physiol* **589**, 4065-4075.
- Namu, Lobster Claw Illustration, <https://www.cleanpng.com/png-snow-crab-claw-drawing-clip-art-claw-836168/>. 2024.
- Nguyen MQ, von Buchholtz LJ, Reker AN, Ryba NJ & Davidson S. (2021). Single-nucleus transcriptomic analysis of human dorsal root ganglion neurons. *Elife* **10**.
- Nieuwenhuis B, Haenzi B, Hilton S, Carnicer-Lombarte A, Hobo B, Verhaagen J & Fawcett JW. (2021). Optimization of adeno-associated viral vector-mediated transduction of the corticospinal tract: comparison of four promoters. *Gene Ther* **28**, 56-74.
- Niloy SI, Strege PR, Hannan EC, Cowan LM, Linsenmeier F, Friedrich O, Farrugia G & Beyder A. (2024). Stretch response of the mechano-gated channel TMEM63A in membrane patches and single cells. *Am J Physiol Cell Physiol* **326**, C622-C631.
- Niu H, Maruoka M, Noguchi Y, Kosako H & Suzuki J. (2024). Phospholipid scrambling induced by an ion channel/metabolite transporter complex. *Nat Commun* **15**, 7566.

- Noel J, Zimmermann K, Busserolles J, Deval E, Alloui A, Diochot S, Guy N, Borsotto M, Reeh P, Eschali r A & Lazdunski M. (2009). The mechano-activated K<sup>+</sup> channels TRAAK and TREK-1 control both warm and cold perception. *EMBO J* **28**, 1308-1318.
- Pan B, Akyuz N, Liu XP, Asai Y, N st-Lund C, Kurima K, Derfler BH, Gyorgy B, Limapichat W, Walujkar S, Wimalasena LN, Sotomayor M, Corey DP & Holt JR. (2018). TMC1 Forms the Pore of Mechanosensory Transduction Channels in Vertebrate Inner Ear Hair Cells. *Neuron* **99**, 736-753 e736.
- Paricio-Montesinos R, Schwaller F, Udhayachandran A, Rau F, Walcher J, Evangelista R, Vriens J, Voets T, Poulet JFA & Lewin GR. (2020). The Sensory Coding of Warm Perception. *Neuron* **106**, 830-841 e833.
- Parpaite T, Brosse L, Sejourne N, Laur A, Mechouioukhi Y, Delmas P & Coste B. (2021). Patch-seq of mouse DRG neurons reveals candidate genes for specific mechanosensory functions. *Cell Rep* **37**, 109914.
- Pomaville MB & Wright KM. (2021). Immunohistochemical and Genetic Labeling of Hairy and Glabrous Skin Innervation. *Curr Protoc* **1**, e121.
- Pomaville MB & Wright KM. (2023). Follicle-innervating Adelta-low threshold mechanoreceptive neurons form receptive fields through homotypic competition. *Neural Dev* **18**, 2.
- Procko C, Murthy S, Keenan WT, Mousavi SAR, Dabi T, Coombs A, Procko E, Baird L, Patapoutian A & Chory J. (2021). Stretch-activated ion channels identified in the touch-sensitive structures of carnivorous Droseraceae plants. *Elife* **10**.
- Qi L, Iskols M, Shi D, Reddy P, Walker C, Lezgiyeva K, Voisin T, Pawlak M, Kuchroo VK, Chiu IM, Ginty DD & Sharma N. (2024). A mouse DRG genetic toolkit reveals morphological and physiological diversity of somatosensory neuron subtypes. *Cell* **187**, 1508-1526 e1516.
- Ranade SS, Woo S-H, Dubin AE, Moshourab RA, Wetzel C, Petrus M, Mathur J, B g y V, Coste B, Mainquist J, Wilson AJ, Francisco AG, Reddy K, Qiu Z, Wood JN, Lewin GR & Patapoutian A. (2014). Piezo2 is the major transducer of mechanical forces for touch sensation in mice. *Nature* **516**, 121-125.
- Royer S, Zemelman BV, Barbic M, Losonczy A, Buzs ki G & Magee JC. (2010). Multi-array silicon probes with integrated optical fibers: light-assisted perturbation and recording of local neural circuits in the behaving animal. *Eur J Neurosci* **31**, 2279-2291.
- Rutlin M, Ho CY, Abaira VE, Cassidy C, Bai L, Woodbury CJ & Ginty DD. (2014). The cellular and molecular basis of direction selectivity of Adelta-LTMRs. *Cell* **159**, 1640-1651.



- Sakuragi T & Nagata S. (2023). Regulation of phospholipid distribution in the lipid bilayer by flippases and scramblases. *Nat Rev Mol Cell Biol* **24**, 576-596.
- Sato M. (1961). Response of Pacinian corpuscles to sinusoidal vibration. *J Physiol* **159**, 391-409.
- Saunders A, Macosko EZ, Wysoker A, Goldman M, Krienen FM, de Rivera H, Bien E, Baum M, Bortolin L, Wang S, Goeva A, Nemesh J, Kamitaki N, Brumbaugh S, Kulp D & McCarroll SA. (2018). Molecular Diversity and Specializations among the Cells of the Adult Mouse Brain. *Cell* **174**, 1015-1030 e1016.
- Schneider MR & Paus R. (2010). Sebocytes, multifaceted epithelial cells: lipid production and holocrine secretion. *Int J Biochem Cell Biol* **42**, 181-185.
- Seal RP, Wang X, Guan Y, Raja SN, Woodbury CJ, Basbaum AI & Edwards RH. (2009). Injury-induced mechanical hypersensitivity requires C-low threshold mechanoreceptors. *Nature* **462**, 651-655.
- Servier, adipocyte-5 icon, <https://smart.servier.com/> is licensed under CC-BY 3.0 Unported <https://creativecommons.org/licenses/by/3.0/>. 2024. Adapted by Daniel Orlin.
- Servier, bladder icon, <https://smart.servier.com/> is licensed under CC-BY 3.0 Unported <https://creativecommons.org/licenses/by/3.0/>. 2024.
- Servier, healthy-colon-3d icon <https://smart.servier.com/> is licensed under CC-BY 3.0 Unported <https://creativecommons.org/licenses/by/3.0/>. 2024.
- Servin-Vences MR, Lam RM, Koolen A, Wang Y, Saade DN, Loud M, Kacmaz H, Frausto S, Zhang Y, Beyder A, Marshall KL, Bonnemann CG, Chesler AT & Patapoutian A. (2023). PIEZO2 in somatosensory neurons controls gastrointestinal transit. *Cell* **186**, 3386-3399 e3315.
- Sharma N, Flaherty K, Lezgiyeva K, Wagner DE, Klein AM & Ginty DD. (2020). The emergence of transcriptional identity in somatosensory neurons. *Nature* **577**, 392-398.
- Stoney SD, Jr. (1990). Limitations on impulse conduction at the branch point of afferent axons in frog dorsal root ganglion. *Exp Brain Res* **80**, 512-524.
- Sukharev SI, Martinac B, Arshavsky VY & Kung C. (1993). Two types of mechanosensitive channels in the Escherichia coli cell envelope: solubilization and functional reconstitution. *Biophys J* **65**, 177-183.
- Szczot M, Liljencrantz J, Ghitani N, Barik A, Lam R, Thompson JH, Bharucha-Goebel D, Saade D, Necaie A, Donkervoort S, Foley AR, Gordon T, Case L, Bushnell MC, Bonnemann CG & Chesler AT. (2018). PIEZO2 mediates injury-induced tactile pain in mice and humans. *Sci Transl Med* **10**.

- Tominaga M. (2007). *TRP Ion Channel Function in Sensory Transduction and Cellular Signaling Cascades*. CRC Press/Taylor & Francis, Boca Raton (FL).
- Tuthill JC & Azim E. (2018). Proprioception. *Curr Biol* **28**, R194-R203.
- Urien L, Gaillard S, Lo Re L, Malapert P, Bohic M, Reynders A & Moqrich A. (2017). Genetic ablation of GINIP-expressing primary sensory neurons strongly impairs Formalin-evoked pain. *Sci Rep* **7**, 43493.
- Usoskin D, Furlan A, Islam S, Abdo H, Lönnerberg P, Lou D, Hjerling-Leffler J, Haeggström J, Kharchenko O, Kharchenko PV, Linnarsson S & Ernfors P. (2015). Unbiased classification of sensory neuron types by large-scale single-cell RNA sequencing. *Nature Neuroscience* **18**, 145-153.
- Vandewauw I, De Clercq K, Mulier M, Held K, Pinto S, Van Ranst N, Segal A, Voet T, Vennekens R, Zimmermann K, Vriens J & Voets T. (2018). Publisher Correction: A TRP channel trio mediates acute noxious heat sensing. *Nature* **559**, E7.
- Vay L, Gu C & McNaughton PA. (2012). The thermo-TRP ion channel family: properties and therapeutic implications. *Br J Pharmacol* **165**, 787-801.
- Vetro A, Pelorosso C, Balestrini S, Masi A, Hambleton S, Argilli E, Conti V, Giubbolini S, Barrick R, Bergant G, Writzl K, Bijlsma EK, Brunet T, Cacheiro P, Mei D, Devlin A, Hoffer MJV, Machol K, Mannaioni G, Sakamoto M, Menezes MP, Courtin T, Sherr E, Parra R, Richardson R, Roscioli T, Scala M, von Stulpnagel C, Smedley D, collaborators TB, Genomics England Research C, Torella A, Tohyama J, Koichihara R, Hamada K, Ogata K, Suzuki T, Sugie A, van der Smagt JJ, van Gassen K, Valence S, Vittery E, Malone S, Kato M, Matsumoto N, Ratto GM & Guerrini R. (2023). Stretch-activated ion channel TMEM63B associates with developmental and epileptic encephalopathies and progressive neurodegeneration. *Am J Hum Genet* **110**, 1356-1376.
- Villarino NW, Hamed YMF, Ghosh B, Dubin AE, Lewis AH, Odem MA, Loud MC, Wang Y, Servin-Vences MR, Patapoutian A & Marshall KL. (2023). Labeling PIEZO2 activity in the peripheral nervous system. *Neuron* **111**, 2488-2501 e2488.
- Von Buchholtz LJ, Ghitani N, Lam RM, Licholai JA, Chesler AT, Ryba NJP & Gov ATC. (2021). Decoding Cellular Mechanisms for Mechanosensory Discrimination. *Neuron* **109**, 1-14.
- Vrontou S, Wong AM, Rau KK, Koerber HR & Anderson DJ. (2013). Genetic identification of C fibres that detect massage-like stroking of hairy skin in vivo. *Nature* **493**, 669-673.
- Wang Y, Leung VH, Zhang Y, Nudell VS, Loud M, Servin-Vences MR, Yang D, Wang K, Moya-Garzon MD, Li VL, Long JZ, Patapoutian A & Ye L. (2022). The role of somatosensory innervation of adipose tissues. *Nature* **609**, 569-574.

- Weinstein S. (1993). Fifty years of somatosensory research: from the Semmes-Weinstein monofilaments to the Weinstein Enhanced Sensory Test. *J Hand Ther* **6**, 11-22; discussion 50.
- Witschi R, Johansson T, Morscher G, Scheurer L, Deschamps J & Zeilhofer HU. (2010). Hoxb8-Cre mice: A tool for brain-sparing conditional gene deletion. *Genesis* **48**, 596-602.
- Woo SH, Lukacs V, de Nooij JC, Zaytseva D, Criddle CR, Francisco A, Jessell TM, Wilkinson KA & Patapoutian A. (2015). Piezo2 is the principal mechanotransduction channel for proprioception. *Nat Neurosci* **18**, 1756-1762.
- Woo SH, Ranade S, Weyer AD, Dubin AE, Baba Y, Qiu Z, Petrus M, Miyamoto T, Reddy K, Lumpkin EA, Stucky CL & Patapoutian A. (2014). Piezo2 is required for Merkel-cell mechanotransduction. *Nature* **509**, 622-626.
- Wu Z, Grillet N, Zhao B, Cunningham C, Harkins-Perry S, Coste B, Ranade S, Zebarjadi N, Beurg M, Fettiplace R, Patapoutian A & Mueller U. (2017). Mechanosensory hair cells express two molecularly distinct mechanotransduction channels. *Nat Neurosci* **20**, 24-33.
- Young M, Lewis AH & Grandl J. (2022). Physics of mechanotransduction by Piezo ion channels. *J Gen Physiol* **154**.
- Yu L, Yang F, Luo H, Liu FY, Han JS, Xing GG & Wan Y. (2008). The role of TRPV1 in different subtypes of dorsal root ganglion neurons in rat chronic inflammatory nociception induced by complete Freund's adjuvant. *Mol Pain* **4**, 61.
- Zhang M, Shan Y, Cox CD & Pei D. (2023). A mechanical-coupling mechanism in OSCA/TMEM63 channel mechanosensitivity. *Nat Commun* **14**, 3943.
- Zhang M, Wang D, Kang Y, Wu JX, Yao F, Pan C, Yan Z, Song C & Chen L. (2018). Structure of the mechanosensitive OSCA channels. *Nat Struct Mol Biol* **25**, 850-858.
- Zhang X, Shao J, Wang C, Liu C, Hao H, Li X, An Y, He J, Zhao W, Zhao Y, Kong Y, Jia Z, Wan S, Yuan Y, Zhang H, Zhang H & Du X. (2024). TMC7 functions as a suppressor of Piezo2 in primary sensory neurons blunting peripheral mechanotransduction. *Cell Rep* **43**, 114014.
- Zheng B, Sage M, Sheppheard EA, Jurecic V & Bradley A. (2000). Engineering mouse chromosomes with Cre-loxP: range, efficiency, and somatic applications. *Mol Cell Biol* **20**, 648-655.
- Zheng W, Rawson S, Shen Z, Tamilselvan E, Smith HE, Halford J, Shen C, Murthy SE, Ulbrich MH, Sotomayor M, Fu TM & Holt JR. (2023). TMEM63 proteins function as monomeric high-threshold mechanosensitive ion channels. *Neuron* **111**, 3195-3210 e3197.

Zheng Y, Liu P, Bai L, Trimmer JS, Bean BP & Ginty DD. (2019). Deep Sequencing of Somatosensory Neurons Reveals Molecular Determinants of Intrinsic Physiological Properties. *Neuron* **103**, 598-616.e597.